International Journal of Computer Science and Application (IJCSA) Volume 3 Issue 1, February 2014 www.ij-csa.org
DOI: 10.14355/ijcsa.2014.0301.01

Design of Open Architecture System to Reduce the Likelihood of a Vehicle Getting Stolen or Carjacking

M. S. Zaghloul

Arab Academy for Science, Technology, and Maritime Transport, Electronic and Communication Department, P.O.1029, Alex, Egypt

dr_mszaghloul@yahoo.com

Abstract

This paper is a practical design and implementation of an electronic protection system for protection from motor vehicle theft and safety for the driver. It is a specific form of computer-based information system that complies with International safety regulations and can be used in any types of cars, ships, trains, and airplanes. Nationwide in the US in 2005, there were an estimated 1.2 million motor vehicle thefts, or approximately 416.7 motor vehicles stolen for every 100,000 inhabitants. (Federal Bureau of Investigation, 2009) It can be interfaced with navigation, control system for the protected vehicles. The system can control and displays information of controlled vehicles which can be powered for the fuel pump, electricity for the ignition system, audio and visual alarms or others. The designed system can prevent the operation of the engine unless the right store code is entered, also it can let the engine operate only for certain specific previously determined time, or reduce the speed of the engine at certain conditions or stop the engine completely in case of danger for example if the driver fell into sleep in this case in our design depending on gyro as a sensor for that. It may also display additional navigation-related information, such as Sailing Directions, speed, or remains fuel. The system is powered by 12 V dc supply available in all types of vehicles, to start operation to enter the password for the key board. Further, it was demonstrated that the program is used in actual work for the system to the microcontroller type16F84A. The software is preferred for design using software PIC Basic for microcontroller. This Program is a window based Software and friendly user. To detect the driver sleep, different techniques can be employed such as camera day or night, passive infrared detector, muscle sensor (neck or hand), flex or pressure sensor, gyro on head (mechanical), and mind activity sensation. A gyro can be designed with USB interface, in which compass model was designed with Honeywell`s HMC5883L-3 axis magnetometer I²C, 2.7 to 6.5 V TTL-USB and microcontroller 16F877, in addition, it was able to electrically resolve better than 0.1 degree rotation and accuracy from 1 to 2 degree. The output from this gyro model is taken via USB port for monitoring purpose and through a relay used as one of the controls to the microcontroller type 16F84A which will result in the required action like reducing the speed or stopping engine. Our design covers various methods of prevention to reduce the likelihood of a vehicle getting stolen. These include physical barriers, which make the effort of stealing the vehicle more difficult by allowing the vehicle to start only if the right password contains the correct code which is present in the stored microcontroller to give start signal for ignition. Adding to those chances of theft can also be reduced with various deterrents which give the impression to the thief that she/he is more likely to get caught if the vehicle is stolen; including: car alarm systems that are triggered if a breaking and entry into the vehicle occurs and trying to start the engine. Kill switch circuits were designed to frustrate or slow down the efforts of a determined car thief. Kill switches are located between crucial parts of the starting system, between the battery source and the coil, or the fuel pump. A car cannot start without first flipping these kill switches to closed position hided in obscured areas, under the dashboard, beneath the seat, behind a chair etc.

Keywords

Safety and Protection; Car Control; Signal Processing; Sensors

Introduction

Motor vehicle theft (sometimes referred to as grand theft auto by the media and police departments in the US) is the criminal act of stealing or attempting to steal a car. Property losses due to motor vehicle theft in 2005 were estimated up to $7.6 billion. (Federal Bureau of Investigation, 2009) Since then the number of motor thefts nationally has declined. The most recent statistics, for 2009, showed an estimated 794,616 thefts of motor vehicles nationwide, representing property losses of nearly $5.2 billion. (Federal Bureau of Investigation, 2009) Different kinds of control were used on vehicle engine like start up and stop, engine speed, supply of electricity to the ignition system, start alarm, Also the sleep of the driver can be detected using our designed gyro model. There are different ways to steal the vehicle like a-theft of an unattended

vehicle without key(s): the removal of a parked vehicle either by breaking and entry, followed by hotwiring or other tampering methods to start the vehicle, or else towing. b-theft with access to keys: known in some places as "Taken Without Owner's Consent (TWOC)". The unauthorized use of a vehicle in which the owner has allowed the driver to have possession or easy access to the keys c-opportunistic theft: the removal of a vehicle that the owner or operator has left unattended with the keys visibly present, sometimes idling. d-carjacking: refers to the taking of a vehicle by force or threat of force from its owner or operator. In most places, this is the most serious form of theft, since assault also occurs. In some carjacking, the operators and passengers are forced from the vehicle while the thief drives it away, while in other incidents, the operator and/or passenger(s) are forced to remain in the vehicle as hostages. Some less common carjacking result in the operator forced to drive the assailant in accordance with the assailant's demands, (Find Law for Legal Professionals) and Fraudulent theft:. In our design, it was not only tried to find the counter action for the previous different ways to steal the vehicle but also protect the driver when fell into sleep. Moreover, our designed system is used to protect from jump an unattended running car while the owner is at the ATM, dropping off videos, etc.

Tool and Ways Commonly Used for Stolen and Various Methods of Prevention

FIG. 1 CARS WITH SMASHED WINDOW

FIG. 2 SHATTERED GLASS MARK THE SPOT WHERE A PARKED VEHICLE WAS STOLEN

The Protction System Circuit Diagram and Mother Board

Tool and ways commonly used for stealing and various methods of prevention to reduce the likelihood of a vehicle getting stolen slide hammer puller to break into the door locks and the cylinder lock, multimeters or a test light to find a power source, spare wires and/or a screwdriver to connect the power source to the ignition and starter wires, a generic rod and hook toolkit to slip between the car window and car frame and to open the lock behind the window. A common one is called the "Slim Jim". Many keyless ignition/lock cars have weak (Eli Biham; Dunkelman, Orr; Indesteege, Sebastian; Keller, Nathan, 2008; Bono, Stephen C.; Green, Matthew; Stubblefield, Adam; Juels, Ari; Rubin, Aviel D.; Szydlo, Michael, 2005)or no cryptographic protection of the unlock Signal. Proof-of-concept "thefts" of top-of-the-line luxury cars have been demonstrated by academic researchers using commercially available tools such as RFID microreaders, but it is unknown whether the attack has been used for actual theft a firearm or other weapon such as a baseball bat, or a utility knife or a box cutter to break open a window or threaten a passenger if inside the car.(Gold Coast City Council, 2014; http://www.edunds.com/car-review/Top-10)

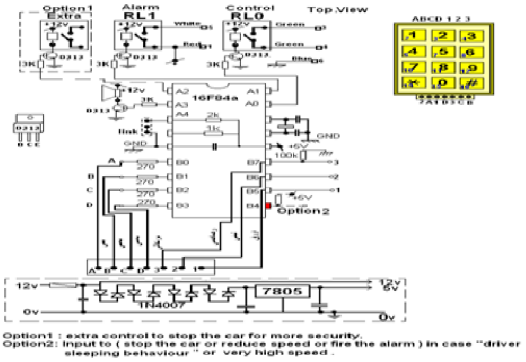

FIG. 3a CIRCUIT DIAGRAM FOR THE PROTECTION SYSTEM

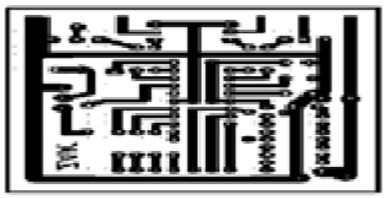

FIG. 3b PROTECTION SYSTEM BOARD LAY OUT

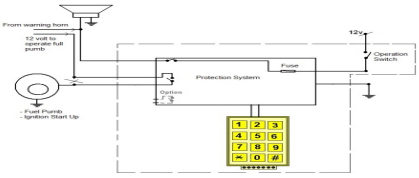

FIG. 4 CAR CONNECTIONS

Methods and Technique to Detect the Driver Sleep

To detect the driver sleeping, different techniques can be applied such as camera day or night, passive

infrared detector, muscle sensor (neck or hand), flex or pressure sensor, gyro on head (mechanical), and mind activity sensation. It was able to design a gyro with USB interface as shown in fig 5, in which Compass Module was used with Honeywell's HMC5883L 3-Axis Magnetometer, I2C, 2.7-6.5V, TTL-USB and micro-controller 16F877. For programming of the micro-controller software PIC basic pro was employed, and we can electrically resolve better than 0.1 degree rotation and accuracy from 1 to 2 degree., thus monitoring the driver head movement, and by analyzing the head movement we can detect driver status, for example the movement of the head to max rear or front inclination angle, in this case of sleep, the pump feeding can be prevented.

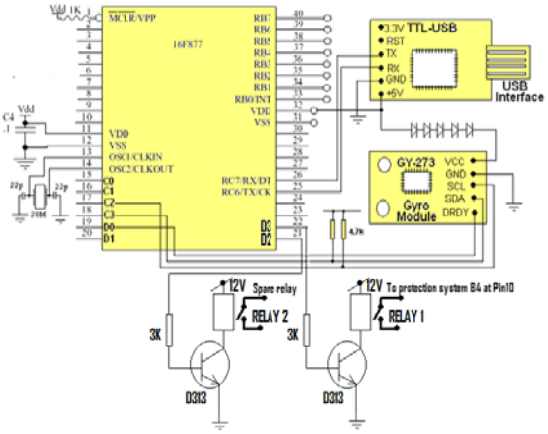

FIG. 5 THE COMPLETE CIRCUIT DIAGRAM FOR GYRO

The Gyro System Design

The designed system is 3-axis digital compass. It was tried to use a cheap and good resolution with a small size. The used Anisotropic Magnetoresistive (AMR) technology provides advantages over other magnetic sensor technologies. These anisotropic, directional sensors feature precision in-axis sensitivity and linearity. These sensors' solid-state construction with very low cross-axis sensitivity was designed to measure both the direction and the magnitude of Earth's magnetic fields, from milli-gauss to 8 gauss.

To get the data from the module, we need I²C interface so a micro controller chip 16F877 can be used to read this data. The design includes a small PCB with Micro Chip "Pic16F877" micro controller and the supporting hardware. We get the I²C data to C2, C3 and an interrupt pin to D0 to indicate data ready. Still the data should be read on a PC displayed that the microcontroller was connected to TTL-USB converter to read Data from Microcontroller. In addition, a small 5v power was made. To supply the Module with 3.3 volts, we applied the 5 v to 4 diodes in forward to have the required voltage drop; then made an external pull up resistor (4.7K) to the SCL & SDA. The I2C software is available. The output from relay 1 is fed to the protection system B4 at pin 10.

Passive Infrared Sensor

FIG. 6 PIR MOTION SENSOR

PIR "Piezoelectric sensors allow sensing motion or movement, which is always used to detect whether a human has moved in or out of the sensors range or not. In our design, this sensor was used to detect driver sleeping then the appropriate action was taken; moreover, PIR output was in connection to the microcontroller inside protection system as shown in figure 4. PIR sensors are small, inexpensive, low-power, easy to use and don't wear out. For that reason, they are commonly found in appliances and gadgets used in homes or businesses; often referred to as PIR, "Passive Infrared", "Piezoelectric", or "IR motion" sensors.

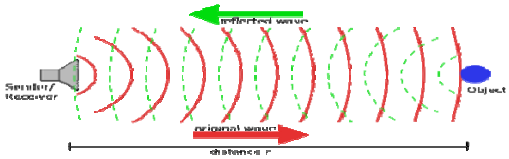

FIG. 7 THEORY OF OPERATION FOR PIR MOTION SENSOR

PIRs are basically made of a piezoelectric sensor (which you can see above as the round metal can with a rectangular crystal in the centre), which can detect levels of infrared radiation. Everything emits some low level radiation, and the hotter something is, the more radiation it emits. The sensor in a motion detector is actually split into two halves. The reason for that is that we are looking to detect motion (change) not average IR levels. The two halves are wired up so that they cancel each other out. If one half sees more or less IR radiation than the other, the output will swing high or low. This output in an input to the microcontroller will lead to stop of fuel pump or ignition coil.

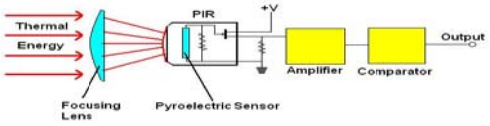

FIG. 8 PIR MOTION SENSOR DIAGRAM

This is suitable for recording the surface temperatures

ranging from about -70 to 1,000°C. In our design, the object was the vehicle driver. The sensors convert the thermal radiation sent from one object in a wavelength range of 0.7 to 20 μ m into an electrical signal that is processed into a signal that can be evaluated. What is important here is the D: S ratio (distance: spot) that the measuring field diameter is indicated at a given distance. Complete coverage of this field by the object's surface whose temperature is to be monitored is optimal.

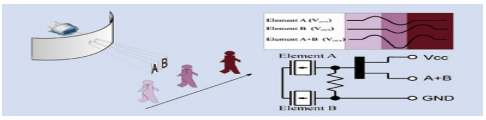

FIG. 9 PIR MOTION SENSOR CIRCUIT

The Complete system design

The complete designed system is shown in figure 10, and this complete system has installed the programmed microcontroller 16F84A. Two types of key board can be employed, as shown in figure 11 they can be of press type or sticker type according to the requirement, then the flat cable was applied which can be used for extension between the key board and the complete system. Figure 12 shows some form of master key.

FIG. 10 REPRESENTS THE COMPLETE DESIGNED SYSTEM

FIG. 11 REPRESENTS THE TWO TYPES OF KEY BOARDS

FIG. 12 SOME SORTS OF MASTER KEY

Conclusion

In this design, it was tried to find the countermeasure for most different ways to steal the vehicle, and the designed system can be used not only to prevent from theft but also to protect from Jump into an unattended running car while the owner is at the ATM, dropping off videos, and protection of the driver when falling into sleep by stopping the engine. Circuits were designed to prevent, or frustrate or slow down the efforts of a car thief, and other circuit for gyro. Moreover, it can reduce the speed of the engine or stopped at certain conditions. Design allows straightforward programming interface to the system used to simplify the task of integration into different user environment. Parallel cable interface to the host makes the system cheaper. The system achieved the high level of security and can be used to more complex designs according to requirements. It can be used in wide scale in commercial as protection and alarm system for any vehicle. Further, a new and systematic design was presented in this paper using microprocessors. A new and comprehensive model is shown that uses appropriate code words, independent of the vehicles details. Protection and alarm are given to any vehicles (M. S. Zaghloul, M Saleh, 2011)

REFERENCES

Bono, Stephen C.; Green, Matthew; Stubblefield, Adam; Juels, Ari; Rubin, Aviel D.; Szydlo, Michael **Jump up^** (2005), *Security Analysis of a Cryptographically-Enabled RFID Device*, 14th USENIX Security Symposium.

Data sheet from Motorola for microcontroller type16F84A of Motorola.

Eli Biham; Dunkelman, Orr; Indesteege, Sebastian; Keller, Nathan **Jump up^**; Pre Neel, Bart (2008), How to Steal Cars—A Practical Attack on Keel Log, Euro crypt 2008

FBI **Jump up^** Motor Vehicle Theft.

Federal Bureau of Investigation **Jump up^** "Motor Vehicle Theft". Crime in the United States 2005 Department of Justice —Release Date: September 2006. Retrieved 2009.

Federal Bureau of Investigation **Jump up^** "Property losses". Crime in the United States 2005 Department of Justice — Release Date: September 2006, Revising 2009.

Find Law for Legal Professionals **Jump up^** - Case Law, Federal and State Resources, Forms, and Code.

Gold Coast City Council **Jump up^** "Car Theft Stats" (PDF). Revising 27 Aug 2012.

http://www.edunds.com/car-review/Top-10**Jump up^** .

M. S. Zaghloul, M Saleh, Field Programmable Gate Array

(FPGA) implementation of the portable automatic testing system for IC'S library and digital circuits, IEEE Applied Imagery Pattern Recognition Workshop, 11-13,2011. Washington, DC, USA.

Manual for Basic pro programming.

DOI: 10.14355/ijcsa.2014.0301.02

Online Ship Control System Using Supervisory Control and Data Acquisition (SCADA)

M. S. Zaghloul

Arab Academy for Science, Technology, and Maritime Transport, Electronic and Communication Department, P.O.1029, Alex, Egypt,

dr_mszaghloul@yahoo.com

Abstract

This paper is a practical design and implementation of open architecture ship control, alarm and monitoring system using Supervisory Control and Data Acquisition (SCADA).Modern ships have an automatic system control which includes control, alarm and monitoring system that have access to all process control station and can monitor them. All the screens for different sensors in our design are considered as the HMI (Human Machine Interface) of the SCADA system monitoring a group of sensors, which can help the operator in the control room to make online control on ship. WinCC Flexible is used to create screens. The control system control several types of self-running process as voyage data recorder, GPS, hull opening, hull stress, radar, ship speed, tank fuel level, fuel and machinery temperature, wind speed and direction, Communication, fire doors control station, and each type is dictated to specific task. The alarm system is connected to sensors everywhere in the ship and continuously monitors them, if any sensor reading is outside the preset limits, alarm occurs. The monitoring system can record any alarm status and save it in hard disk or printer with time stamp. The alarm system depends mainly on data coming from different sensors connected to corresponding measuring points, also an inhibit control can be applied to certain alarm group for disable at certain conditions for the system.

Keywords

IMO; SOLAS; Ship Control; Signal Processing; Sensors

Introduction

SCADA is Supervisory Control and Data Acquisition. SCADA systems that use to monitor and control a plant or equipment in industries such as water and waste water control, energy, oil, telecommunications and gas refining and transportation. Within the environment of a marine plant there are many parameters which need to be controlled or monitored including: temperatures, pressure, level, viscosity, flow control, speed, torque control, voltage, current, machinery status (on/ off), and equipment status (open/ closed).In olden times it was the role of the watch keeping engineers to monitor and control the machinery plant. This was achieved by periodically taking rounds around the engine room and manually inspecting the condition of the running machinery. Often the engineer was totally dependent on his natural senses, frequently supported by only the minimum of widely distributed simple monitoring devices. (NATIONAL TRANSPORTATION SAFETY BOARD, 2007) This is an example design of an open architecture system. The intention here is to Supervisory Control and Data Acquisition (SCADA). To be able to use different number of screens and with different types of man machine interface such that it can display and control different sensor or system status, these sensors can be voyage data recorder, GPS, hull opening, hull stress, Radar, ship speed, tank fuel level, fuel and machinery temperature, wind speed and direction. Communication, fire doors control station.

Typical SCADA system and its benefit

Typical SCADA system consists of one more field data interface devices usually RTUs or PLCs which interface to field sensing devices, local control switch boxes and valve actuators. A communication system is used to transfer data among field data interface devices, control units and the computers in the SCADA central host which is a central host computer server or servers. A collection of standard and/or custom software, sometimes called Human Machine Interface HMI software, is used to provide the SCADA central host and operator terminal application, supporting the communications system, monitor and control remotely located field data interface devices. Devices such as level meters, water flow meters, valve position transmitters, temperature transmitters, power consumption meters, and pressure meters all provide

information that can tell an experienced operator how well a system performs. Benefits SCADA Systems provide operational costs reduction, immediate knowledge of system performance, improvement on system efficiency and performance, increasing equipment life, reducing cost of repairs, as well as number of man-hours (labor costs) required for troubleshooting or service, frees up personnel for other important tasks, facilitating compliance with regulatory agencies through automated report generating

FIG. 1 A NETWORKED SCADA SYSTEM

SCADA Software

a. Central Host Computer Operating System It is the software used to control the central host computer hardware.

b. Operator Terminal Operating System the software used to control the RTU computer hardware. It is usually the same as the central host computer operating system, and usually contributes to the networking of the central host and the operator terminals.

c. Central Host Computer Application the software that handles the transition and reception of data between the RTU and the central host computer. The software also provides the graphical user interface, which offers site mimic screens, alarm pages, trend pages, and control functions**.**

d. Operator Terminal Application it is the application that enables users to access information available on the central host computer application.

e. Communication Protocol Drivers the software that is usually based on the central host and the RTUs, and required to control the translation and interpretation of the data between ends of the communications links of the system.

Automation Protocols

a. Standard Protocol VS Vendors Protocols

SCADA protocols have been designed for extremely compact and a major portion is also designed for sending information to master station only when the RTU is polled by master station. Typically, the legacy of SCADA protocols consists of Conitel, Profibus, Modbus RTU and RP-570. These protocols of communication are specifically SCADA-vendor but they are popularly used and adopted. Standard protocols mainly are IEC 61850, DNP3 and IEC 60870-5-101 or 104. These protocols of communication are recognized and standardized by all big SCADA vendors. Several of these protocols contain extensions for operation over the TCP/IP. It is considered good practice of security engineering to avoid the SCADA systems from connection to Internet for reducing attack surface.

b. Compilation of automation protocols Due to this creation of multitude of control protocols by the developers and its management. In order to 'lock in' their own customer base amongst the many vendors an incentive was there to create own protocols. Compilation of automation protocols is given here. For the better intercommunication between the different software and hardware, PLE for Process Control (OPC) is a widely accepted solution, which then even allows communication between the devices which were originally not even intended to be part of the industrial network

WinCC Flexible

1. Automation Levels are: a. Controllers b. Machine HMI c. Process visualization

2. WinCC Flexible Stages The first stage is to configure the HMI devices for operating and monitoring at machine level using the WinCC flexible engineering system, so it replaces the complete functionality of protocol, while the second stage is to permit configuration of WinCC functionality, i.e. it will also take over as successor to WinCC". Uniform Engineering "will then exist for the complete visualization sector from a small panel in the lower performance range of operation at machine level up to powerful and redundant client/server structure in the upper performance range of process visualization

3. Components of WinCC Flexible

3.1 Engineering System (ES) the Engineering System is the software with which all configuration tasks required to create a GUI for operation and monitoring of machines and plants can be carried out.

3.2 Runtime (RT) WinCC flexible Runtime is the software for process visualization on the HMI device to execute the project in process mode

3.3 Options The options depend on the target system used. An HMI device which does not support a

particular functionality cannot use the corresponding option either.

The Screens

These systems encompass the transfer of data between a SCADA central host computer and a number of Remote Terminal Units RTUs and/or Programmable Logic Controllers PLCs, as well as the central host and the operator terminals. A SCADA system gathers information, transfers the information back to a central site, then alerts the home station that a leak has occurred, carrying out necessary analysis and control, and displaying the information in a logical and organized fashion. WinCC Flexible is used to create screens, to help the operator in monitoring the following sensors: Communications, Echo Sounder, Fire Doors, GPS, Hull Openings, Hull Stress, Radar, ship speed, level of tank Fuel, Temperature, Wind Speed, and the basic window VDR. Figure 2 shows the VDR window.

FIG. 2 VOYAGE DATA RECORDER

Moving among screens takes place through the main screen. Choose what sensor you need.

Figure 3 shows the communication screen, which can detect the voice call between the ship crew.

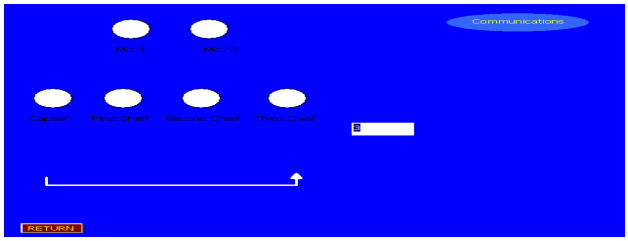

FIG. 3 COMMUNICATION WINDOW

FIG. 4 FIRE DOOR WINDOWS

Figure 4 shows fire alarm status. The screen contains three sections; each one has three indication levels. The first level ranges from 1 to 40, which is considered to be safe. The second level ranges from 41 to 70, which indicates the smoking level. The third level ranges from 71 to 100, indicating the danger level.

Figure 5 shows the Echo Sounder screen. It will be the depth under the keel of ship using acoustic technology.

FIG. 5 ECHO SOUDER WINDOW

Figure 6 shows the GPS screen, which indicates the current location of the ship based on the longitude and latitude.

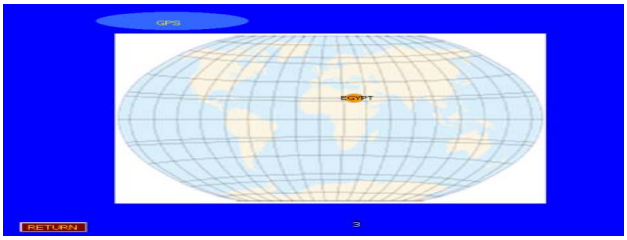

FIG. 6 GPS WINDOW

Figure 6 shows the Hull Opening screen, which indicates the current water level on the sides of the ship that inform user the stability status

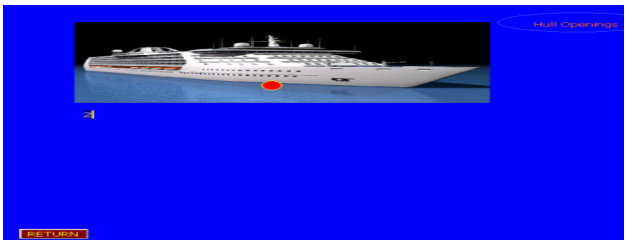

FIG. 7 HULL OPENINGS WINDOW

Figure 8 shows the Hull Stress screen, which indicates the current ship weight and the extra weight

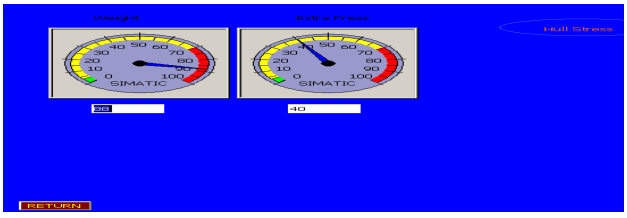

FIG. 8 HULL STRESS WINDOW

Figure 9 shows the Radar screen, which will detect the moving and fixed targets nearby the ship.

Figure 10 shows the ship Speed screen used to displays the current speed of the ship and the direction of movement.

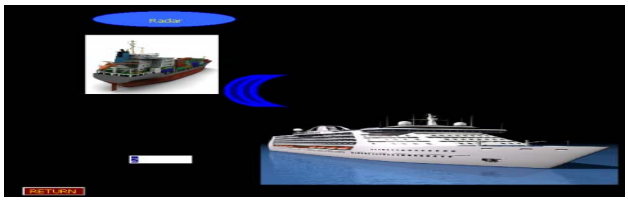

FIG. 9 RADAR WINDOW

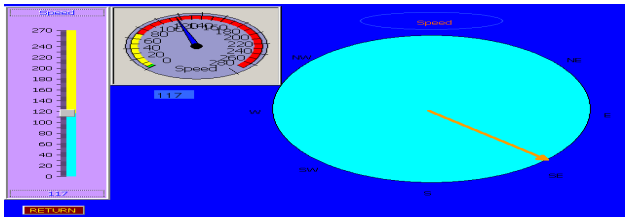

FIG. 10 SHIP SPEED WINDOW

Figure 11 shows the Tank Fuel screen, which detects the fuel level in the fuel tank

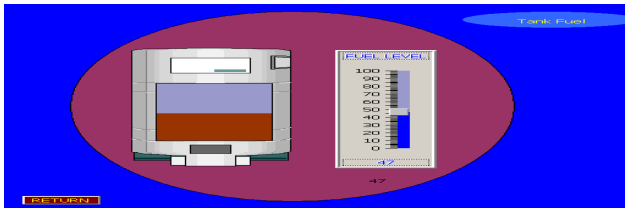

FIG. 11 TANK FUEL WINDOW

Figure12 shows the Temperature screen, which displays the internal and external temperature of the ship.

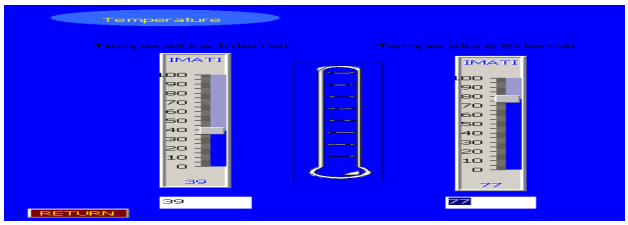

FIG. 12 TEMPERATURE WINDOW

Figure 13 shows the Wind Speed screen, which indicates the speed of the wind and its direction.

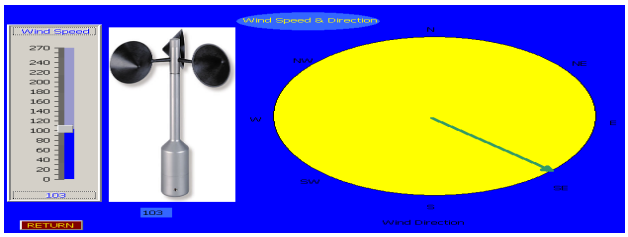

FIG. 13 WIND SPEED AND DIRECTION WINDOW

All the previous screens are considered as the HMI (Human Machine Interface) of the SCADA system monitoring a group of sensors, which can help the operator in the control room to make online control on ship control system.

Summary

The offered designed SCADA is Supervisory Control and Data Acquisition. SCADA systems are used to monitor and control a ship or equipment in industries such as water and waste water control, energy, oil, telecommunications and gas refining and transportation. These systems encompass the transfer of data between a SCADA central host computer and a number of Remote Terminal Units RTUs and/or Programmable Logic Controllers PLCs, as well as the central host and the operator terminals. A SCADA system gathers information, transfers the information back to a central site, then alerts the home station that a leak has occurred, carrying out necessary analysis and control, and displaying the information in a logical and organized fashion. These systems can be relatively simple, such as one that monitors environmental conditions of a small ship, or very complex, such as a system that monitors all the activity in large ship system. Traditionally, SCADA systems have made use of the Public Switched Network (PSN) for monitoring purposes.

REFERENCES

Castine, "Illustration of Variation" Maine Maritime Academy, MA, Sept 8, 2003.

Department of Energy http://www.doe.gov/engine/content.

Hatem Khater, M. S. Zaghloul," Acoustic Targets Identification Using Hybrid Classifier", ICCTA, 2009, 17-19 October 2009, Alexandria, Egypt.

http://www.amimarine.net Parham Drive, "AMI - GFV MARINE Ltd", Eastleigh, Southampton, SO50 4NU UK,

http://www.titanicinquiry.org/BOTInq/BOT01.html.

International convention for the safety of life at sea (SOLAS)", International maritime organization, December 2000

M. S. Zaghloul, "Replay Software of Voyage Data Recorder for Real Marine Accident", ICCTA 2009. Alexandria, Egypt, 17-19 October 2009.

NATIONAL TRANSPORTATION SAFETY BOARD, Office of Research and Engineering, 20594, 8 March 2007 Washington, D.C.

Newton-Evans Research Company, June 2003, Worldwide Market Survey of SCADA, Energy Management Systems and Distribution Management Systems in Electrical Utilities, vol,1Noth America Market 2003-2005.

Office of the Manager, National Communications System, October 2004 By Communication Technologies, Inc.14151 New brook Drive, Suite 400 Chantilly, Virginia 20151,

703-961-9088 (Voice) 703-961-1330 (Fax) www. comtechnologies.com.

Wreck Commissioners' Court Proceedings, Titanic Inquiry Project, 5 Sept 2003.

DOI: 10.14355/ijcsa.2014.0301.03

Applying CAD for Multi Sensors in Voyage Data Recorder

M. S. Zaghloul

Arab Academy for Science, Technology, and Maritime Transport, Electronic and Communication Department, P.O.1029, Alex, Egypt

dr_mszaghloul@yahoo.com

Abstract

This paper is a practical design and implementation of software developed to enhance the best use of the VDR. This software uses visual basic 6.0, and consists of VDR home page, and has a system configuration, operation, operation procedure, and operation in remote alarm panel, removing VDR and release of DRU. It was tried to comply with International Maritime Organization (IMO) regulations. The system displayed information integrates position information from the Global Positioning System (GPS) and other navigational systems, such as Radar, echo sounder, gyrocompass, day and night cameras etc; as well as additional navigation-related information, such as Sailing Directions. This project has a general background about all inputs to VDR, and concerned with the different inputs to this system such as GPS, Radar, Echo Sounder and Gyrocompass. It was demonstrated that the program deals with VDR, all interfaces with Rader, GPS, Speed log, etc. The software was preferred for design using visual basic 6.0. This program is a window based Software. Moreover, both the flow chart and the program steps are shown. (Browning et al, 2007; John Bell, 2008; Department of transportation, 2001)

Keywords

IMO; SOLAS; Ship Control; Signal Processing; Sensors; Voyage Data Recorder (VDR)

Introduction

In this research, software developed to enhance the best use of the VDR used visual basic 6.0, and consisted of VDR home page as shown in Fig. 1 as follow:

FIG. 1 SAMPLE SCREEN SHOT OF THE VDR HOME PAGE

To login the system and enter the password as shown in Fig. 2

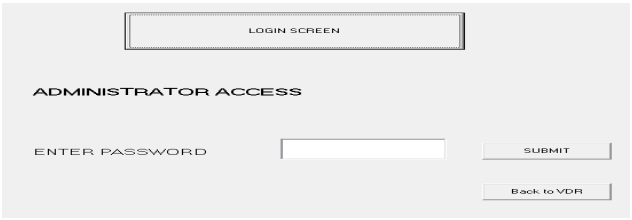

FIG. 2 SAMPLE SCREEN SHOT OF THE VDR LOGIN PAGE

System includes network setup page that has current and new volume as shown in Fig. 3 as follow:

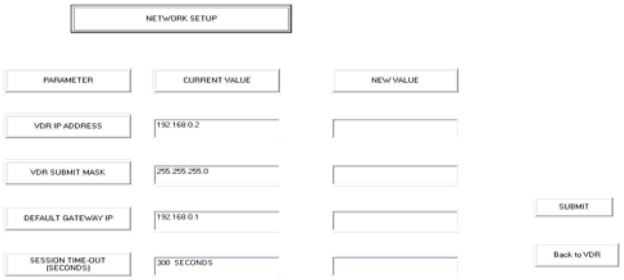

FIG. 3 SAMPLE SCREEN SHOT OF THE VDR NETWORK SETUP PAGE

This system has VDR device update page that updates device allocations and stream names as shown in Fig. 4

FIG. 4 SAMPLE SCREEN SHOT OF THE VDR DEVICE UPDATE PAGE

Press on manual, this window will appear as shown in Fig. 5

The software has a system configuration, operation,

operation procedure, and operation in remote alarm panel, removing VDR and release of DRU including: Maintenance (annual refraction, cleaning, software maintenance, software list, checking software, version of system program, checking of software version of RAP, replacing batteries, replacing acoustic beacon, replacing backup VDR, replacing fuses and replacing consumable parts. Trouble shooting: general trouble shooting, error codes and testing display of remote alarm panel, Location of spares and their list. Interface, data sentences and interface circuits.

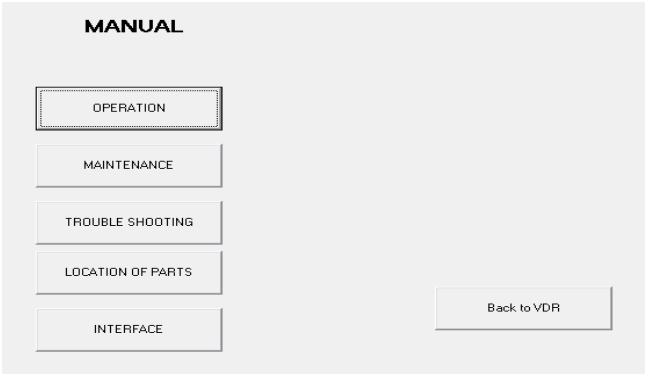

FIG. 5 MANUAL OF SOFTWARE

The Applied Software

Visual Basic (6.0) is used with this applied soft ware. The flow chart of the applied program as shown in appendix (A) and the complete program is available. The program will deal with eighteen sensors as inputs with different data format according to sensor data format, and also this is an open architecture in which a new sensor inputs can be added.

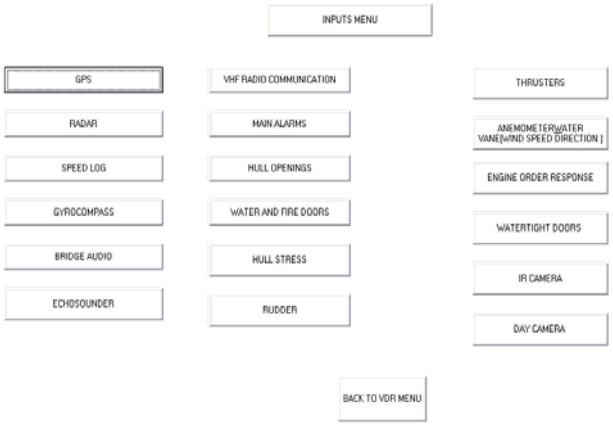

FIG. 6 SENSORS APPEAR ON THIS WINDOW

Replying of Software

This software is used in voyage data recorder in both recording and reply back to obtain the recorded data during the accident events. Press on readings, the following window will appear in Fig. 6 which shows all sensors.

To read any of the sensor data, press the sensor name, so it will appear the data record of this sensor.

GPS data will be appear as shown in Fig. 7

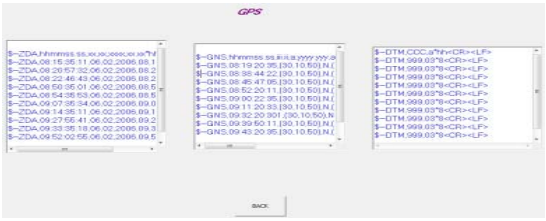

FIG. 7 GPS SENSOR DATA RECORDED

RADAR data will appear as shown in Fig. 8

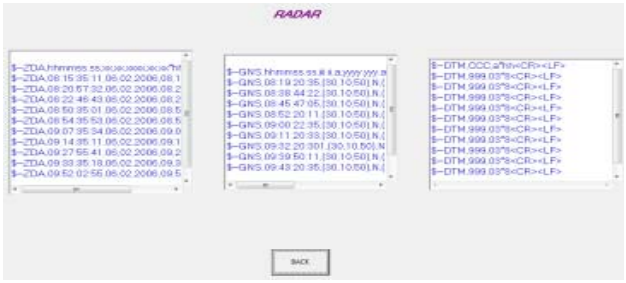

FIG. 8 RADAR SENSOR DATA RECORDED

SPEED LOG data will appear as shown in Fig. 9

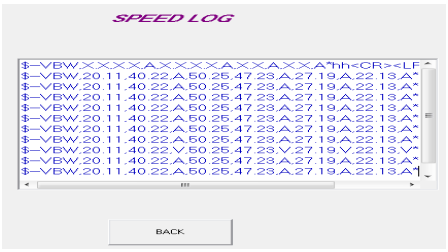

FIG. 9 SENSOR DATA RECORDED

GYROCOMPASS data will appear as shown in Fig. 10

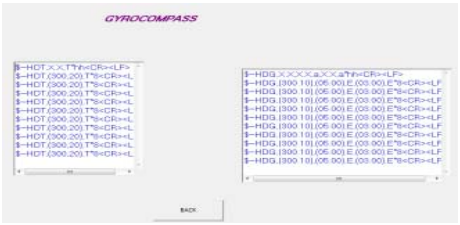

FIG. 10 GYROCOMPASS SENSOR DATA RECORDED

BRIDGE AUDIO: the data will appears shown in Fig. 11 as follow:

FIG. 11 BRIDGE AUDIO SENSOR DATA RECORDED

ECHOSOUNDER data will appear as shown in Fig. 12

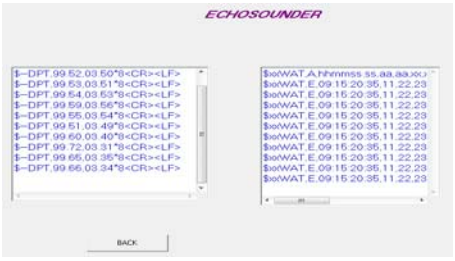

FIG. 12 ECHOSOUNDER SENSOR DATA RECODED

VHF RADIO COMMUNICATION data will appear as shown in Fig. 13

FIG. 13 VHF RADIO COMMUNICATION SENSOR DATA RECORDED

MAIN ALARMS: the data will appear as shown in Fig. 14

FIG. 14 MAIN ALARMS SENSOR DATA RECORDED

HULL OPENINGS data will appear as shown in Fig.15

FIG. 15 HULL OPENINGS SENSOR DATA RECORDED

WATER AND FIRE DOORS data will appear as shown in Fig. 16

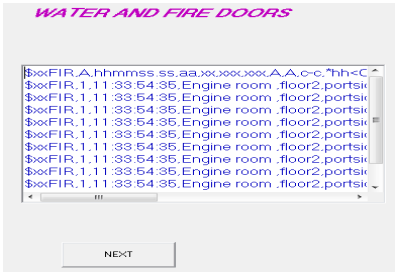

FIG. 16 WATER AND FIRE DOORS SENSOR DATA RECORDED

RUDDER: the data will appear as shown in Fig. 17

FIG. 17 RUDDER SENSOR DATA RECORDED

THRUSTERS: the data will appear as shown in Fig. 18

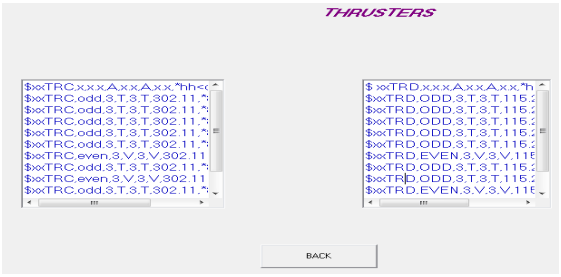

FIG. 18 THRUSTERS SENSOR DATA RECORDED

WIND SPEED DIRECTION: the data will appears shown in Fig. 19

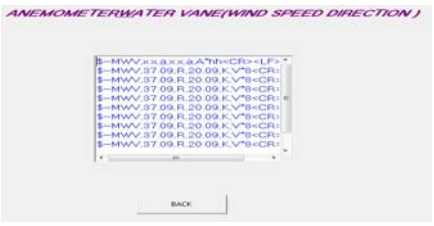

FIG. 19 WIND SPEED DIRECTION SENSOR DATA RECORDED

ENGIN ORDER RESPONSE: the data will appear as shown in Fig. 20

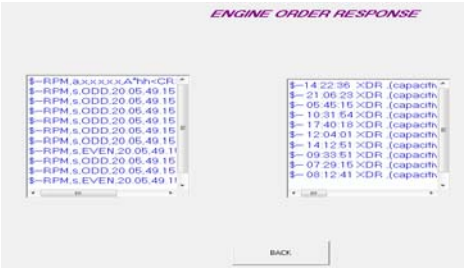

FIG. 20 ENGIN ORDER RESPONSE SENSOR DATA RECORDED

WATERTIGHT DOORS: the data will appears shown in Fig. 21

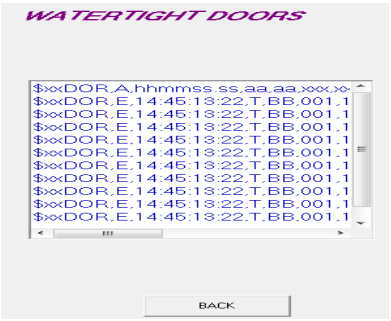

FIG. 21 WATERTIGHT DOORS SENSOR DATA RECORDED

HULL STRESS data will appear as shown in Fig. 22

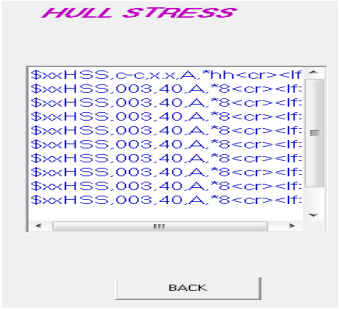

FIG. 22 HULLS STRESS SENSOR DATA RESPONSE

IR CAMERA: the data will appear as shown in Fig. 23 as follow:

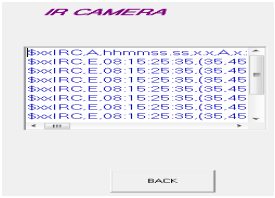

FIG. 23 IR CAMERA SENSOR DATA RECORDED

DAY CAMER data will appear as shown in Fig. 24

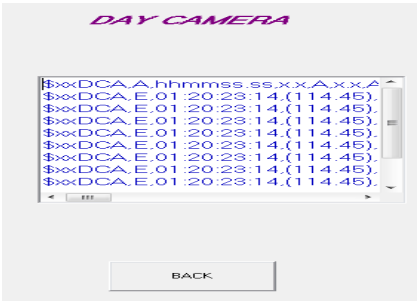

FIG. 24 DAY CAMERA SENSOR DATA RECORDED

The flow chart

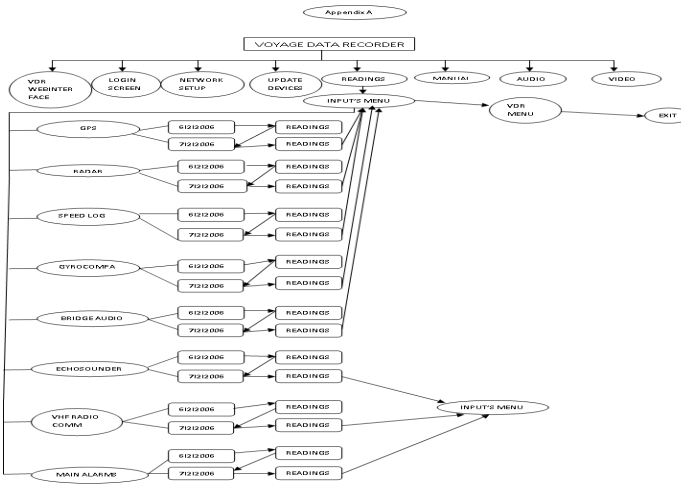

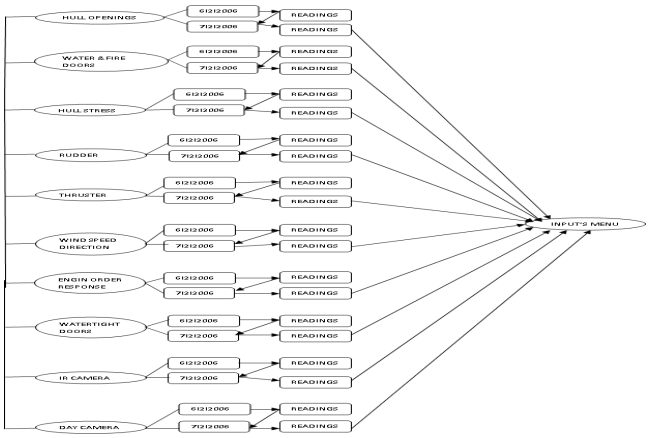

REFERENCES

Bowditch, Nathaniel, "American Practical Navigator: an Epitome of Navigation", Hydrographic Center, 1995".

Browning et al United States Patent, Patent No. US7.208.685B2, Apr. 24, 2007.John Bell, "Basic GPS Navigation .A practical guide to GPS navigation", 2008.

Department of transportation "National highway traffic safety administration event data recorder working group. Washington, DC, US 2001.

Gabauer, DJ Newel, H. Land O'Neill, M. E, "use of event data recorders (EDR) technology for highway crash data analysis", 2004.

Hatem Khater, M. S. Zaghloul, "Acoustic Targets Identification Using Hybrid Classifier", ICCTA, 2009, 17-19 October 2009, Alexandria, Egypt.

M. S. Zaghloul, "Replay Software of Voyage Data Recorder for Real Marine Accident", ICCTA 2009. Alexandria, Egypt, 17-19 October 2009.

"NATIONAL TRANSPORTATION SAFETY BOARD", Office of Research and Engineering, Washington, D.C. 20594, March 8 2007.

Office of the federal register," title 14 aeronautics and space, part 121 operating requirements", federal aviation administration, 2008.

"Wreck Commissioners' Court Proceedings", Titanic Inquiry Project, 5 Sep 2003. http://www.titanicinquiry.org/BOTInq/BOT01.html.

International Journal of Computer Science and Application (IJCSA) Volume 3 Issue 1, February 2014 www.ij-csa.org
DOI: 10.14355/ijcsa.2014.0301.04

Research on the Impact of Interaction Factors on Online Group-buying Sites

Ranzhe Jing

School of Information Management and Engineering, Shanghai University of Finance and Economics
Shanghai, China

jing.ranzhe@mail.shufe.edu.cn

Abstract

With the prosperous development of e-commerce, group-buying on internet becomes also rapidly popular. This article gave an illustration from internal and external influencing factors of group-buying development and analyzed the influencing factors on the development of group-buying sites with the YaAHP system.

Keywords

Online Group-buying; Online Customer; Influencing Factors; Customer Loyalty; YaAHP System

Introduction

Recently, online group-buying has been one of the most popular shopping ways as the development of Internet and e-commerce. Therefore, how to assure the steady development of group-buying sites has become a problem which the operator of sites must pay attention to. Among the current researches, the products of common group-buying are determined by the site and the customers cannot directly determine the type of products he or she could buy currently (Alan and Basu, 1994). And the customer may just follow the trend instead of actual needs. The other influencing factors are very important, especially who buys and whether he will buy are the most important factors for the realization of group-buying. Customer behavior process mainly includes the reorganization of problems, information collection, products evaluation, purchase decisions and behaviors after purchase (Israr et al, 2009). The customers of online group-buying have definite requirements on the name, brand, model, specification, style, color and price. At the same time, they will think twice very sensibly before buying and they are very sensitive about the price of products. However, few scholars directly explored the concrete model of online group-buying from the viewpoint of the nature and influencing factors of online group-buying (Basu, 1994; Wang and Jing, 2011).

This article analyzed the influencing factors of online group-buying, made empirical research on the current domestic mainstream sites based on model research and provided some valuable suggestions for the future development of group-buying sites from the perspective of consumers choosing the sites while buying online and through questionnaire conducted on the consumers of online group-buying.

Factors Analysis

Group-buying is a new thing and a recognized e-commerce model with good development prospects, influenced by internal and external factors.

Internal Influencing Factors

1) Expectations of Buyer

The buyers expect that the price of goods or service will go down with the increase of buyers or purchase in the near future, so they choose to join in group-buying, which comes from the positive retail demand externalities. The nature of group-buying is that the more the buyers are, the lower the price is (Israr et al, 2009; Hean and Xie, 2009). Therefore, during a cycle of group-buying, people who have already joined in the group-buying have positive external effect for consumers who wait and see to buy at a lower buy.

At the same time, the expectations of buyers will have a negative impact on group-buying, leading to uncertainty of online group-buying. Only the reservation price is lower than current price and higher than discounted price of next approaching phrase that the consumers are driven to join in group-buying (Underwood, 2010). Therefore, it is important to take corresponding mechanism to stimulate the expectations of buyers, offset their wait-and-see attitude and strengthen their willing to join in. Only under the premise that some buyers have joined in, can more buyers be attracted to join in and the deadlock is avoided thus contributing to the establishment of group-buying.

2) Zone of Agreement

The existence of zone of agreement enables the realization of dynamic price mechanism. During group-buying, if the zone of agreement is bigger, the simulative effect of price is greater, so it is more likely to stimulate the willingness of buyers to join in so that the purchases meet the conditions for the establishment of group-buying which contributes to its establishment.

3) Discrete Levels of Price

Nowadays, no matter common online shopping or online group-buying, search engine and shopping pages reduce the search cost of consumers and increases the number of searches for commodity information. When consumers search for a commodity and browse same commodity at different prices, the discrete space of price for the commodity increases. If the discrete space is big, it will take consumers more time to search for the price information of commodities and the cost is increasing respectively, therefore, consumers will sense a lower reservation price to make up for their transaction cost (Kim et al, 2008). However, their reservation price will not affect the actual price, on contrary, the price gap between expected and actual price will reduce their willingness to join in group-buying. Therefore, for a commodity, the lower the discrete level of price is, the more likely more buyers are attracted and the higher the success rate of the group-buying is.

4) Degree of Credibility

Online group-buying is influenced by the credit of buyers and sellers at the same time. Just like ordinary established commodity price transactions, the higher the degree of seller's credit is, the bigger success rate the transaction is. The difference is that online group- buying pays more attention to the credit of buyers; that is when group-buying is realized, whether buyers could purchase the commodity or service with the negotiated price (Wang and Jing, 2011). If buyers regret making such decisions and withdraw group-buying unilaterally, the establishing conditions for group-buying is destroyed, the seller cannot provide commodities or service with negotiated price and other consumers cannot obtain corresponding commodities or service. This will result in a great waste of time, material and other sources. And the enthusiasm of the seller and other consumers to join in group-buying again is dampened, which will seriously hinder the development of online group-buying.

5) Online Group-buying Cycle

For buyers and sellers in online group-buying, they all face two major problems of wait and uncertainty before the end of group-buying. The reason for wait is that group-buying takes some time to ensure that sufficient consumers know and visit the page of a group-buying sites and the visitors have access to the pages and their willingness to buy will further affect the price of commodities or service (Jing, 2011). However, the waiting time is too long, the opportunity cost and uncertainty of the realization of group-buying will increase for both buyers and sellers, which will have a negative effect on the buyers.

6) Characteristics of Commodities or Service

The characteristics of different commodities directly determine whether it is suitable for online group-buying. According to the latitude of purchase time and the characteristics of product quality, marketing abroad divides the product into three categories: querying products, experiencing products and trusting products. Therefore, consumers shall spend some time and energy to search the information about the products including cars, houses, and household appliances and so on. Trusting products refers to the products whose quality cannot be judged in a short time until after use for a long time, such as cosmetics and home decorations and so on. Among the three products, the price of querying products on the market is not flexible (Teo and Liu, 2007). It is suitable to buy on a fixed price instead of group-buying. However, for experiencing and trusting products, there is a certain zone of agreement and the elasticity of price is relatively big, therefore, it is suitable for dynamic pricing mechanism of online group-buying.

External Influencing Factors

1) The Development of Online Group-buying

Global online group-buying derives from Groupon U.S. No matter in China, Europe, Japan and the United States, group-buying sites like Groupon are growing very fast with good expansion prospects. Practitioners of world's internet business generally think that online group-buying model will hold a promising development prospect (Underwood, 2010). Therefore, the development trends of global

online group-buying are one of the most important external factors.

2) Situation of Market Competition

Competition will lead to the survival of the fittest, closure of group-buying sites with bad reputation and service level, optimization of sites with good reputation and service level, which will improve general level of entire online group-buying markets. However, when the competition of the market is fierce enough, consumers with same demand who are willing to join in group-buying are limited at the same period. When they face so many sites providing similar products or service, limited demand is dispersed. If a single group-buying site cannot meet the minimum volume, the result is that consumer's satisfaction will go down so that they will give up online group-buying market (Hean and Xie, 2009). The result is that consumer's satisfaction will go down so that they will give up online group-buying market.

3) Level of Economic Development

Online group-buying is a new form of online shopping that requires certain infrastructure (such as computers, broadband, etc.) and income level to support. Therefore, the development trend of a country will also influence the development of online group-buying.

4) 4) Development of E-commerce

Online group-buying is a brand-new model of e-commerce and factors influencing the development of e-commerce will also have an impact on online group- buying. For example, electronic means of payment, logistics, safety of network information and relevant legal environment will have a direct impact on the development of online group-buying (Jing, 2011; Wei, 2011). The higher level the development of e-commerce is, the more conductive to the development of online group-buying is.

Research Model

The method for this research is a combination of reviewing papers and surveying through questionnaire. Since decision-makers for group- buying websites can hardly change the external conditions, the external factors influencing the group-buying websites have been ignored. Then factors affecting the development of group-buying were analyzed from two points of view-Website and service/products.

Convenience, security, design of Interface and credit of the website are supposed to be taken into consideration. From service/products' point of view, the category, price and quality of service or products should be considered. After subdividing the above-mentioned factors and measuring them in different dimensions, we built up the structural model for the factors affecting group-buying online as presented in table 1. The target level aimed at analyzing the importance of factors that influence group-buying online while the rule layer includes convenience, security, design of Interface and credit of the website and category, price and quality of service or products. For those six aspects, after measured by some key questions, sub-rule layers were acquired.

TABLE 1 AFFECTING FACTORS MODEL OF ONLINE GROUP-BUYING

The Importance of the Factors Affecting Online Group-buying	
Convenience and security	Online communication is convenient and timely
	The buying process convenient and efficient
	Good navigation and search engine
	Visit the Web site is quick and easy
	Security guarantee
Interface design	The comments, suggestions and comments can been seen
	Shopping information is easy to find
Reputation	Good after-sale protection mechanism
	Consumers reputation
Service/product range	The diversity of the goods
	To provide appropriate goods and services for customer requirements
	Meet the needs of consumer entertainment, social and other multi-level
Services /products prices	Group-buying certificates are easy to use
Service/product quality	Information objective and true, updated timely
	The quality of goods or services
	Goods or services at lower prices

TABLE 2 AFFECTING FACTORS MODEL OF ONLINE GROUP-BUYING

Criterion	Weights	Adjust the weights	Summary
Visit the Web site is quick and easy	0.0337	3.64%	18.97%
Good navigation and search engine	0.0309	3.34%	
The buying process convenient and efficient	0.0428	4.62%	
Online communication is convenient and timely	0.0383	4.14%	
Security guarantee	0.0299	3.23%	
The comments, suggestions and comments can been seen	0.0889	9.60%	20.51%
Shopping information is easy to find	0.101	10.91%	
Good after-sale protection mechanism	0.0797	8.61%	18.61%
Consumers reputation	0.0926	10.00%	
The diversity of the goods	0.0455	4.91%	13.59%
To provide appropriate goods and services for customer requirements	0.0352	3.80%	
Meet the needs of consumer entertainment, social and other multi- level	0.0451	4.87%	
Group-buying certificates are easy to use	0.0607	6.56%	20.30%
Information objective and true, updated timely	0.0654	7.06%	
The quality of goods or services	0.0618	6.68%	
Goods or services at lower prices	0.0743	8.03%	8.03%
Goods or services at lower prices	0.0743	-	-

Then, judgment matrix can be obtained, the weight of every factor was calculated according to which the weight of rule layer can be calculated. Finally, the importance of factors influencing online group-buying was determined.

Practical Research

The questionnaire was designed based on AHP which makes multiple comparisons in one layer. Number 9, 7, 5, 3, 1 were set to be absolutely important, very important, more important, slightly important and equally important. Sample of our research came from internet, 285 questionnaires were sent back among which 278 are effective.

When YaAHP system was applied to data processing, it was able to get instant consistency ratio of judgment matrix. The sub-rule of price of products/service added was deleted when the model was built up from weights (the second column).

Conclusions

The result obtained from data processing using YaAHP showed that design of interface is the most important factor and its importance takes up 20.51% of all the six factors while quality of product/service takes up 20.3%, convenience and security of website takes up 18.97%, credit is 18.61%, category is 13.59% and price is 8.03%.

According to the analysis above, the online experience of consumers should be taken into consideration, and the interactive experience between websites and consumers should be strengthened. The information of products or service should be complete. The description made by vendor helps form the consumers' expectation for the product/service, which will surely dissatisfy consumers if the description is not appropriate.

ACKNOWLEDGMENT

The research was supported by the National Natural Science Foundation of China (NSFC Program No.71072037) and 211 Project for Shanghai University of Finance and Economics(the 4th phase).

REFERENCES

Dan J. Kim, Donald L. Ferrin, H. Raghav Rao. A Trust-based Consumer Decision-making Model in Electronic Commerce: The Role of Trust, Perceived Risk, and Their Antecedents. Decision Support Systems, Vol 44(2), 544-564, 2008.

Dick Alan, Kunal Basu. Customer Loyalty: Toward an Integrated Conceptual Framework. Journal of Marketing Science, 1994, 22: 100-102.

Israr Qureshi, Yulin Fang, Elaine Ramsey, Patrick McCole, Patrick Ibbotson, Deborah Compeau. Understanding online customer repurchasing intention and the mediating role of trust-an empirical investigation in two developed countries. European Journal of Information Systems. No.18, pp. 205-222,2009.

Jincheng Wang, Ranzhe Jing. Exploring on the Ways to improve Online Customer Loyalty. International Conferenceon Logistics, Informatics and Services Sciences. 38-46, 2011.

Keh Hean, Yi Xie, Corporate Reputation and Customer

Behavioral Intentions: The Roles of Trust, Identification and Commitment, Industrial Marketing Management, vol.7, No. 38, pp.732-742, 2009.

Ranzhe Jing. Online Customer Value Structure: a Network Analysis Approach. International Conference on Intelligent Systems and Knowledge Engineering. 219-226, 2011.

Thompson S. H. Teo, Jing Liu. Consumer Trust in e-commerce in the United States, Singapore and China. Omega, Vol 35(1), 22-38, 2007.

Underwood, R. Groupon versus the world. Inc. Vol 32(8), 116-118. 2010.

Yujie Wei, D. W. Staub, Amit Poddar. The Power of Many: An Assessment of Managing Interent Group Purchasing. Journal of Electronic Commerce Research, Vol 12(1), 19-43, 2011.

DOI：10.14355/ijcsa.2014.0301.05

Spectral Nodal Element Simulation of Conjugate Heat and Mass Transfer: Natural Convection Subject to Chemical Reaction Along A Circular Cylinder

Yifan Wang[1], Don Liu[*2], Haibo Zhang[1]

[1] Mathematics & Statistics, Louisiana Tech University, Ruston, LA 71272, USA

[2] Mathematics & Statistics and Mechanical Engineering, Louisiana Tech University, Ruston, LA 71272, USA

[*2] DonLiu@latech.edu

Abstract

This paper used nodal spectral element method and 4th order Runge-Kutta method to solve the conjugate heat and mass transfer problem coupled with chemical reaction within free convection boundary layer in cylindrical coordinates. The numerical results showed details of this natural convective phenomenon and the accuracy of the algorithm.

Keywords

Spectral Element Method; Runge-Kutta Method; Chemical Reaction; Buoyancy; Boussinesq Approximation; Heat and Mass Transfer; Natural Convection; Boundary Layer

Introduction

Conjugate heat and mass transfer caused by the difference in temperature and concentration between different materials is of importance to engineering. (Hills 1966) and (Bergles and Webb 1970) investigated conjugate heat and mass phenomenon in early 1960s. Later, three theoretical research, (Kearney et. al. 1973); (Chen 1973); and (Nixon 1975) were conducted for engineering applications. Since 1990s, heat and mass transfer through porous mediums has been of interest to researchers and widely researched and applied to industry (Bejan 1993), such as migration of mass and energy through porous media (Lauriello 1974; Nield and Bejan 1998), and transfer of moisture through dehumidifying materials (Oliveira et. al. 1994; Zhang et. al. 2012; Defraeya et. al. 2012). Conjugate heat and mass transfer involving vertical cylinders has occurred in various engineering areas (Dorfman 1985; Dorfman and Renner 2009), such as heat and mass transfer along a vertical cylinder (Kawala and Odda 2013), solar energy retrieving, food sciences (Nitin and Karwe 2004) and biological materials (Liu et. al. 2004).

The composite phenomenon of heat and mass transfer together with chemical reaction near a free convection boundary layer of a vertical circular cylinder was studied in this paper. Boussinesq approximation was used so that the governing equations were simplified. A high accuracy (both the space and time) simulation model was developed and results were discussed.

Mathematical Description

We considered the problem of a quiescent fluid having chemical reaction with a vertical cylinder that is surrounded by the fluid. The cylindrical surface has variable heat and mass fluxes. Using the Boussinesq approximation and boundary layer approximation (Kundu and Cohen 2008), the governing equations in cylindrical coordinates are given as below:

$$\frac{\partial(ru)}{\partial x}+\frac{\partial(rv)}{\partial r}=0, \tag{1}$$

$$\frac{\partial u}{\partial t^{'}}+u\frac{\partial u}{\partial x}+v\frac{\partial u}{\partial r}= g\beta_T(T^{'}-T_{\infty}^{'})+g\beta_C(C^{'}-C_{\infty}^{'})+\frac{\mu}{r}\frac{\partial}{\partial r}(r\frac{\partial u}{\partial r}), \tag{2}$$

$$\frac{\partial T^{'}}{\partial t^{'}}+u\frac{\partial T^{'}}{\partial x}+v\frac{\partial T^{'}}{\partial r}=\frac{\alpha}{r}\frac{\partial}{\partial r}(r\frac{\partial T^{'}}{\partial r}), \tag{3}$$

$$\frac{\partial C^{'}}{\partial t^{'}}+u\frac{\partial C^{'}}{\partial x}+v\frac{\partial C^{'}}{\partial r}=\frac{D}{r}\frac{\partial}{\partial r}(r\frac{\partial C^{'}}{\partial r})-kC^{'}. \tag{4}$$

In which, μ is viscosity, α is thermal diffusivity, D is mass diffusivity, β_T and β_C are thermal expansion coefficient and concentration expansion coefficient, respectively, k is chemical reaction coefficient. For free convection, the pressure term is substituted by $-g\beta_T T_{\infty}^{'}-g\beta_C C_{\infty}^{'}$ (Rohsenow 1998).

After proper scaling, nondimensionalized equations of

the corresponding equations are given below:

$$R\frac{\partial U}{\partial X}+R\frac{\partial V}{\partial R}+V=0, \tag{5}$$

$$\frac{\partial U}{\partial t}+U\frac{\partial U}{\partial X}+V\frac{\partial U}{\partial R}=\frac{T}{r_0}+\frac{NC}{r_0}+\frac{1}{R}\frac{\partial U}{\partial R}+\frac{\partial^2 U}{\partial R^2}, \tag{6}$$

$$\frac{\partial T}{\partial t}+U\frac{\partial T}{\partial X}+V\frac{\partial T}{\partial R}=\frac{1}{\Pr R}\frac{\partial T}{\partial R}+\frac{1}{\Pr}\frac{\partial^2 T}{\partial R^2}, \tag{7}$$

$$\frac{\partial C}{\partial t}+U\frac{\partial C}{\partial X}+V\frac{\partial C}{\partial R}=\frac{1}{ScR}\frac{\partial C}{\partial R}+\frac{1}{Sc}\frac{\partial^2 C}{\partial R^2}-kC. \tag{8}$$

Where U and V are the axial and the radial velocity, respectively; T is temperature; C is concentration; r_0 is the radius of the cylinder; Pr is the Prandtl number; Sc is Schmidt number; and N is the coefficient of buoyancy ratio of temperature over concentration. Mathematically, this problem is well-posed and subject to the below initial and boundary conditions:

1). Initially, all variables U,V,T,C are set to be zero.

2). On cylindrical surface

$$t>0: U=0, V=0, q_T=\lambda\frac{\partial T}{\partial R}=-X^{0.5}, q_C=D\frac{\partial C}{\partial R}=-X^{0.5}$$

3). $U=0, T=0, C=0$ at $X=0, R>R_0$

4). $U\to 0, T\to 0, C\to 0$ as $R\to\infty$

Numerical Approach

Spatial Discretization

Galerkin projection in space to Equs. (5)-(8) was used to obtain the variational forms and spectral element discretization was used in space. An arbitrary element denoted as "e" in the cylindrical coordinates, was mapped to a standard element in ξ_0 and ξ_1, both ranging from -1 to 1. Particularly, for the solution of U as shown below, it was expanded in terms of a tensor product of two one-dimensional Lagrangian basis functions. Each of the basis function is denoted as h on quadrature points which are zeros of Legendre polynomials

$$U^e(\xi_0,\xi_1)=\sum_{p}^{Po}\sum_{q}^{Po}U^e_{pq}h^e_p(\xi_0)h^e_q(\xi_1)=\sum U^e_{pq}\Phi^e_{pq} \tag{9}$$

Where, Po is the highest polynomial order of the basis functions. Because of the collocation property of the nodal spectral element method, coefficients U^e_{pq} in above equation are the numerical solutions at those quadrature points. The test function in a standard element is chosen to be the same as basis functions.

$$\Psi^e_{rs}=\sum_{r}^{Po}\sum_{s}^{Po}h^e_r(\xi_0)h^e_s(\xi_1) \tag{10}$$

Using the Galerkin projection, the weak forms of Equs. (5)-(8) can be obtained. We used the following short notations for particular matrices.

The global mass matrix:

$$\underline{\underline{M}}=\sum_{e}^{Total}\left[\int_{\Omega_e}\Phi^e_{pq}\Psi^e_{rs}\left|J\right|_e d\xi_0 d\xi_1\right] \tag{11}$$

The global advection matrix:

$$\underline{\underline{Adv_X}}=\sum_{e}^{Total}\left[\int_{\Omega_e}(\Phi^e_{pq})'_{\xi_0}\Psi^e_{rs}(\frac{2}{L_R})\left|J\right|_e d\xi_0 d\xi_1\right] \tag{12}$$

$$\underline{\underline{Adv_R}}=\sum_{e}^{Total}\left[\int_{\Omega_e}(\Phi^e_{pq})'_{\xi_1}\Psi^e_{rs}(\frac{2}{L_X})\left|J\right|_e d\xi_0 d\xi_1\right] \tag{13}$$

The global Laplacian matrix:

$$\underline{\underline{K}}=\sum_{e}^{Total}\left[\begin{array}{l}\int_{\Omega_e}(\Phi^e_{pq})'_{\xi_0}(\Psi^e_{rs})'_{\xi_0}\frac{L_X}{L_R}d\xi_0 d\xi_1\\ +\int_{\Omega_e}(\Phi^e_{pq})'_{\xi_1}(\Psi^e_{rs})'_{\xi_1}\frac{L_R}{L_X}d\xi_0 d\xi_1\end{array}\right] \tag{14}$$

Where J is the Jacobian for the transformation in the typical element "e". In our simulation, in the element "e", L_X is the length in X and L_R is the length in R.

Temporal Discretization

At the initial time step, values of U_0, V_0, T_0, and C_0 were initialized to zero. Equs. (6)-(8) was treated as a system of initial-value problem by moving the convective terms on the left hand side to the right hand side of the equations. Then 4th order Runge-Kutta method in time was used to solve the system of ordinary differential equations. Let k_{1U}, k_{1T}, and k_{1C} stand for coefficients of the 4th order Runge-Kutta method, in the first stage. Then we have:

$$\begin{aligned}\underline{\underline{M}}k_{1U}=\Delta t\Big[&-U_0.*(\underline{\underline{Adv_X}}U_0)-V_0.*(\underline{\underline{Adv_R}}U_0)+\underline{\underline{M}}\frac{T_0}{r_0}\\&+\underline{\underline{M}}\frac{NC_0}{r_0}+\frac{1}{R}(\underline{\underline{Adv_R}}U_0)+\underline{\underline{M}}U_X\Big|_\Omega-\underline{\underline{K}}U_0\Big]\end{aligned} \tag{15}$$

$$\begin{aligned}\underline{\underline{M}}k_{1T}=\Delta t\Big[&-U_0.*(\underline{\underline{Adv_X}}T_0)-V_0.*(\underline{\underline{Adv_R}}T_0)\\&+\frac{1}{\Pr R}(\underline{\underline{Adv_R}}T_0)+\frac{1}{\Pr}\underline{\underline{M}}T_X\Big|_\Omega-\frac{1}{\Pr}\underline{\underline{K}}T_0\Big]\end{aligned} \tag{16}$$

$$\begin{aligned}\underline{\underline{M}}k_{1C}=\Delta t\Big[&-U_0.*(\underline{\underline{Adv_X}}C_0)-V_0.*(\underline{\underline{Adv_R}}C_0)\\&+\frac{1}{ScR}(\underline{\underline{Adv_R}}C_0)+\frac{1}{Sc}\underline{\underline{M}}C_X\Big|_\Omega-\frac{1}{Sc}\underline{\underline{K}}C_0-k\underline{\underline{M}}C_0\Big]\end{aligned} \tag{17}$$

Where, Ω represents the boundary of the problem. The intermediate value of V_i was computed from the value of U_i in the below equation:

$$(\underline{\underline{Adv_R}}+\frac{\underline{\underline{M}}}{R})V_i=\underline{\underline{Adv_X}}U_i \tag{18}$$

where U_i was computed from U_0+k_{iU}. Then, k_{1V} was computed from $V_i - V_0$. To compute the values of k_{2U}, k_{2T}, k_{2C}, we used the following equations:

$$\underline{\underline{M}}k_{2U} = \Delta t\begin{bmatrix} -(U_0+\frac{1}{2}k_{1U}).*[\underline{\underline{Adv_X}}(U_0+\frac{1}{2}k_{1U})] \\ -(V_0+\frac{1}{2}k_{1V}).*[\underline{\underline{Adv_R}}(U_0+\frac{1}{2}k_{1U})] \\ +\underline{\underline{M}}\frac{(T_0+\frac{1}{2}k_{1T})}{r_0}+\underline{\underline{M}}\frac{N(C_0+\frac{1}{2}k_{1C})}{r_0} \\ +\frac{1}{R}[\underline{\underline{Adv_R}}(U_0+\frac{1}{2}k_{1U})]+\underline{\underline{MU_X}}\Big|_\Omega \\ -\underline{\underline{K}}(U_0+\frac{1}{2}k_{1U}) \end{bmatrix} \quad (19)$$

$$\underline{\underline{M}}k_{2T} = \Delta t\begin{bmatrix} -(U_0+\frac{1}{2}k_{1U}).*[\underline{\underline{Adv_X}}(T_0+\frac{1}{2}k_{1T})] \\ -(V_0+\frac{1}{2}k_{1V}).*[\underline{\underline{Adv_R}}(T_0+\frac{1}{2}k_{1T})] \\ +\frac{1}{\Pr R}[\underline{\underline{Adv_R}}(T_0+\frac{1}{2}k_{1T})]+\frac{1}{\Pr}\underline{\underline{MT_X}}\Big|_\Omega \\ -\frac{1}{\Pr}\underline{\underline{K}}(T_0+\frac{1}{2}k_{1T}) \end{bmatrix} \quad (20)$$

$$\underline{\underline{M}}k_{2C} = \Delta t\begin{bmatrix} -(U_0+\frac{1}{2}k_{1U}).*[\underline{\underline{Adv_X}}(C_0+\frac{1}{2}k_{1C})] \\ -(V_0+\frac{1}{2}k_{1V}).*[\underline{\underline{Adv_R}}(C_0+\frac{1}{2}k_{1C})] \\ +\frac{1}{ScR}[\underline{\underline{Adv_R}}(C_0+\frac{1}{2}k_{1C})]+\frac{1}{Sc}\underline{\underline{MC_X}}\Big|_\Omega \\ -\frac{1}{Sc}\underline{\underline{K}}(C_0+\frac{1}{2}k_{1C})-k\underline{\underline{M}}(C_0+\frac{1}{2}k_{1C}) \end{bmatrix} \quad (21)$$

Procedures similar to Equs. (19)-(21) were performed to compute k_{3U}, k_{3T} and k_{3C}; while, k_{4U}, k_{4T} and k_{4C} were computed from the following equations:

$$\underline{\underline{M}}k_{4U} = \Delta t\begin{bmatrix} -(U_0+k_{3U}).*[\underline{\underline{Adv_X}}(U_0+k_{3U})] \\ -(V_0+k_{3V}).*[\underline{\underline{Adv_R}}(U_0+k_{3U})] \\ +\underline{\underline{M}}\frac{(T_0+k_{3T})}{r_0}+\underline{\underline{M}}\frac{N(C_0+k_{3C})}{r_0} \\ +\frac{1}{R}[\underline{\underline{Adv_R}}(U_0+k_{3U})]+\underline{\underline{MU_X}}\Big|_\Omega \\ -\underline{\underline{K}}(U_0+k_{1U}) \end{bmatrix} \quad (22)$$

$$\underline{\underline{M}}k_{4T} = \Delta t\begin{bmatrix} -(U_0+k_{3U}).*[\underline{\underline{Adv_X}}(T_0+k_{3T})] \\ -(V_0+k_{3V}).*[\underline{\underline{Adv_R}}(T_0+k_{3T})] \\ +\frac{1}{\Pr R}[\underline{\underline{Adv_R}}(T_0+k_{3T})]+\frac{1}{\Pr}\underline{\underline{MT_X}}\Big|_\Omega \\ -\frac{1}{\Pr}\underline{\underline{K}}(T_0+k_{3T}) \end{bmatrix} \quad (23)$$

$$\underline{\underline{M}}k_{4C} = \Delta t\begin{bmatrix} -(U_0+k_{3U}).*[\underline{\underline{Adv_X}}(C_0+k_{3C})] \\ -(V_0+k_{3V}).*[\underline{\underline{Adv_R}}(C_0+k_{3C})] \\ +\frac{1}{ScR}[\underline{\underline{Adv_R}}(C_0+k_{3C})]+\frac{1}{Sc}\underline{\underline{MC_X}}\Big|_\Omega \\ -\frac{1}{Sc}\underline{\underline{K}}(C_0+k_{3C})-k\underline{\underline{M}}(C_0+k_{3C}) \end{bmatrix} \quad (24)$$

After all coefficients of four stages of Runge-Kutta scheme were determined, the value of U at the next time level could be calculated from the following fomula:

$$U_1 = U_0 + \frac{1}{6}(k_{1U}+2k_{2U}+2k_{3U}+k_{4U}). \quad (25)$$

Using the similar formula, values of T and C can be computed. V was calculated from Equ. (18).

Numerical Approach

Before discussing the simulation results, we first performed temporal and spatial convergence tests to ensure the consistency of our algorithm. Fig. 1 shows the results of temporal convergence test. The domain of computation was discretized into 20 elements, and 6th order Lagrangian polynomials were used as basis function. A 4th order temporal convergence was achieved by varying the time step from 0.0000125, 0.000025, 0.00005, to 0.0001. Result agreed well with theoretical expectation, because the 4th order Runge-Kutta method was used in all temporal derivatives.

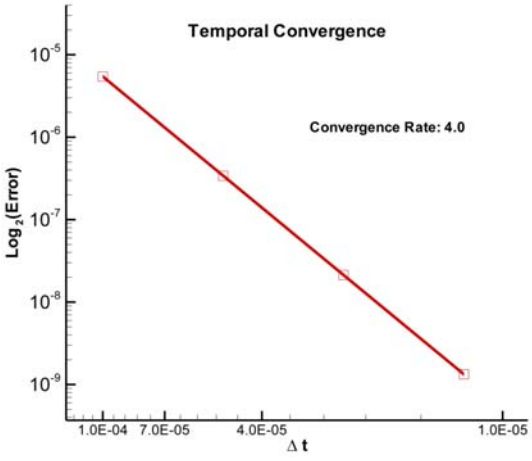

FIG. 1 TEMPORAL CONVERGENCE

Fig. 2 illustrates the exponential convergence in space. By increasing the polynomial order of basis functions, the L_2 norm of nodal errors decreased exponentially. Spatial and temporal convergence indicated that our algorithm is consistent and stable. Fig. 3 and Fig. 4 present the numerical results of the free convection conjugate heat and mass transfer with chemical reaction around a vertical cylinder. The left plot of Fig. 3 shows the mesh used for the computation. A total of 20 elements was used and 8th order basis functions in

each direction and each element were adopted. The right plot of Fig. 3 is the velocity profile of U. At the cylinder surface the velocity is equal to zero and a boundary layer is formed near the cylinder surface. Velocity increased in the boundary layer and then decreased away from the cylinder surface due to subsided driving force – buoyancy and concentration difference.

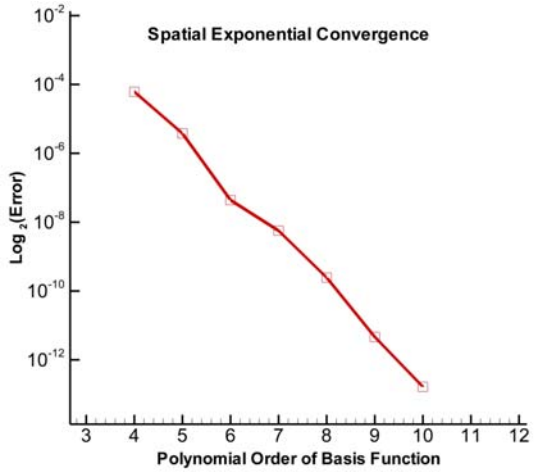

FIG. 2 SPATIAL CONVERGENCE

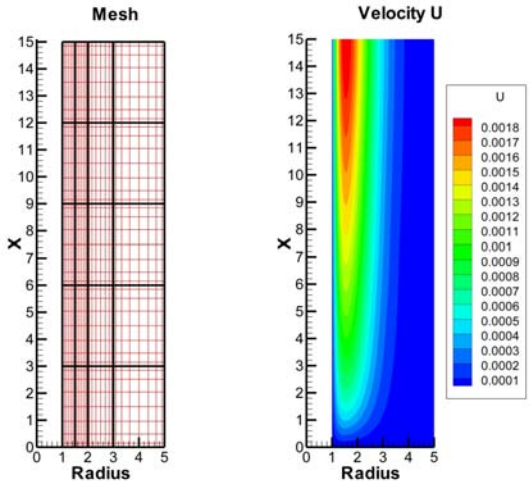

FIG. 3 MESH AND CONTOUR OF VELOCITY U

Fig. 4 reveals the distribution of temperature (left) and concentration (right) from the cylindrical surface to the far away region. It can be seen that the major variation of temperature and concentration happens within the free convection boundary layer, as expected from the boundary layer theory (Kundu and Cohen 2008). In the simulation, Sc=0.7 and Pr=7.0, which assumes mass diffusion rate is larger than thermal diffusion rate. Therefore, the thickness of mass boundary layer is greater than the thickness of thermal boundary layer. Fig. 5 presents the vector field of the fluid velocity. For a better visual effect, the enlarged bottom portion of the whole domain with X chosen from 0 to 6 was shown. Fig. 5 indicates that the fluid rises naturally from the bottom to the top due to the uneven heat and mass flux specified in boundary conditions. We have attempted a variety of different setting. Due to limited space in the paper, we could not present all.

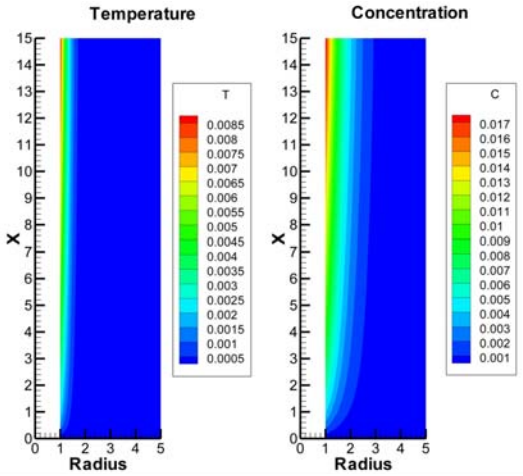

FIG. 4 CONTOUR OF TEMPERATURE AND CONCENTRATION

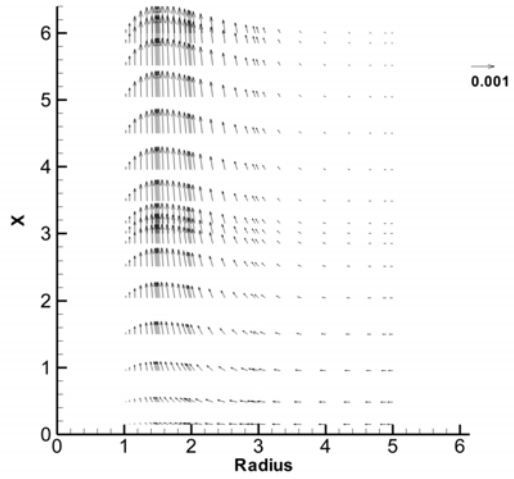

FIG. 5 LOCAL VELOCITY PROFILE

Conclusions

Conjugate heat and mass convection with chemical reaction around a vertical cylinder was modelled with a nodal spectral element method and 4th order Runge-Kutta method in time. Results indicated good accuracy and field details. This algorithm helped understand the complex phenomenon with conjugated heat, mass transfer and chemical reaction.

Appendix (Nondimensionalization)

Within the boundary layer, the radius of the cylinder r_0 was chosen as the length scale, and the diffusive velocity scale, $\mu/(\rho r_0)$ is chosen to be the velocity scale. We summarize these scaling as below:

$$X = \frac{x}{r_0},\ R = \frac{r}{r_0},\ U = \frac{\rho u r_0}{\mu},\ V = \frac{\rho v r_0}{\mu},\ t = \frac{\mu t'}{\rho r_0^2},$$

$$T = \frac{(T^{'} - T_{\infty}^{'})\lambda}{q_T},\ T = \frac{(C^{'} - C_{\infty}^{'})D}{q_C},\ \Pr = \frac{\mu}{\rho\alpha},$$

$$Sc = \frac{\mu}{\rho D},\ N = \frac{\beta_C q_C \lambda}{\beta_T q_T D}.$$

Where q_T and q_C are heat and mass fluxes.

ACKNOWLEDGMENT

This study was funded by National Science Foundation grants DMS-1115546 and DMS-1318988.

REFERENCES

Bejan A. "Convection Heat Transfer." 2nd Edition, Wiley, New York, 1993.

Bergles A. E. and Webb. R. L. "Augmentation of Convective Heat and Mass Transfer." Papers presented at the winter annual meeting of The American Society of Mechanical Engineers, New York, Dec. 2, 1970.

Chen C. S. "Simultaneous Heat and Mass Transfer in Convective Drying of Biological Materials." Annales De Technologie Agricole, (1973):165-172.

Defraeya T., Blocken B. and Carmeliet J. "Analysis of Convective Heat and Mass Transfer Coefficients for Convective Drying of a Porous Flat Plate by Conjugate Modelling." International Journal of Heat and Mass Transfer, 55(1-3), 2012.

Dorfman A. S. "Methods of Estimation of Coefficients of Heat Transfer from Nonisothermal Walls." Heat Transfer-Soviet Research, 15(6), 1985: 35–57.

Dorfman A. and Renner Z. "Conjugate Problems in Convective Heat Transfer: Review." Mathematical Problems in Engineering, 2009.

Evans L. B., Reid T. C. and Drake E. M. "Transient Natural Convection in Vertical Cylinder." AIChE Journal, 14(2), 1968: 251-256.

Ganesan P. and Rani H. P. "Transient Natural Convection along Vertical Cylinder with Heat and Mass Transfer." Heat and Mass Transfer, 33(5-6), 1998: 449-455.

Hills A. W. D. "Heat and Mass Transfer in Process Metallurgy." Proceedings of a symposium held by the John Percy Research Group In Process Metallurgy, Imperial College, London, April 1966.

Kawala A. M. and Odda S. N. "Numerical Investigation of Unsteady Free Convection on a Vertical Cylinder with Variable Heat and Mass Flux in the Presence of Chemically Reactive Species." Advances in Pure Mathematics, 3, 2013: 183-189.

Kearney D. W., Kays W. M. and Moffat R. J. "Heat Transfer to a Strongly Accelerated Turbulent Boundary Layer: Some Experimental Results, Including Transpiration." International Journal of Heat and Mass Transfer, 1973, 16(6):1289-1305.

Kundu P. and Cohen I.M, "Fluid Mechancis." 4th Edition, Elsevier Inc., 2008.

Lauriello P. J. "Application of a Convective Heat Source to the Thermal Fracturing of Rock." International Journal of Rock Mechanics and Mining Sciences & Geomechanics Abstracts. 11(2), 1974: 75–81.

Liu Z., Wan R., Muldrew K., Sawchuk S. and Rewcastle J. "A Level Set Variational Formulation for Coupled Phase Change/Mass Transfer Problems: Application to Freezing of Biological Systems." Finite Elements in Analysis and Design, 40(12), 2004: 1641-1663.

Nield D. A. and Bejan A. "Convection in Porous Media." 2nd Edition, Springer, New York, 1998.

Nitin N. and Karwe M. V. "Numerical Simulation and Experimental Investigation of Conjugate Heat Transfer between a Turbulent Hot Air Jet Impinging on a Cookie-Shaped Object." Journal of Food Science, 69, 2004:59-65.

Nixon J. F. "The Role of Convective Heat Transport in the Thawing of Frozen Soils." Canadian Geotechnical Journal Revue Canadienne de Geotechnique, 12(3), 1975: 425-429.

Oliveira L. S., Fortes M. and Haghighi K. "Conjugate Analysis of Natural Convective Drying of Biological Materials." Drying Technology, 12(5), 1994: 1167-1190.

Rohsenow W. M. "Handbook of Heat Transfer." ISBN, 0-07-053576-0, 1998.

Zhang L. Z., Huang S. M. and L. X. Pei "Conjugate Heat and Mass Transfer in a Cross-Flow Hollow Fiber Membrane Contactor for Liquid Desiccant Air Dehumidification." International Journal of Heat and Mass Transfer, 55(25–26), 2012: 8061–8072.

International Journal of Computer Science and Application (IJCSA) Volume 3 Issue 1, February 2014 www.ij-csa.org
DOI：10.14355/ijcsa.2014.0301.06

Adaptive Spread Coefficient-based RBF-NN for Complex Signals Modeling

Yibin Song*[1], Zhenbin Du[2]

School of Computer Science, Yantai University, Shandong, China

*[1]syb2874@163.com; [2]zhenbindu@163.com

Abstract

As an efficient method on the fitting or approximating for complex signals, the Radial Base Function Neural Network (RBF-NN) is widely used in signal modeling. During the training process, the spread coefficient (Sc) is one of important parameters in the RBF-NN learning algorithm. A suitable Sc can speed up the signal fitting process. This paper presents an improved RBF-NN learning method based on the adaptive spread coefficient for the signal approximation of complex systems. The improved algorithm is applied to the learning and approximating process of the nonlinear signal. The simulations showed that the presented RBF-NN has good effects on speeding up the training and approaching process. Meanwhile, the learning convergence of the improved algorithm is more excellent than that of normal algorithm.

Keywords

RBF Neural Networks, Adaptive Spread Coefficient, Complex Signals Modelling, Learning Convergence.

Introduction

RBF Neural Network (RBF-NN) is widely used on the fitting or approximating for the complex signals or the model recognition of the nonlinear systems. In RBF - NN, the Radial Base Function is adopted as mapping function. The mapping relation between different layers will be confirmed as soon as the centre point being confirmed. But the linear mapping is applied between hidden layer and output layer, and the weighted linearly sum of hidden layers is used for the output of Neural Network (NN). The linking weights are adjustable parameters of Network. So, the linking weights of network can be evaluated by linear equation sets or by RLS method directly. The learning speed of NN will be more quickly. Meanwhile, the fussy calculation and the local minimizing can be avoided.

The RBF-NN is a typical local approaching network. Only a few weights need to be adjusted for the output of network. Therefore, the RBF-NN could complete the learning process more quickly than that of BP-NN.

Based on the principle of RBF-NN, this paper presents an improved RBF-NN for the signal approximating, which is based on the adaptive spread coefficient. It is also suitable for the identification of the structure-unknown complex signals. An actual signal approximating of a nonlinear model is applied to validate the effects of the improved algorithm. The simulations showed that the presented method has good effects on speeding up the learning process and approximating performance, especially suitable for the real-time request of complex signals modeling.

Improved Algorithm for RBF-NN

RBF-NN Structure Analysis

For the RBF-based Neural Network architecture, direct mapping was adopted between input and hidden layer. But the mapping between hidden layer and output layer adopts the weighted linearly sum of hidden layers as the mapping mode (shown as Fig. 1).

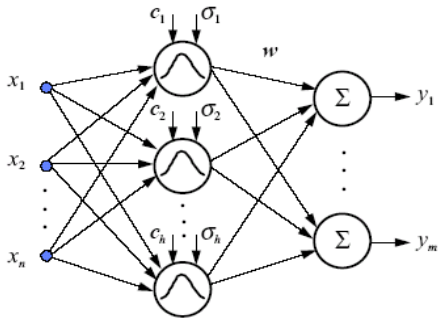

FIG. 1: NORMAL STRUCTURE OF RBF-NN

This structure of NN can reduce the complexity of computational problems so as to speed up the learning process. It is suitable especially for accomplishing the function approaching, model identification and sorting process quickly.

Adaptive-Parameter-Based algorithm for RBF-NN

In RBF-NN, the input vectors of lower dimensions are mapped to the hidden space of higher dimensions at first. The hidden cells selected the base function to realize the vector conversion, and then, sorted or identified by output layer. The form of base function F

can be described as:

$$f(X) = \Lambda_0 + \sum_{j=1}^{M} \Lambda_j \Phi(\|X - C_j\|) \quad (1)$$

Where: $\phi(\| X - X_i \|)$ is the Radial Base Function (RBF).

$\| \bullet \|$ denotes Euclid Norm.

$X \in R^n$, $\Lambda_j \in R^m$ (j=1,2,…… M)

$C_j \in R^n$ is the center of RBF.

$\Lambda_0 \in R^m$ is the constant vector.

Suppose $\Lambda = [\lambda_{mj}]^T$ (j=1,2,…… M), the equation (1) can be re-described as:

$$f_i(X) = \lambda_{i0} + \sum_{j=1}^{M} \lambda_{ij} \Phi(\|X - C_j\|) \quad (2)$$

If Gauss function is adopted as the Radial Base Function (RBF), it can be presented as:

$$\Phi = G(\| X - C_j \|^2) = \exp(-\frac{M}{d_m^2} \| X - C_j \|^2) \quad (3)$$

Where, d_m is the longest distance between the selected centres.

According to the different ways for selection of RBF center, RBF-NN is usually applied the methods as random selection, Self-Organization Learning (SOL) or supervisory learning, etc. This paper applied self-organization learning algorithm to choose the center of RBF so as to complete the network learning. In SOL algorithm, the central position of RBF is set automatically. The weights of output layer can be calculated by error-correction-learning algorithm. So, it is known that the SOL algorithm is a mixed learning algorithm essentially. The function of SOL is to adjust the center of RBF to the key area of input space.

To cluster, least distance is the learning goal of SOL algorithm. The k-mean clustering algorithm was adopted. The input samples were decomposed to M classes and M clustering centres were obtained. The steps of clustering algorithm are:

Step 1: To choose randomly M samples, from the input samples Xj(j=1,2,…,N), as the initial clustering centres Ci (i=1,2,…,M),

Step 2: To distribute input samples Xj（j=1,2,…,N）to every Ci and to form clustering sets θi (i=1,2,…,M). The following condition should be met:

$$d_i = \min_i \| X_j - C_i \| \quad (4)$$

(j=1,2,…,N i=1,2,…,M)

Where d_i is the minimal Euclidean distance.

Step 3: To calculate the sample's mean (i.e. clustering centre ti) in θi:

$$C_i = \frac{1}{M_i} \sum_{X_j \in \theta_j} X_j \quad (5)$$

Where M_i is the number of input sample in θi

Step 4: To repeat above calculation till the change of distribution of clustering centre less than designed value ε is obtained.

Step 5: After the decision of RBF centre, the mean square error $\sigma = d_m / \sqrt{2M}$ can be calculated and then the output of hidden layer is acquired by equation (2).

The Error-Correction-Learning algorithm can calculate the linear weights between hidden and output layer. Suppose that the output of the *k*th neuron of output layer is $\hat{y}_k$ and that of the jth neuron of hidden layer is g_j. The relation is:

$$\hat{y}_k = \sum_j w_{kj} \cdot g_j \quad (6)$$

If the actual output is yk, the error is:

$$\varepsilon_k = y_k - \hat{y}_k$$

The purpose of BP learning is to amend linking weights so as to minimize the error index $E = f(\sum \varepsilon^2_k)$ and to meet the desired performance J. When input mode is $\mathbf{X}_P$, therefore, the correcting value of w_{kj} should be:

$$\Delta_p w_{kj} = -\alpha \frac{\partial E_p}{\partial w_{kj}} \quad (7)$$

Where, α is adjusting factor for learning rate.

The correcting equation is:

$$w_{kj}(k+1) = w_{kj}(k) + \Delta_p w_{kj} \quad (8)$$

In order to improve the convergence of algorithm and its learning effects, a dynamic correcting factor can be set in the correcting equation, that is:

$$w(k+1) = w(k) + \alpha[(1-\eta)T(k) + \eta T(k-1)] \quad (9)$$

where, $0<\alpha<1$, $0 \le \eta < 1$ is a dynamic factor and $T(k) = -\partial E / \partial w(k)$ is the direction of negative grads in the kth time learning.

However, simulations showed that this method is not perfect to improve the learning process. The key question is how to select the learning rate. Sometimes, it is a very difficult decision for the algorithm. The difficulty is how to give attention to both the learning speed and the convergence of algorithm. If a rate-adaptive factor δ(k) is used in the learning algorithm,

the learning performance can be improved significantly. The improved equation is described as equation (10). Where, λ= Sign [T(k)T(k-1)] is the direction of grads, δ(k) is the adaptive factor associated with learning error ε.

$$\begin{cases} w(k+1) = w(k) + \alpha(k)T(k) \\ \alpha(k) = \delta(k)\alpha(k-1) \\ \delta(k) = \varepsilon \cdot 2^{\lambda} \end{cases} \quad (10)$$

The spread coefficient (Sc) is one of important parameters in the RBF-NN learning algorithm. The different decision of Sc will affect the learning performance directly. In fact, a suitable Sc can speed up the signal fitting process obviously. This paper presented an improved RBF learning method based on the adaptive spread coefficient for the signal approximation of complex models. The adaptive spread coefficient is described as:

$$Sc = Sc + \eta \cdot (e^{\zeta} - 1) \quad (11)$$

Where, $\zeta = \left| \max(err) - err^* \right|$,

η is fitting factor,

err*≤0.0001 is the desired learning error.

In order to get a suitable spread factor, the relative error of learning ζ has been introduced into the training algorithm. The value of Sc can be modified adaptively with the training errors. Simulations showed that the amended algorithm can improve the training performance and simplify the structure of neural network satisfactorily.

Simulations

According to the characteristic of RBF-NN, RBF-NN was employed to identify the complex model via learning about the sampled I/O data. For the structure-unknown system, RBF-NN needs to model the unknown object and identify the behaviours of the system by learning the sampling data.

Suppose that the complex model is described as the following equations:

Input:

$$u(k) = 0.25 \cdot [u^2(k-1) - Sin^3(\frac{3k\pi}{97})] \quad (12)$$

Output of the model:

$$y(k) = \frac{[y^2(k-1)+1] \cdot y(k-2) \cdot u^3(k-1) + \exp[u^2(k-2)]}{1 + y^3(k-1)} \quad (13)$$

As an example, 200 pairs and 400 pairs of input data ***u(k)*** and output data ***y(k)*** were sampled respectively as the learning samples. The training results and the learning errors are shown in Fig. 2 ~ Fig. 5.

The simulations showed that the RBF-NN could accomplish the desired signal fitting and model identifying satisfactorily. The desired learning aim had been achieved by the improved RBF-NN with the adaptive Spread coefficient (Sc) only after 155-epoch trainings. It is more speedy and accurate than normal RBF-NN, which needs the trainings for 197 epochs. On the other hand, it means that there are only 155 hidden neurons needed to construct the improved RBF-NN. But the normal RBF-NN needs 197 hidden neurons to get the same training aim. Detail comparing results are shown in table 1.

Simulations showed clearly that the learning effect of improved RBF-NN is much significantly than that of normal RBF-NN, on not only the training speed but also the network structure.

It can be found that the improved RBF-NN is much suitable for the modelling and signal fitting of complex plants or systems. It is also an effective method for the prediction and control of complex systems.

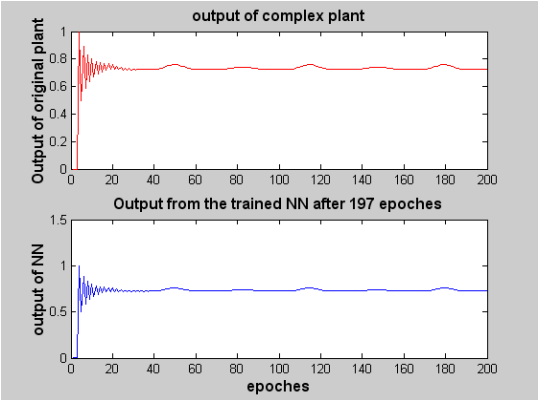

FIG. 2: LEARNING RESULTS OF FIXED SC-BASED RBF-NN

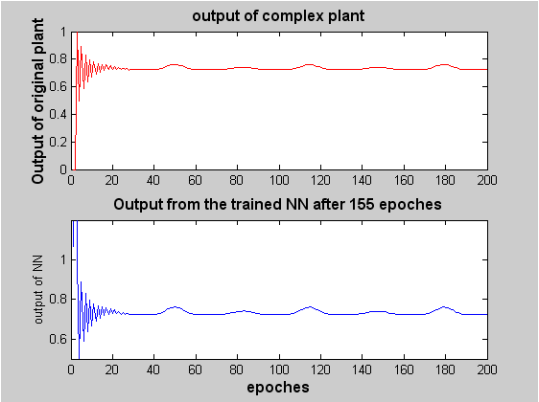

FIG. 3: LEARNING RESULTS OF ADAPTIVE SC-BASED RBF-NN

Conclusions

The outstanding feature of RBF-based Neural

Network are its accurate learning results and quick convergence. This paper has presented an improved algorithm for the RBF-NN. After applying to the identification of a typical nonlinear system and simulations, some conclusions can be made.

Although the RBF-NN can take effect on speeding up the learning process, the improved RBF-NN with adaptive Sc has quicker training speed, more simplified network structure and more excellent learning performance. It can improve the modelling and identifying process of complex plants obviously. Therefore, the presented RBF-NN is an effective way for the realization of the real-time control of complex systems.

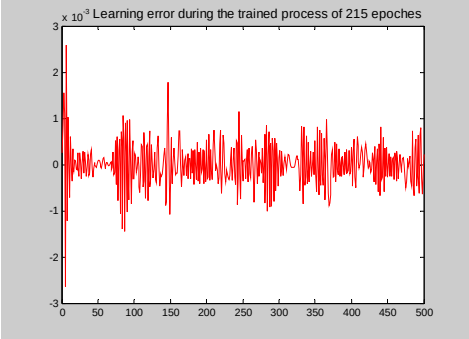

FIG. 4: LEARNING ERRORS OF OF FIXED Sc-BASED RBF-NN

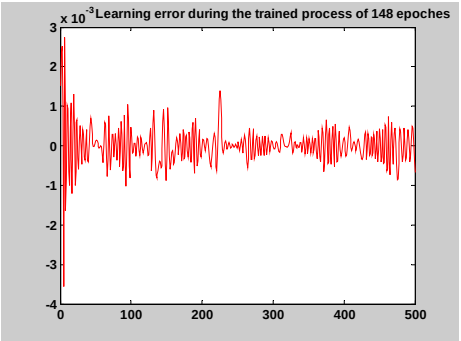

FIG. 5: LEARNING ERRORS OF ADAPTIVE Sc-BASED RBF-NN

TABLE : COMPARISON OF THE LEARNING RESULTS

Training algorithm	Pair of samples	Training epochs	Desired variable of learning error	Mean-Squared Error of NN
RBF-NN	200	197	0.0001	4.32e-3
Improved RBE-NN	200	155	0.0001	4.76e-3
RBF-NN	400	215	0.0001	2.04e-3
Improved RBE-NN	400	148	0.0001	2.85e-3

ACKNOWLEDGMENT

This work was sponsored by National Natural Science Foundation of China (61175053). The first author is the primary contact.

REFERENCES

A. Delgado, C. Kambhampati, K. Warwick. "Dynamic recurrent neural network for system identification and control". IEE Proc. Control Theory Application, 142(6), 1995, 307-314.

Biehl M, Ghosh A, Hammer B. "Dynamics and Generalization Ability of LVQ Algorithms". Journal of Machine Learning Research,8, 2007, 323-360.

Desheng Wu and Liang Liang. "An application of pattern recognition on scoring Chinese corporations financial conditions based on back-propagation neural network". Management Science of China,12 (1),2004. 68-76.

Kosmatopulos E B "high-Order Neural Network Structures for Identification of Dynamical Systems". IEEE Trans. On Neural Networks. 6(2), 1995. 422~ 431.

M. Bianchini, P. Frasconi and M. Gori. "Learning without local minima in radial basis function networks", IEEE Trans. on Neural Networks, 6(3), 1995, 749-756.

Siefkes C, Siniakov P. "An Overview and Classification of Adaptive Approaches to Information Extraction". Journal of Data Semantics. Vol. 4, 2005, 172-212.

Schneider P, Biehl M, Hammer B. "Distance Learning in Discriminative Vector Quantization". Neural Computation. 21(10), 2009, 2942-2969.

Xue zhen-kuang, Li Shao-yuan. "A Multi-Model modeling Approach to MIMO Nonlinear Systems". Acta Electronics Sonia, 33(1). 2005. 52-56.(in Chinese)

Yibin Song. was **b**orn in Anhui, China. Oct. 01, 1957. Graduated in Hefei University of Technology, China, and earned Bachelor's degree in Hefei University of Technology (1982), majoring in industrial automation; Master's Degree in industrial automation in Hefei University of Technology (1988), China.

Up to now, he has worked in the university for 30 years. His research interests include artificial intelligence, machine learning, complex system modeling, etc and has published about 40 academic papers.

At present, Prof. Song is the member of IEEE SMC Society, the Chinese automation society, the Chinese computer society.

Zhenbin Du. PHD, associate professor. Majoring in automation. The member of Chinese automation society. His research interests include intelligent control methods, nonlinear system modeling, etc.

International Journal of Computer Science and Application (IJCSA) Volume 3 Issue 1, February 2014 www.ij-csa.org
DOI: 10.14355/ijcsa.2014.0301.07

A New Path Search Algorithm for Providing Paths among Multiple Origins and One Single Destination

Liang Zhao[1], Wenjia Wang[2]

Hitachi (China) Research & Development Corporation,
301 North Wing Tower C Raycom Infotech Park,
2 KexueyuanNanlu, Beijing, China

[1]lzhao@hitachi.cn; [2]wjwang@hitachi.cn

Abstract

Route planning services provide directional functionalities allowing people to make transport plan in which such services are now closely interrelated to people's daily life. Existing route planners such as digital map sonly offer the path search services originated from one place which cannot fulfill the increasing needs of people. In this paper, we first described a new service for digital map that provides route plans for people from different origins towards the same destination for the purpose of group travelling. Since the performance of route planner highly depends on the shortest path search algorithms, in this paper, weal so introduced our newly proposed path search algorithm, namely, Multi-origins Common Destination algorithm. The initial evaluation results showed that it out performs the counterparts.

Keywords

Group Travel; Route Planning; Multiple Origins

Introduction

Modern lifestyle propels the intensive needs of people's movement, i.e. transportation. Therefore, it is of vital importance for providing navigation or map services to transportation among places, in order to meet the fast-paced life. Nowadays, the popularity and proliferation of navigation technologies and services are growing rapidly and especially used for route planning in densely-populated metropolitan areas. The provisioning of intelligent navigation services to citizens and business has been a strategic objective for organizations and governments worldwide to promote the quality of life. The intelligent route planning technologies provide point-to-point (s) route planning for both public transports and private transports through digital devices such as PC, laptop, smart phone or on-board navigation system etc., which allow users to find the most efficient route with saving up gasoline prior to one's trip or during one's trip. A lot of people like traveling, shopping, or hanging out in a group. While travelling together, a group of friends can first gather in a place from various departure places, then move together to the same destination. This allows participant familiar with the route that can guide others to the destination. Moreover, it also saves gasoline if participants gather in the rendezvous point then drive together towards the destination. However, with regards to such service, there is no existing map service and efficient technology to provide route plans for meeting such needs. In addition, in this context, this problem is to find a rendezvous-point before destination with the total minimized distance of paths on road network. However, existing path search algorithms cannot be applied directly to solve this problem as all of existing algorithms are designed for finding paths originated from single node. Therefore, to address this problem, in this paper, we proposed a new algorithm to find the approximate optimal rendezvous-point and the corresponding routes. The reminder of this paper is organized as following: Section 2 reviews the related work. Section 3 describes the Dijkstra's algorithm and Section 4 introduces the proposed algorithm (MOD). In Section 5, the performance of MOD is evaluated. Finally, Section 6 concludes and directs the future work.

Related Work

In recent years, route planning services and technologies have attracted a lot of research attention. In the service point of view, existing route planning services can be divided into followings, the single-origin-to-single-destination route planning service, and the single-origin-to-multiple-destinations route planning service, which are offered by the major map search engine such as Google Map, and Bing Map for providing driving, public transports, walking and

hybrid transportations. Basically, single-origin-to-single-destination route planning service provides travel route from one origin to one destination. In contrast, the single-origin-to-multiple-destinations route planning service plans the routes from one origin to a final destination through one or multiple waypoints. In the technology point of view, route planning technologies are instances designed to solve the shortest path problem. As a type of shortest path problem, the single-pair shortest path problem is to find the shortest path from one source (origin) to one destination. The algorithms designed for this problem commonly are referred to making the single- origin-to-single-destination route plans in the digital map services.

There is quite a number of existing shortest path search algorithms designed for the single-pair shortest path problem. Among them, Dijkstra's shortest path algorithm is the most commonly known to find the optimal shortest path from one origin to all vertices, while it is also can be used to find the route from one origin to one destination. Bidirectional Dijkstra's algorithm is a variant of Dijkstra's algorithm with improved calculation speed. A Star algorithm, Bidirectional A Star algorithm and the variants etc., are the most popular path search algorithms designed for the single-pair shortest path problem, implemented by major web- based map services to find the approximate shortest path between two nodes due to its low computational time and low memory consumption. These algorithms are heuristics while they estimate the minimum possible distance to the destination end during the calculating. In A Star algorithm, it estimates the distance from the current node (including the origin and all other nodes along the search) to the destination node in order to narrow the search direction and reduce the search complexity. Its bidirectional derivative, i.e. Bidirectional A Star algorithm runs two searches simultaneously, and sets the opposite end-node as the target to estimate the distance, i.e. a search state originated from origin node sets the destination node as the distance estimation target, while the origin node is the destination estimation target for the search state originated from destination node. Existing algorithms for the single-pair shortest path problem cannot provide effective solution to realize the group route planning, i.e. 'the rendezvous-point shortest path problem'-finding of paths from multiple sources to single destination via a common rendezvous-point. Unlike the fixed positions of origin and destination, the location of rendezvous-point is vague until the route search is completed. For this reason, modifications of the heuristic algorithms are required to determine the rough position of rendezvous-point in the starting of the algorithms to estimate the distance to each search end, in order to be applied to solve the rendezvous-point shortest path problem. In contrast, Dijkstra's algorithm and A Star algorithm can be implemented to find the rendezvous-point with some minor modifications. The modified algorithms should calculate the shortest paths from each starting point (including the origins and destination) to rest of vertices on the map, then these paths are compared to get one node with the minimum cost to all starting points where this node is the rendezvous-point. Although the modifications simple and straight forward, the modified algorithms are inefficiency due to its nature of full graph search, which are infeasible for route planning system to handle thousands of multiple queries at the same time.

Deng etal, presents a multi-source skyline query processing scheme for road networks, where as this work focuses on providing the shortest paths from multiple origins to a common destination. Compared to the objective of proposal in this paper, the work is only designed to find the paths from multiple origins to the same destination where the paths are not through a common rendezvous-point for allowing participators to meet before moving towards the destination.

In order to provide efficient route search algorithm for the group travel planning system, we proposed new algorithm where the detailed algorithm is describe in Section 4. To better understand MOD, the basic computing process of Dijkstra's algorithm has been described which can in Section 3.

Dijkstra's Algorithm

A road network can be defined as a graph $G = (E, V)$, where V is a set of nodes corresponding to road junctions and E is a set of non-directional edges (an edge can be either a straight line or a polyline) between two nodes from V corresponding to road segments. If two nodes in V are linked as an edge in E, then they are adjacent to each other. All the adjacent nodes of $v \in V$ are stored in set U. Let $d(v, v')$ be the total length of the edges along a path (i.e. distance) between the two nodes, v and v'. If v and v' are not connected on any path, then $d(v, v') = \infty$. The shortest distance of path length of the shortest path between v and v' is denoted as $d_s(v, v')$.

Dijkstra's algorithm finds the shortest route from a

given origin node, v_s to a destination node v_d in the graph. During the search, if a shortest path from v_s to a node v' is found, v' will be moved from set U to set S in which S is a set to store all the shortest-path-founded nodes. In the first step of this algorithm, every node $v \in U$ with the distance $d(v_s, v)$ is put into S. Then, the algorithm iterates to replace a node $v \in S$ (if $d(v_s, v)$ is the minimum for all nodes in S), by all the nodes in set U. For example, for each node $v' \in U$, $d(v_s, v')$ is set to $d(v_s,v) + d(v, v')$ if v' has not yet been moved to S or (in case v' in S) the existing estimate of $d(v_s, v')$ is larger than $d(v_s, v) + d(v, v')$. This process terminates when v_d is selected from S while $d_s(v_s, v_d)=d(v_s, v_d)$. If the termination condition is not set as finding the shortest path to v_d, Dijkstra's algorithm then continues to compute the shortest paths from v_s to all other nodes in the graph.

TABLE 1 COMPUTATION PROCESS OF DIJKSTRA'S ALGORITHM

Step	Set S	Set U
1	Move *A* toset *S*, then *S*={*A*}, Shortest paths: *A*->*A*=0 Start search by applying *A* as mid-point	*U*={*B, C, D, E*} Tentative distances: *A*->*B*=6 *A*->(other nodes in *U*)=∞ Find *A*->*C*=3 is the shortest path to *C*. Tentative distances: *A*->*B*=6
2	Move *C* to set *S*, then *S*={*A, C*} Shortest paths: *A*->*A*=0，*A*->*C*=3 Applying *C* as mid-point，and start search from the shortest path of *A*->*C*=3	U={*B, D, E*} Find new path *A*->*C*->*B*=5 as the shortest path to *B* (shorter than the path *A*->*B*=6 from last step). Tentative distances: *A*->*C*->*D*=6, *A*->*C*->*E*=7
3	Move *B* to set *S*，then *S*={*A, C, B*} Shortest paths: *A*->*A*=0，*A*->*C*=3，*A*->*C*->*B*=5 Applying *B* as mid-point，and start search from the shortest path of *A*->*C*->*B*=5	*U*={*D, E*} Find new path *A*->*C*->*B*->*D*=10(longer than path *A*->*C*->*D*=6 from step 2) Therefore, *A*->*C*->*D*=6 is the shortest path to *D* Tentative Distance: *A*->*C*->*E*=7
4	Move *D* to set *S*，then *S*={*A, C, B, D*} Shortest paths: *A*->*A*=0，*A*->*C*=3，*A*->*C*->*B*=5，Applying *D* as mid-point, and start from the shortest path *A*->*C*->*D*=6	*U*={*E*} Find new path *A*->*C*->*D*->*E*=8(longer than path *A*->*C*->*E*=7 from step 2) Therefore, *A*->*C*->*E*=7 is the shortest path to *E*
5	Move *E* to set *S*，then *S*={*A, C, B, D, E*} Shortest paths: *A*->*A*=0，*A*->*C*=3，*A*->*C*->*B*=5，*A*->*C*->*E*=7	Now set *U* is empty, search ends.

Figure 1 shows an example of a five nodes topology with weight value beside each link. In this example, Dijkstra's algorithm is applied to find paths from node *A* to rest of nodes in this weighted graph, while Table 1 lists the detailed computing process of using this algorithm.

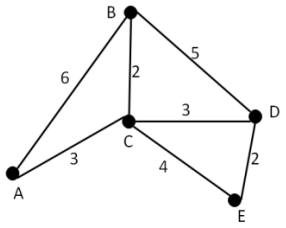

FIGURE 1 A FIVE NODES EXAMPLE OF DIJKSTRA'S ALGORITHM

Group Travel Planning for People from Multiple Origins towards the Same Destination

This system is designed for group travelling to find the travel routes, while especially driving routes can be found for people originated from multiple places towards the same destination and intend to meet in a rendezvous-point before moving to the destination. The system requires user to put in search requirements, including the name of departure place of each participator in this group travel event, and the name of common destination place and other information such as e-calendar, email address, and mobile phone numbers etc. In particular, a new algorithm has been proposed which finds paths for group travel, to realize this system. Our proposed algorithm finds the rendezvous-point on the shortest paths to participators' location and the destination. In addition, by implementing the proposed algorithm, system then can generate estimated driving time, gasoline cost and distance for paths from each participator to rendezvous-point and from rendezvous-point to destination respectively. All search results are shown on the GUI. In this paper, anew algorithm was proposed, namely, Multi-Origins Common Destination algorithm (MOD). For multiple given source vertices (origin nodes) and one common destination vertex (destination node) in the graph, this algorithm finds a suitable rendezvous-point, in which the total cost of paths from each given vertex via the rendezvous-point to the destination vertex is the approximate lowest.

Figure 2 shows the operation process of MOD algorithm. The MOD is an algorithm trying to solve the following problem: given a number of origins S and a single destination node v_d, find a rendezvous-point r that minimizes $d(v_d, t) + \text{sum}(d(s, v_d))$, where $\forall s \in S$, $d(s, r)$ is the shortest distance between node s and node r. Each starting node (including origins and destination)

starts the searches. MOD algorithm operates one search each time. For each search state, one step of Dijkstra's algorithm is implemented. Here, *one step of Dijkstra* is one single step or an iteration of Dijkstra's algorithm shown in Table 1 in which all search states run one-by-one simultaneously in round-robin fashion. The MOD algorithm terminates when a node is visited by all search states. Hence, this node is the rendezvous-point in which the corresponding paths are also generated. As the searching ends at a premature termination, the rendezvous-point is possible to be non-optimal which means continuing the search could still lead better solution. However, our current solution of finding the optimal rendezvous-point is not quite efficient. Therefore, in this paper, we only showed the MOD with the approximate optimal rendezvous-point and related paths.

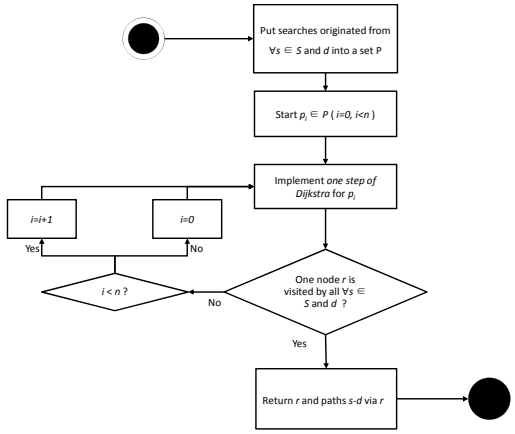

FIGURE 2 FLOWCHART OF MULTI-ORIGINS COMMON DESTINATION ALGORITHM

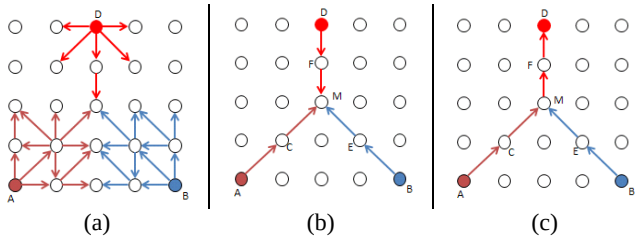

FIGURE 3AN EXAMPLE OF MOD

In Figure 3, the shown example of MOD algorithm intends to find the rendezvous-point and paths from two origins *A* and *B* to a common destination node *D*. Figure 3 (a) illustrates that the search states start from three ends, *A*, *B* and *D*. As the first node visited by all three searches, node M is found as the rendezvous-point in Figure 3 (b). As shown in Figure 3 (c), the rendezvous-point node *M* is found. Then the paths are generated by the algorithm: (1) MOD reverses the path from *D* to *M* as *D* is the destination node and has *M->F->D*, (2) the path from *A* to *D* via *M* is *A->C->M->F->D* and the path from *B* to *D* via *M* is *B->E->M->F->D*.

Performance Evaluation

The performance of MOD has been primarily evaluated with comparison to Dijkstra's Algorithm with modification (MAD) in terms of two evaluation metrics, *computation time* and *the number of nodes visited*. In Section 4.1, we first describe our comparison target, MAD. Then we show the evaluation results in Section 4.2.

To set the comparison target, the Dijkstra's algorithm has been modified to have MAD. First of all, MAD applies the Dijkstra's algorithm to compute and record the shortest paths from each origin nodes to rest of nodes, and the shortest paths from destination node to rest of nodes on the map. Then these paths are compared to find the rendezvous-point, where a node on the shortest paths to the pre-set origins and destination is chosen as the rendezvous-point.

We implemented the simulation model of the MOD algorithm and MAD algorithm in Java to examine the efficiency, where the experimental environment for analyzing the performance of algorithms in this article is as following:

Processor: Intel Core i7-2640M @ 2.80GHz

Memory: 4 GB (DDR3 1333MHz)

GPU: Nvidia NVS 4200M 1GB

Map: New York City and Florida City of US

The primary evaluation program models the simulation of up-to six origins, i.e. participators of the group travelling are from six different places towards one same destination. The evaluation program randomly selects the position of origins and destination. In this paper, MOD was compared with MAD with evaluation metrics, *the number of nodes visited* and *computation time. The number of nodes visited* expresses the efficiency of a path search algorithm, where the less nodes visited by a path search algorithm leads to better search speed. *The computation time* simply counts the time duration between the beginning and end of running an algorithm, which presents the overall effectiveness of a path search algorithm.

In Figure 4, the comparison of *the number of nodes visited* between MAD and MOD is shown. In average, MAD visits more than twice of nodes compared to MOD when there are two origins and one destination. However, in the figure, the trend line gradually moves downward as the number of origin nodes increases. This is due to the nature of MOD algorithm. According to our evaluation data, average 1.15 times of the total

nodes are visited to find a rendezvous-point by MOD when there are only two origins and one destination. This number rises to around 4.65 when there are six origins and one destination. As MOD sets the first node visited by all searches to be the Rendezvous-point, it creates search overlaps on the map, causing more search overlaps when there are more search states, i.e. more origins. Consequently, it costs more if the number of searches increases. In contrast, the number of nodes visited by MAD is directly proportional to the number of origin nodes. Figure 5 shows the comparison of *the computation time* between MAD and MOD. As the number of origin nodes goes up, the running time rapidly increases. This clearly presents the advantage of MOD in saving time cost, and proves that MOD is suitable for the group travel system which can instantly generate the search results based on each query. There may be perplexing about the downward trend line of Figure 4, and upward trend line of Figure 5. The reason is that the evaluation metric the *number of nodes visited* only considers the total cost of finding the shortest paths from origin to all nodes in the graph, where it does not take the cost of comparison of these paths to find the best rendezvous-point. However, for evaluation metric computation time, it counts the total running time of each algorithm considering the node-visiting and path-finding.

To sum up the performance evaluation, with simulated two evaluation metrics, MOD outperforms its counterparts MAD, especially in processing speed.

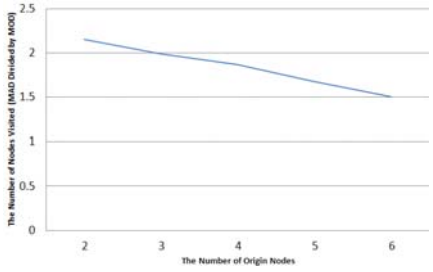

FIGURE 4 THE COMPARISON OF THE NUMBER OF NODES VISITED BETWEEN MAD AND MOD

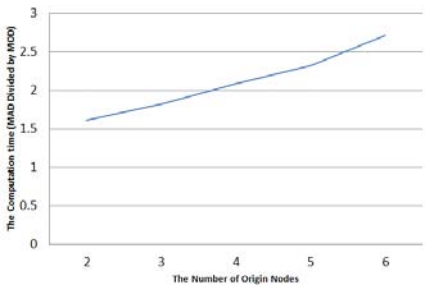

FIGURE 5 THE COMPARISON OF COMPUTATION TIME BETWEEN MAD AND MOD

Conclusion and Future Work

This paper has presented a new path search algorithm, MOD to realize the route planning service providing group travel plans for people. To best of our knowledge, MOD is first algorithm that was special designed for group travel planning. The primary performance results also show that MOD outperforms existing shortest algorithms in terms of computational speed. For our future research direction, first of all, in that MOD only provides the approximate optimal solution, MOD was expected to refine in order to find an effective way to achieve the optimal rendezvous-point and shortest paths. In addition, the feasibility of applying the heuristics search strategy in MOD has also been investigated to strengthen the performance.

REFERENCES

Bellman, R. 1958. On a routing problem. Quarterly of Applied Mathematics 16, 87–90.

Bing Map, http://www.bing.com/maps/.

deChampeaux, D., and Sint, L. 1977. An improved bidirectional heuristic search algorithm, Journal of the ACM 24 (2), 177–191.

Dijkstra, E. W. 1959. A note on two problems in connexion with graphs. Numerische Mathematik 1. 269–271.

Google Map, http://maps.google.com.

Hart, P. E., Nilsson, N. J., and Raphael, B. 1968. A Formal Basis for the Heuristic Determination of Minimum Cost Paths. In IEEE Transactions on System Science and Cybernetics, volume 4.

K. Deng, X. Zhou and H. T. Shen. 2007. "Multi-source Skyline Query Processing in Road Networks", ICDE 2007, 796 – 805.

Nissan announces results of new traffic information system model project, http://www.nissan-global.com/EN/NEWS/2013/_STORY/130913-03-e.html.

Pijls, W. and Post, H. 2009. A new bidirectional search algorithm with shortened post processing. European Journal of Operational Research, Elsevier, 363-369.

Pohl, I. 1969. Bidirectional Heuristic Search in Path Problems. Ph.D. Dissertation, Stanford University.

Taeg-KeunW. 2007. Efficient Modified Bidirectional A * Algorithm for Optimal Route-Finding, New Trends in Applied Artificial Intelligence, Lecture Notes in Computer Science, 344-353.

DOI: 10.14355/ijcsa.2014.0301.08

Mathematical Model for Predicting Arterial Drug Diffusion from Drug-Eluting Stents

Carrie V. Falke[1], Abdul Khaliq[2], Tammy R. Dugas[3], James J. Kleinedler[4], Weizhong Dai*[5]

[1,2,5] Mathematics and Statistics, College of Engineering and Science, Louisiana Tech University Ruston, LA 71272
[3,4] Department of Pharmacology, Toxicology and Neurosciences, LSU Health Sciences Center at Shreveport, LA 71130

[1]cfv003@ latech.edu; [2]khaliq@latech.edu.edu; [3]tdugas@lsuhsc.edu; [4]jkleinedler@gmail.com; [*5]dai@coes.latech.edu

Abstract

Arterial blockages are a common and significant clinical problem. One clinical method to clear these blockages is to deploy drug-eluting stents (DES) to restore blood flow through a narrowed artery. However, the design of a DES poses a unique challenge, because the concentration of drug within the arterial tissue must be therapeutically sufficient to interrupt the pathogenesis of restenosis. Characterizing the factors that determine drug kinetics and partitioning within the arterial wall is of paramount importance, especially when delivering drugs with narrow safety margins. This article presents a three-dimensional mathematical model for accurately predicting arterial drug concentration and flux after the drug is released from a stent, so that drug-eluting stents can be designed more efficiently to treat arterial blockages. The mathematical model is then solved using the COMSOL solver.

Keywords

Drug-eluting Stents; Mathematical Modelling; Arterial Drug Concentration

Introduction

One of the most important classes of cardiovascular disease affecting humans is atherosclerosis, a condition in which the wall of a blood vessel thickens as a result of the accumulation of fatty materials such as cholesterol. Atherosclerosis is a degenerative disease that affects coronary, carotid and other peripheral arteries in the body. Arterial blockages due to atherosclerosis are a common and significant clinical problem in the USA, in which cardiovascular diseases having resulted in 26% of all deaths [website 1]. Due to the plaque accumulation in the artery, the artery may be narrowed and eventually blocked, severely restricting blood flow and culminating in cardiac events such as myocardial infarction. One clinical method to restore, and mainstain blood flow through the narrowed vessels is to insert stents (as shown in Figure 1) in the diseased vessel (as illustrated in Figure 2).

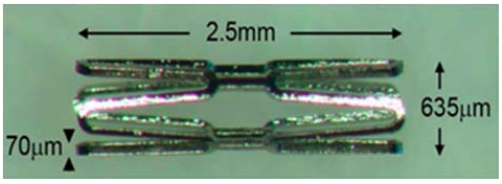

FIG. 1 STENT FEATURING 4 RADIAL CELLS, THAT WAS CUT BY A YAG LASER [website 2].

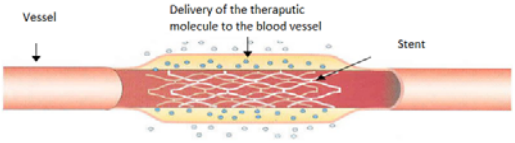

FIG. 2 DRUG ELUTING STENT EMBEDDED IN THE ARTERY [website 2].

Stent placement typically follows angioplasty, the mechanical widening of a diseased artery using an endovascular balloon catheter. At the site of treatment, angioplasty causes local damage the arterial wall and the stent provides mechanical support during the healing process to assist in keeping the artery open. However, the stent tends to incite a local immune response. This may cause scar tissue to rapidly grow over the stent. In addition, there is a possibility for clots to form at the site where the stent damages the arterial wall. The accumulation of scar tissue, cell proliferation, and clot formation (thrombosis) may cause the standard stents to become blocked, a process called restenosis. The result is that a basic "bare metal" stent has the long term potential to defeat its own purpose. Although bare metal stents (BMS) are still used in the clinical regimen, drug-eluting stents (DES) are becoming increasingly popular. These drug-coated devices aim to deliver drugs locally at the site of angioplasty to reduce the incidence of restenosis–a re-narrowing of the artery due to medial and intimal hyperplasia [Babapulle and Eisenburg 2002]. DES were designed to cope with this problem. These devices were developed to limit restenosis and maintain long-term blood flow by providing controlled release of compounds to interfere with

restenosis. By releasing an anti-proliferative drug (drugs typically used against cancer or as immuno-suppressants), DES can help avoid this in-stent restenosis. However, DES design poses a unique challenge because the concentration of drug within the arterial tissue must be sufficient to interrupt the pathogenesis of restenosis; but at the same time, the intended drug in the tissue layers must not exceed the therapeutic range, as non-selective action of current therapies has been shown to interfere with re-endothelialization, a critical component of the vascular healing process [Finn et al, 2005]. Additionally, if excessive drug is delivered to the tissue, local toxicity can result, putting the patient at risk for thrombosis [van den Heuvel et al. 2009]. On the other hand, insufficient drug release can result in an ineffective device. Thus, characterizing the factors that determine drug kinetics and partitioning within the arterial wall is of paramount importance, especially when delivering drugs with narrow safety margins. Accumulating evidence suggests that arterial pharmacokinetics ultimately determine the biological effect and potential toxicity of stent-based therapeutics. Thus, the motivation of this article is to present a three-dimensional mathematical model for accurately predicting the arterial drug concentration and flux after a drug is released from a stent, so that drug-eluting stents can be designed to more efficiently deliver drugs within the therapeutic window. We have presented preliminary results obtained based on the software COMSOL solver.

Mathematical Model

A small-animal stent and arterial geometry were taken into consideration, as shown in Figures 1 and 3-4. A cylindrical three-dimensional domain contains the stent and artery interface. A 1/8 potion of domain is shown in Figure 5. Within this domain, the governing equation for diffusion of the drug in the complex system is considered as

$$\frac{\partial A^{(m)}}{\partial t} = \frac{D_r^{(m)}}{r}\frac{\partial}{\partial r}\left(r\frac{\partial A^{(m)}}{\partial r}\right) + \frac{D_\varphi^{(m)}}{r^2}\frac{\partial^2 A^{(m)}}{\partial \varphi^2} + D_z^{(m)}\frac{\partial^2 A^{(m)}}{\partial z^2} + Others \quad (1)$$

where $A^{(m)}$ is the concentration of drug, $D_r^{(m)}, D_\varphi^{(m)}, D_z^{(m)}$ are diffusion coefficients in the cylindrical coordinates (r, φ, z), respectively, and t is the time. Here, m represents those tissue layers in the arterial tissue and the drug-coated stent layer, respectively. The "Others" term in the above equation may include the influences from drug polarity, drug load, and protein binding. In particular, the reversible binding of drug with tissue elements in the arterial wall plays an important role as reported in the literature [Balakrishnan et al., 2008; Borghi et al., 2008; Levin et al., 2004; Lovich and Edelman, 1996; Sakharov et al., 2002]. This is the bound-drug which attaches itself to the arterial wall. The reversible binding in the wall can be described in the reaction expression as follows:

$$C + S \underset{k_b}{\overset{k_a}{\Leftrightarrow}} B, \quad (2)$$

which is characterized by an association (binding) rate constant k_a forming bound drug (B) and a dissociation (unbinding) rate constant k_b [Lovich and Edelman, 1996; Sakharov et al., 2002, Borghi et al., 2008]. The associated mathematical expression can be written as

$$\frac{\partial B}{\partial t} = k_a(S_0 - B) - k_d B, \quad (3)$$

where B is the bound drug with the arterial wall. Here, the amount of available binding sites S at each position within the wall is tracked by the difference between the initial binding sites level S_0 and bound drug level B which we will investigate in later research. With appropriate initial and boundary conditions, and interfacial conditions between layers, the diffusion of the drug may be solved numerically.

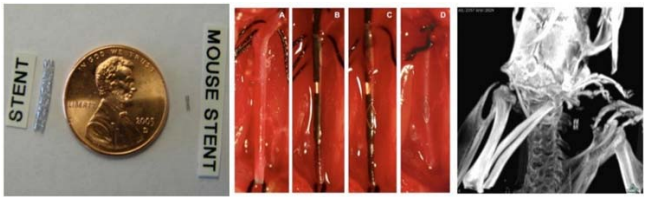

FIG. 3 SIZE OF A STENT COMPARED TO A PENNY AND COMPARED TO THE STENT USED IN RODENTS (LEFT). STENT BEING INSERTED INTO THE ARTERY WHERE A BLOCKAGE IS LOCATED (MIDDLE). A CT IMAGE OF THE STENT PLACED INTO THE COMMON CAROTID ARTERY (RIGHT).

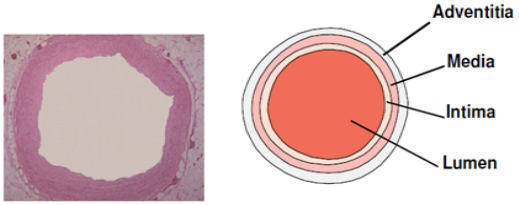

FIG. 4 ANATOMEY OF THE THREE-LAYERS ARTERY WALL [van der Woude et al 2003].

Results and Discussion

Finite Element Method was used in the software COMSOL Multiphysics version 4.3b to create our 3D finite element mesh, as shown in Figure 5. The Chemical Species Transport and the Transport of Diluted Species User Interface modules were selected to provide a modeling environment that is predefined for the study of a chemical species transported by

diffusion and convection. Because the diffusion coefficient is unknown, we had to adjust the value of diffusion coefficient based on the experimental results. Finally, the numerical result was then compared to the experimental values obtained from LSU Health Sciences Center and the values of parameters were adjusted accordingly based on a mathematical inverse analysis.

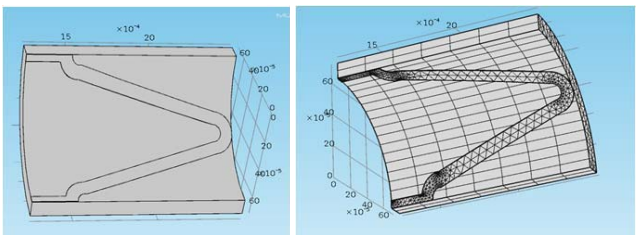

FIG. 5 ACUTAL STENT GEOMETRY AND FINITE ELEMENT MESH.

In this study, we simulated the release of resveratrol (RESV), a vascular-protective polyphenol. Dr. Dugas' laboratory at LSU Health Sciences Center - Shreveport measured the amount of drug coated on the stent and resulting molar drug concentration in arterial tissue following stent placement in a rat model. To determine the amount of drug coated on the stent, residual drug was extracted from the stent coatings using acidified methanol supplemented with 1 mM ascorbic acid. [van der Woude et al., 2003]. After 24 h incubation at 37°C in the extraction buffer under gentile agitation, the samples were centrifuged at 1000 *xg* and drug content in the supernatant was quantified using HPLC [Kleinedler et al., 2011]. The limit of detection with this analytical method is 0.1 ng/mL. To determine the molar drug concentration in the arterial tissue, tissues were weighed and finely minced. RESV was extracted under agitation into acidified methanol solution supplemented with 1 mM ascorbic acid at 37°C for 30 minutes. After vortexing and centrifugation at 1000 *xg* (10 minutes), an aliquot of supernatant was collected and drug content quantified using HPLC [Kleinedler et al., 2011]. Molar drug concentration was then determined based on tissue weight [Finn et al., 2005]. The average amount of RESV present on the stent at the corresponding day was calculated from the experimental data collected from 4-5 different rats.

Figures 6-7 show the simulation for the drug release from the stent and the drug residence time in the artery compared to the experimental data. From these two figures, it can be seen that simulation of drug release from the stent obtained based on various diffusion coefficients in the artery (ranging from 2.60 $\times 10^{-15}$ m²/s to 2.60 $\times 10^{-14}$ m²/s) agrees well with the experimental data; however, the profile of drug residence time in the artery is still significantly different from the experimental data. This is probably the diffusion coefficient for drug diffusion within the artery. Ongoing studies are aimed at determining these factors for further model development.

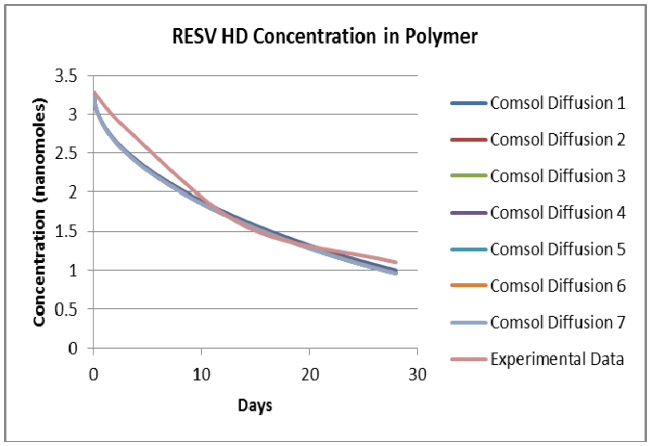

FIG. 6 DRUG RELEASE PROFILES FROM STENT. HERE, COMSOL DIFFUSIONS 1-7 WERE OBTAINED BASED ON DIFFUSION COEFFICIENTS OF 2.60 x 10^{-15} m2/s, 6.50 x 10^{-15} m2/s, 1.04 x 10^{-14} m2/s, 1.44 x 10^{-14} m2/s, 1.82 x 10^{-14} m2/s, 2.21 x 10^{-14} m2/s, AND 2.60 x 10^{-14} m2/s, RESPECTIVELY.

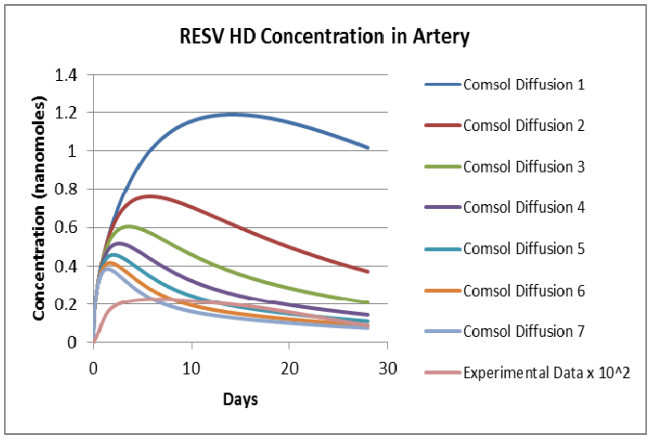

FIG. 7 DRUG RESIDENCE TIME IN THE ARTERY. HERE THE VALUE OF EXPERIMENTAL DATA IS MULTIPLIED BY 100.

Conclusion

We have proposed a three-dimensional model for predicting accurately the arterial drug concentration and flux after the drugs are released from a stent, so that drug-eluting stents can be used more efficiently in treating arterial blockages. The preliminary results obtained based on the COMSOL solver have been presented. Further research will focus on the model adjustment and parameter analysis in order to predict accurately the arterial drug concentration and flux after the drugs are released from a stent, so that drug-eluting stents can be used more efficiently in treating arterial blockages.

ACKNOWLEDGMENT

This research was supported by a NSF-Louisiana P-Fund grant.

TRD and JJK are intellectual property peripherally related to this work. Moreover, TRD is co-founder of ReQuisite Biomedical, LLC.

REFERENCES

Babapulle M.N., M.J. Eisenburg 2002. Coated stents for the prevention of restenosis: part I. Circulation 106:2734-2740.

Balakirshnan, B. , J.F. Dooley, K.G. Kopia, E.R. Edelman 2008. Thrombus causes fluctuations in arterial drug delivery from intravascular stents. J Control Release 131:173-180.

Borghi, A., E. Foa, R. Balossino, F. Migliavacca, G. Dubini 2008. Modelling drug eluting from stents: Effect of reversible binding in the vascular wall and degradable polymeric matrix. Comput Meth Biomech Biomed Eng 11:367-377.

Finn, A.V., F.D. Kolodgie, J. Harnek, L.J. Guerrero, E. Acampado, K. Tefera, S.K. Skorija, D.K. Weber, H.K. Gold, R. Virmani 2005. Differential response of delayed healing and persistent inflammation at sites of overlapping sirolimus- or paclitaxel-eluting stents. Circulation 112:270-278.

Grassi, G., M. Grassi, G. Pontrelli, L. Teresi 2007. Modelling drug release in cardiovascular eluting stents, in Modelling cardiovascular system and mechanical circulatory support. (C. De Lazzari Ed.), CNR, pp. 135-151.

Kleinedler, J.J., J.D. Foley, J.S. Alexander, V.Y. Hebert, T.R. Dugas 2011. Synergistic effect of resveratrol and quercetin released from drug-eluting polymer coatings for endovascular devices. J Biomed Mater Res B Appl Biomater 99B:266-275.

Levin, A.D., N. Vukmirovic, C.W. Hwang, E.R. Edelman 2004. Specific binding to intracellular proteins determines arterial transport properties for rapamycin and paclitaxel. Proc Natl Acad Sci. USA 101:9463-9467.

Lovich, M.A., E.R. Edelman 1996. Computational simulations of local vascular heparin deposition and distribution. Am J Physiol 271:H2014-H2024.

Sakharov, D.V., L.V. Kalachev, D.C. Rijken 2002. Numerical simulation of local pharmacokinetics of a drug after intravascular delivery with an eluting stent. J Drug Targeting 10:507-513.

Website 2. Is a Drug Eluting Stent Always the Best Option? Retrieved from http://heartheavy.com/are-drug-eluting-stnts-always-the-best-option/.

Website 1. Heart Disease Facts. Retrieved from http://www.cdc.gov/heartdisease/facts.htm.

van den Heuvel, M., O. Sorop, H.M. van Beusekom, W.J. van der Geissen 2009. Endothelial dysfunction after drug eluting stent implantation. Minerva Cardioangiol 57:629-643.

van der Woude, H., A. Gliszczynska-Swiglo, K. Struijs, A. Smeets, G.M. Alink, I.M. Rietjens 2003. Biphasic modulation of cell proliferation by quercetin at concentrations physiologically relevant in humans. Cancer Letter 200:41-47.

Carrie V. Falke is a Ph.D. student in the Program in Computational Analysis and Modeling at Louisiana Tech University, Ruston, LA 71272.

Abdul Khaliq received his Ph.D. degree in Engineering from Louisiana Tech University. Currently, he is a research staff at Louisiana tech University.

James J. Kleinedler received his Ph.D. in Pharmacology from the LSU Health Sciences Center in Shreveport, LA**.**

Tammy R. Dugas received her Ph.D. degree from Louisiana State University, USA, in 1996. She is an associate professor at Louisina State University Health Sciences Center at Shreveport. She has extensive experience in laboratory experiments to measure drug diffusion in different artery layers and drug release profiles. She has published many papers related to pharmacological research and cardiovascular toxicology.

Weizhong Dai received his Ph.D. degree in Applied Mathematical and Computational Sciences from the University of Iowa, USA, in 1994. He is a McDermott International Professor of Mathematics and the Chair of Ph.D. Program in Computational Analysis and Modeling at Louisiana Tech University, USA. His research interests include numerical solutions of partial differential equations, numerical heat transfer and bioheat transfer, numerical simulations for bioeffect of electromagnetics, and numerical methods for microfabrication systems, such as LCVD, melt crystallization, and X-ray lithography. He has published four book/book chapters and more than 140 research articles in refereed journals and international conference proceedings.

DOI: 10.14355/ijcsa.2014.0301.09

The Coupling Analysis and Research of Temperature and flow Field

Wang Lin[1], Wu Jianxin[*2]

College of Mechanical engineering, Inner Mongolia University of Technology
Hohhot 010051 China

[*2] wujx@imut.edu.cn

Abstract

To the solid rocket axisymmetric thrust-vectoring nozzle, under the action of flow field and temperature field, Comsol Multiphysics is used for this mechanism to simulate the load deformation and thermal deformation of the convergent plate, sheet, rod expansion regulation and other components, and to analyze the dynamic characteristics of the system in the generator mode under the two field coupling. Simulation and analysis to forecast the deformation of the mechanism accurately have important theoretical significances to the design of the system.

Keywords

Axisymmetric Vectoring Exhaust Nozzle; Dynamics; Coupling; Simulation

Introduction

In this paper axisymmetric jet engine thrust- vectoring nozzle treated as the prototype which is based on axisymmetric vectoring nozzle (AVEN) to model. From the beginning to the maximum swing angle of the swing and then to restoration because of the dual role of flow-temperature field, the divergent flap, the convergence closure disk of nozzle will produce dynamic load. In order to verify if the kinematic parameters (displacement, velocity and acceleration) meet the requirements of the system design, it's necessary to analyze its multi-field coupling.

Currently, it's very common to research the solid rocket motor of full swing axis TVC system. Dual Stewart platform driven thrust-vectoring nozzle is developed on the conventional mechanical nozzle and has been applied to the latest foreign aircraft engine (fighter). However, there is no report on the application of Stewart platform driven thrust-vectoring nozzle to the solid rocket motors (Comsol Multiphysics). Authors used Solid works, three-dimensional graphics software, to model and then Comsol Multiphysics was applied for physical field coupling analysis. Comsol Multiphysics an advanced numerical simulation software, developed by the Swedish Comsol and widely used in various fields of science and engineering computing is the first truly multi-physics of any direct coupling analysis software and with its efficient computational performance and outstanding multi-field coupling analysis capabilities, it has achieved an accurate numerical simulation of arbitrary multi-physics highly, which is widely used in the global leader field of numerical simulation (Huang ZhenYu, Xu WenCan, Mao HongYu. 2000); as well, it has a powerful solver for solving multi-field coupling analysis, which differs from other simulation software and can help improve the design accuracy of axisymmetric vectoring nozzle (AVEN).

AVEN Model

There is widely existent large drive torque, contact stress of moving parts, deformation and other issues in the thrust vector control system of domestic solid rocket motor. This subject includes a scheme, simultaneously adjusting the thrust-vectoring and throat diameter of nozzle and the fixed body is guaranteed on the divergent of the nozzle during the process of adjusting the thrust and direction, of dual Stewart platform thrust-vector which is driven by the linear motor. When a small amount of load is distributed in the expansion piece of the nozzle which is driven by a linear motor, moving parts change from a high-load, high-temperature and high-pressure into a relative low-load, low-temperature region. As nozzle is far away from the center of gravity of the rocket, a small deflection angle will produce enough torque deflection (generally the deflection angle requires only 6° ~ 8°), at this time, the impact on the axial thrust is only 10% or so. Therefore, even if the thrust of rocket engine is great, the driving force required for the vector nozzle in this program is very limited, which provided the conditions of directly using the linear motor to driven. Reducing the driving force of the system means to reduce the weight of the system (if

the engine is reduced by 1 kg, the range will be increased by 20 ~ 30 km). Compared with conventional hydraulic drive, Linear motor drive is not only reduces the weight of the rocket nozzle but also improves control accuracy (Comsol Multiphysics). The composition of thrust-vector of dual Stewart platform system driven by linear motor is shown in Fig. 1. The basic structure of the apparatus is: the divergent section of the nozzle (stationary object), A1 regulation ring,A2 steering regulation ring, the convergent flap 1, the expansion closure disk 2, the divergent flap 3, pull rod 4, cross joint 5,the convergence closure disk 6 and other components.

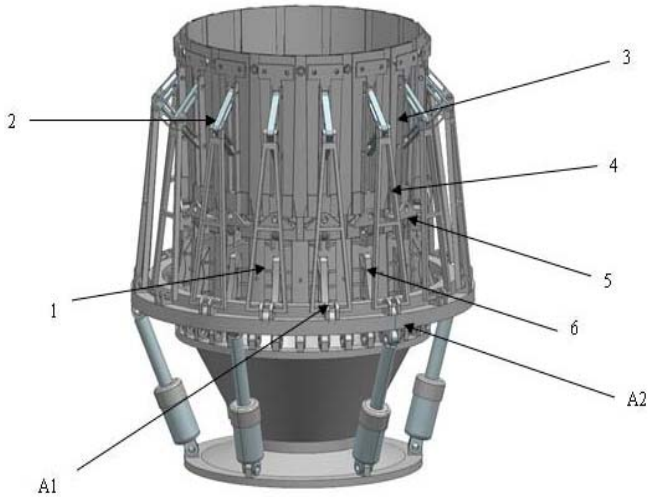

FIG. 1 THE COMPOSITION STRUCTURE OF DOUBLE STEWART PLATFORM THRUST-VECTOR SYSTEM

For the perspective of mechanism, the device is a dual-Stewart platform complex spatial mechanism. Between the dual-Stewart platforms; there are dozen pairs of space hinge mechanism in parallel. The space combined guide convergent flap and expansion space flap is a closed expansion nozzle. The position and orientation of convergent flap are determined by the regulation ring A1; while the position and orientation of expansion flap are determined by steering adjustment ring of A1 and adjustable ring of A2. In order to achieve the oscillating motion of the nozzle, regulation rings A1, A2 are driven by a linear motor. The device consists of the three components which are front, middle and rear.

The front portion connected to the diffuser of nozzle for controlling the area A1, central portion is actuation mechanism for the expansion flap, and rear portion is expansion flap. In order to withstand rocket gas jet effect, the nozzle consists of convergent flap, expansion flap and the convergence closure disk. During the process of adjusting the thrust vector, the flap and the expansion sheet are always subjected to the pressure of the gas and the pressure changes with the nozzle. During the operation, it is the core issue of this new type of nozzle's development that how to ensure coordinated movement of the convergence (expansion) flap and adjust of thrust vector

Coupling Numerical Methods and Turbulence Models of Flow-Temperature Field

The problem of multi-field coupling in the system, consisting of two or more than two interacting field, is widespread phenomenon in the nature or electromechanical products. Mechanisms in the flow field, temperature field, electromagnetic fields, and force field are affected by all kinds of coupling parameters and have effects on the system dynamic performance. It is necessary to study the coupling mechanism of the physical field parameters, explore the essential rules of multi-field coupling. From the view of the system theory, considering the dynamics performance of the physical field of the system and establishing the partial differential equations which is a unified description of the dynamic characteristics of the system are necessary (Comsol Multiphysics). Flying at high altitude, the motor working temperature generated inside the nozzle and the fluid will produce stress and strain on the part of convergent and expansion section. In the literature (Wang YuXin, 2006), for the flow field of axisymmetric thrust vectoring nozzle is a typical transonic flow field, using Jameson's finite volume method and three-dimensional Euler/NS equations to solve flow field of vectoring nozzle. In order to overcome the pulsation of the central difference scheme smooth area and oscillation of discontinuous solutions, it used artificial viscosity technique; in order to accelerate the convergence speed of solution, the local time step, enthalpy damping technology, average implicit residual, as well as Runge-Kutta time advance technologies of mixed step are utilized. Comsol Multiphysics is employed for coupling analysis of the mechanism.

When the nozzle at the position of 0°, the high temperature fluid which burst forth by the combustion chamber get to the outside world through the nozzle, the temperature of the fluid decrease from the high to low, the velocity increases gradually. Using the NS equations of time-dependent 3-dimensional Cartesian coordinates conservation to solve the problem of the nozzle in temperature and flow field. Turbulence type using $k-\varepsilon$ model, based on the development of eddy viscosity model contains part of the history effects of eddy viscosity. Specifically, it is associated with the

eddy viscosity and turbulent kinetic energy and turbulent kinetic energy dissipation; and the k and ε can solved by using them (Wang Tao, 1999). The following equations (1)~(6) are the control equations of the coupled field.

$$\rho\frac{\partial\vec{u}}{\partial t}+\rho(\vec{u}\cdot\nabla)\vec{u}= \nabla\cdot\left[-p\vec{I}+(\mu+\mu_T)\left(\nabla\vec{u}+(\nabla\vec{u})^T\right)-\frac{2}{3}(\mu+\mu_T)(\nabla\cdot\vec{u})\vec{I}-\frac{2}{3}\rho k\vec{I}\right]+\vec{F} \quad (1)$$

$$\frac{\partial\rho}{\partial}+\nabla(\rho\vec{\mu})=0 \quad (2)$$

$$\rho\frac{\partial k}{\partial t}+\rho(\vec{u}\cdot\nabla)k=\nabla\cdot\left[\left(\mu+\frac{\mu_T}{\sigma_k}\right)\nabla k\right]+P_k-\rho\varepsilon \quad (3)$$

$$\rho\frac{\partial\varepsilon}{\partial}+\rho(\vec{\mu}\cdot\nabla)\varepsilon=\nabla\left[(\mu+\frac{\mu_T}{\sigma_e})\nabla\varepsilon\right]+C_{e1}\frac{\varepsilon}{k}P_k-C_{e2}\frac{\varepsilon^2}{k}, \quad (4)$$

$$\varepsilon=ep$$

$$\mu_T=\rho C_\mu\frac{k^2}{\varepsilon}, \quad (5)$$

$$P_k=\mu_T\left[\nabla\vec{\mu}:\left(\nabla\vec{\mu}+(\nabla\mu)^T\right)-\frac{2}{3}(\nabla\cdot\vec{\mu})^2\right]-\frac{2}{3}\rho k\nabla\cdot\vec{\mu}$$

$$\rho C_p\frac{\partial T}{\partial t}+\rho C_p\vec{\mu}_{trans}\cdot\nabla T=\nabla\cdot(k\nabla I)+Q \quad (6)$$

In the equations:

ρ —Flow density

p —Stream Pressure

$\vec{u}$ —Airflow velocity field

k —Turbulent kinetic energy

C_p —Atmospheric heat capacity

C_μ —specific heat capacity

Nozzle and air physical parameters in Table I and Table II:

Boundary Conditions and Mesh Generation

Boundary conditions of the flow field of nozzle include: Inlet boundary condition: given total temperature, total pressure and velocity direction of import nozzle. Outlet boundary conditions include: total external pressure. Wall boundary conditions: no penetration, no-slip condition, pressure gradient is zero. Inlet velocity is150m/s. Pressure is 6e6Pa, outlet velocity is 2000m / s, the outlet pressure is 0.11e6Pa.

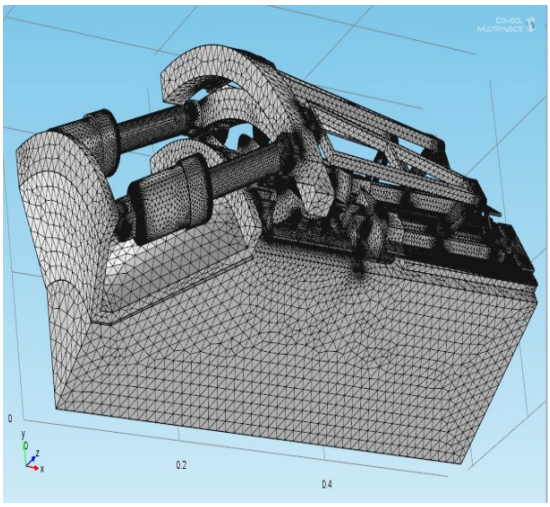

FIG. 2 COMSOL MULTIPHYSICS MESHED

Temperature field of the nozzle boundary conditions: Inlet and outlet boundary conditions: Temperature of given inlet is 3000K, outlet temperature is 1300K. Calculation parameters: inlet radius of nozzle is 81.25 mm; throat radius is 167mm; convergence length is 123 mm; expansion length is 191mm; vector deflection angle is 0°; airflow inlet total temperature is t_0 ; pressure ratio is 2~8. This mechanism is axisymmetric and the one third of model is desirable to do analysis.

Comsol Flow Field-Temperature Field Coupling to Solver Results

Temperature Change Map

Figure 3 shows Bodies high temperature concentrated at the entrance to the nozzle diffuser in the given constraints. The maximum temperature is 3000 K.

TABLE I THE NATURE OF STEEL

steel	density	Viscosity	thermal conductiviy	Specific heat ratio
Value (units)	7850 kg/m^3	1	46.1	43.53

TABLE THE RELATION OF ATMOSPHERIC HEAT CAPACITY AND TEMPERATURE OF STEEL

T/℃	100	200	300	400	500	600	700	755	900
Cp/(J/Kg)	480	498	524	560	615	700	854	1064	806

TABLE II PHYSICAL PROPERTIES OF DRY AIR

Temperature (t)	Density (ñ)	specific heat (c)	thermal conduct ivity ($\lambda\times10^2$)	dynamic viscosity ($u\times10^5$)	Specific heat ratio
(℃)	(kg/m)	(kJ/kg•℃)	(W/m•℃)	($pa*s$)	1
20	1.205	1.013	2.593	1.81	1.4
300	0.615	1.047	4.605	2.97	
800	0.329	1.114	7.176	4.43	

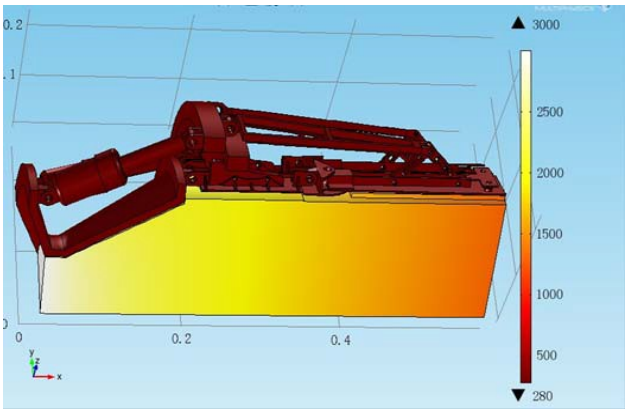

FIG. 3 CHANGES IN TEMPERATURE

Pressure Change Map

In the given constraints, fluid pressure changes within the organization shown in Figure 4. Maximum pressure pmax=8.2304e19Pa on the side of convergent flap. In Figure 4, the structure shows the Pressure value in Yellow area p=1Pa, Minimum pressure is 0 Pa.

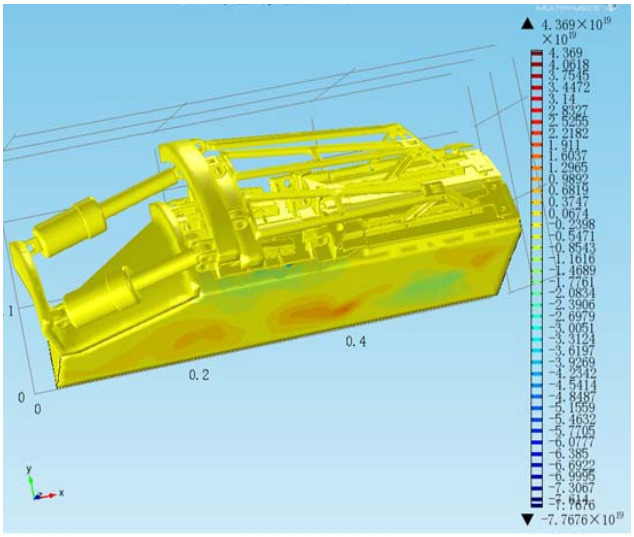

FIG. 4 CHANGES PRESSURE

Conclusion

Based on the problem of multi-physics coupling of nozzle, it has been researched how to do with the process of multi-physics coupling and delimit on a variety of constraints and boundary conditions of multi-physics problems. Through assembling Three-dimensional model, Comsol Multiphysics three coupling method (Flow field - temperature field - Solid Mechanics) was adopted for solving simulation. Research showed the exact stress in the three coupling method combined effect and heat conditions was clear through using multi-physics coupling analysis software. The operator interface of Comsol Multi-physics Software was simple to understand. Coupling method was directly coupled but not sequentially coupled. This article was significant to study and analyze the sxisymmetric vectoring nozzle (AVEN).

ACKNOWLEDGMENT

This work was sponsored by Natural Science Foundation of Inner Mongolia 2013MS0712.

REFERENCES

Comsol Multiphysics. Chinese User Manual.

Huang ZhenYu, Xu WenCan, Mao HongYu.” the numerical calculation of nozzle flow and Thrust vector”. Ordnance learned journal, 2000,21(2):31~34.

Liu WenZhi. Wu JianXin, Gong YongZhi, Yan LiXia. “Solid rocket motor mechanical dynamics device TVC system research and development momentum” Mechanical Design .

Lu Yan, Fan SiQi, Ma HuiMin. “Axisymmetric vectoring nozzle Numerical Simulation and Mathematical model Research.” Northwestren Polytechnical University Press. 2002, 20(3): 383~386.

Luo Jing,Wang Qiang, Erijitai. “The calculation Axisymmetric vectoring nozzle Internal flow feature in different kind of turbulence”, 2003, 24(4):326~340.

Pu LiangGui, Ji MingGang.” Mechanical Design (Eighth Edition)” Beijing: Higher Education Press, 2006.5.

Wang YuXin, “Axisymmetric jet engine thrust vectoring nozzle” Beijing: National Defense Industry Press, 2006.3.

Wang Tao, Meng QingMing.” Integrated flight with vectoring nozzle in order to promote control technology research”. Aviation pow learned journal, 1999, 14(4): 437~457.

DOI: 10.14355/ijcsa.2014.0301.10

Dynamic Analysis and Optimization of Parallel Manipulator

Wang KaiJie, Wu JianXin*

College of Mechanical engineering, Inner Mongolia University of Technology
Hohhot 010051 China

wujx@imut.edu.cn

Abstract

Electromechanical coupling dynamic model of parallel manipulator is a kind of a complicated electromechanical system which is multi-input, multi-output, nonlinear and strong coupling. There is not a perfect method to calculate dynamic modeling and simulation of parallel manipulator at present. 6UPS-parallel manipulator dynamic model was set up by Lagrange method; PID position controller was designed; and the controller parameters were optimized by inertia weight adaptive particle swarm optimization in the article. It was proved that the modeling of electromechanical coupling dynamic model was right and the manipulator was controlled well by the controller through the simulation result of computer.

Keywords

Parallel; Manipulator; Dynamics; Optimization

Introduction

Parallel manipulator appeared while robotics and CNC technology was combined. It can provide flexibility of robots, also has rigidity and precision of the machine tools, and it is a new type of electromechanical device with multiple functions (Jack Hollingum, 1997; Khalil W, Guegan S., 2004; Liu M J, Li C X, Li C N., 2000). Features of the manipulator are: high-rigidity, fast response speed, capacity of multiple degrees of freedom movement, capacity to display space posture, and so on. Building and analysis of parallel manipulator dynamic modeling is an important theoretical basis of the manipulator trajectory planning, dynamic design and the controller parameter setting, which can contribute to solving internal force and driving force of each joints after the cutting tools movement regularity (path, velocity and acceleration) was available. Its dynamic model is usually a complex system which contains multiple degrees of freedom multiple variable, high nonlinearity and multi-parameter coupling. Almost all of dynamic theory available such as Newton-Euler method, Lagrange equation, virtual work principle, Kane Formulation can be used in its modeling. Many scholars at home and abroad engaged in the research (Ohn M Fitzgerald, 1993; Stanley Modic, 1994; Yiu Y K, Cheng H Xiong, Z H Liu, et al., 2001), but there isn't a perfect method to calculate dynamic modeling and simulation of parallel manipulator so far because of the complexity. 6UPS-parallel manipulator dynamic model was set up by Lagrange method; PID position controller was designed; the controller parameters were optimized by inertia weight adaptive particle swarm optimization and dynamic simulation calculation was processed in the article.

Building of 6-UPS Parallel Manipulator Dynamic Model

The manipulator was decomposed into two sub-systems (moving platform and six legs) in order to solve its kinetic energy and potential energy. The two subsystems' kinetic energy and potential energy were droved at first, and then the whole manipulator's dynamical equation was droved.

Kinetic Energy and Potential Energy of the Moving Platform

Kinetic energy of the moving platform in three-dimensional space (including translation and rotation):

$$K_{Plat} = \frac{1}{2}[m_{Plat}(\dot{x}_p^2 + \dot{y}_p^2 + \dot{z}_p^2) + (\dot{\alpha}^2 I_z + \dot{\beta}^2 I_y + \dot{\gamma}^2 I_x)] \quad (1)$$

where m_{Plat} denotes the mass of the moving platform; $(\dot{x}_p, \dot{y}_p, \dot{z}_p)$ denotes the time derivative of the moving platform position parameter; $(\dot{\alpha}, \dot{\beta}, \dot{\gamma})$ denotes the time derivative of the moving platform azimuth parameter; I_x denotes the X-axis rotary inertia of the moving platform; I_y denotes the Y-axis rotary inertia of the moving platform; I_z denotes the Z-axis rotary inertia of the moving platform; g denotes acceleration of gravity.

Potential energy of the moving platform:

$$P_{Plat} = [0 \quad 0 \quad m_{Plat}g \quad 0 \quad 0 \quad 0]q \quad (2)$$

Kinetic Energy and Potential Energy of the Driving Leg

The structure of driving leg is shown in Fig 1, where m_1 is mass of the non-moving leg; m_2 is mass of the moving leg; e_1 denotes the distance between the mass center of the non-moving leg and the corresponding hook hinge mass center of the fixed platform; e_2 denotes the distance between the mass center of the moving platform and the corresponding spherical hinge mass center of the moving platform; l_i denotes the length of the drive leg which is marked as i.

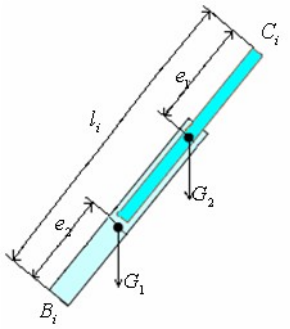

FIG. 1 STRUCTURE OF DRIVE LEG

Kinetic energy of the driving leg:

$$K_{Legs} = \frac{1}{2}\sum_{i=1}^{6}\left[m_{Leg}(V_i^T V_i)\right] \tag{3}$$

Where m_{Leg} mass of the drive leg which is marked as i; V_i is velocity of it; V is velocity vector of the driving leg. Potential energy of the driving leg:

$$P_{Legs} = m_1 g\sum_{i=1}^{6} e_1\overrightarrow{(B_iC_i)_z} + m_2 g\sum_{i=1}^{6}(l_i - e_2)\overrightarrow{(B_iC_i)_z} \tag{4}$$

Where $\overrightarrow{(B_iC_i)_z}$ is Z-axis vector component of the driving $legB_iC_i$; g denotes acceleration of gravity.

Building of 6UPS-parallel Manipulator Dynamical

Then the Lagrange function will be:

$$\tau_i = \frac{d}{dt}(\frac{\partial L(q,\dot{q})}{\partial \dot{q}_i}) - \frac{\partial L(q,\dot{q})}{\partial q_i} \quad i = 1,2,\cdots,6 \tag{5}$$

Transforming Eq. (11) and substituting it into Eq. (12):

$$\begin{aligned}\tau_i = &(\begin{bmatrix} M_{Plat} & 0 \\ 0 & I_{Plat}\end{bmatrix} + m_{Leg}J^T J)\ddot{q} + \\ &m_{Leg}(\dot{J}^T J + m_{Leg}J^T\dot{J})\dot{q} - m_{Leg}\dot{q}^T(\frac{\partial J}{\partial q_i})^T J\dot{q} + \\ &[0 \quad 0 \quad m_{Plat}g \quad 0 \quad 0 \quad 0]^T + m_1 g\sum_{i=1}^{6} e_1(\frac{\partial\overrightarrow{(B_iC_i)_z}}{\partial q_i}) \\ &+m_2 g\sum_{i=1}^{6}(\frac{\partial l_i}{\partial q_i}\overrightarrow{(B_iC_i)_z} + l_i\frac{\partial\overrightarrow{(B_iC_i)_z}}{\partial q_i} - e_2\frac{\partial\overrightarrow{(B_iC_i)_z}}{\partial q_i})\end{aligned} \tag{6}$$

Setting:

$$D = \begin{bmatrix} M_{Plat} & 0 \\ 0 & I_{Plat}\end{bmatrix} + m_{Leg}J^T J \tag{7}$$

$$H = m_{Leg}(\dot{J}^T J + m_{Leg}J^T\dot{J}) \tag{8}$$

$$\begin{aligned}G = &-m_{Leg}\dot{q}^T(\frac{\partial J}{\partial q_i})^T J\dot{q} + [0 \quad 0 \quad m_{Plat}g \quad 0 \quad 0 \quad 0]^T \\ &+m_1 g\sum_{i=1}^{6} e_1(\frac{\partial\overrightarrow{(B_iC_i)_z}}{\partial q_i}) \\ &+m_2 g\sum_{i=1}^{6}(\frac{\partial l_i}{\partial q_i}\overrightarrow{(B_iC_i)_z} + l_i\frac{\partial\overrightarrow{(B_iC_i)_z}}{\partial q_i} - e_2\frac{\partial\overrightarrow{(B_iC_i)_z}}{\partial q_i})\end{aligned} \tag{9}$$

And then dynamical equation of the system can be transformed into:

$$\tau_i = D\ddot{q} + H\dot{q} + G \quad i = 1,2,\cdots,6 \tag{10}$$

Where τ_i is not really driving force which is acted on the driving leg but the fictitious force and moment acting on the position x_p, y_p, z_p and the azimuth α,β,γ, so it could be called generalized force. The really driving process is that the change of the driving leg result in the change of the moving platform, and then 6-dimentions generalized force acting on the moving platform is transformed into driving force of the driving leg. According to virtual work principle:

$$f^T\cdot\delta l = \tau^T\cdot\delta q \tag{11}$$

So

$$\tau = J^T f \tag{12}$$

Where, τ is the 6-dimention generalized force acting on the moving platform.

The system dynamical equation that regards driving force as an external force can be easily got:

$$J^T f = D\ddot{q} + H\dot{q} + G \tag{13}$$

It can be transformed into:

$$\ddot{q} = D^T(J^T f - H\dot{q} - G) \tag{14}$$

Inertia Weight Adaptive Particle Swarm Optimization of PID Controller

In PSO algorithm, great influencing parameters on the result of optimization and efficiency are w, c_1, c_2. Inertia weight coefficient w is a key influence coefficient of PSO algorithm, which balances global exploration and local exploitation abilities of the swarm. A large inertia weight facilitates exploration, but it makes the particle long time to converge. Conversely, a small inertia weight makes the particle fast converge, but it sometime leads to local optimum. Empirical results have shown that w is given a large value in the in the initial search to enhance the global search capability, and then decrease w gradually to obtain more accurate result. Exponential decreasing function is used to determine the weight coefficient w:

$$w = e^{-\alpha k} \tag{15}$$

Now the update velocity equation is:

$$v_i^d(k+1) = e^{-\alpha k} v_i^d(k) + c_1 r_1[p_i^d(k) - x_i^d(k)] + c_2 r_2[p_g(k) - x_i^d(k)] \quad (16)$$

Where α is an adjustment coefficient, it's used for the regulation of inertia weight decay rate.

Design variables of optimization algorithm are the control parameters of the position PID controller:

$$K = [K_p, K_i, K_d]$$

Constraint condition will be: $0 < K < +\infty$;

Objective function is position error of moving platform given as following equation:

$$Obj(q_j) = \min(q_j^* - q_j) \quad (17)$$

Dynamic differential equations (10) are solved by Runge-Kutta method that is easy to carry out and stability.

Results of optimization are as follow:

$$K_p = 881,\ K_i = 1821,\ K_d = 878.$$

Dynamic Analysis and Optimization

Dynamic parameter of parallel manipulator is shown in Table 1.

TABLE 1 SIZE PARAMENTER OF 6UPS PARALLEL MANIPULATOR

Parallel manipulator parameter	Value
Radius of non-moving platform(m)	0.480
Thickness of non-moving platform(m)	0.030
Hinge point distributed radius of non-moving platform (rad)	π/12
Radius of moving platform(m)	0.080
Thickness of platform(m)	0.050
Hinge point distributed radius of moving platform(rad)	π/6
Diameter of moving leg(m)	0.035
Length of moving leg(m)	0.460
Moving distance of the moving leg(m)	0.250
Outside diameter of non-moving leg(m)	0.070
Inside diameter of non-moving leg(m)	0.035
Length of non-moving leg(m)	0.460
Diameter of screw leg(m)	0.020
Length of screw leg(m)	0.300
Guiding distance of screw leg(m)	0.004

The movement of moving platform defines a helix moving in the coordinate space $O-xyz$. The curve of given displacement and velocity is shown in Fig 2 and Fig 3:

The displacement and velocity real changing curve of the moving platform center can be gotten by solving 6UPS parallel manipulator system dynamic differential equation, which is shown in Fig 4 and Fig 5:

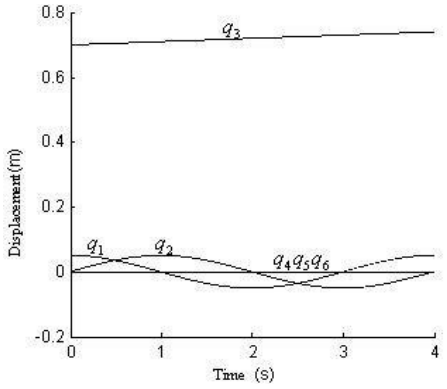

FIG. 2 DISPLACEMENT CURVE OF THE MOVING PLATFORM CENTER

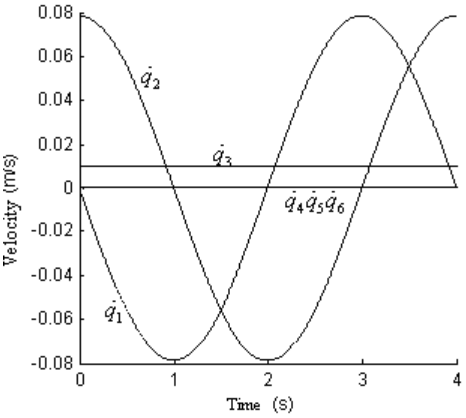

FIG. 3 VELOCITY CURVE OF THE MOVING PLATFORM CENTER

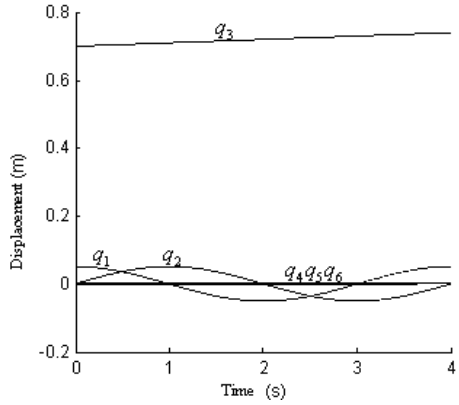

FIG. 4 THE REAL CHANGING CURVE OF THE MOVING PLATFORM CENTER DISPLACEMENT

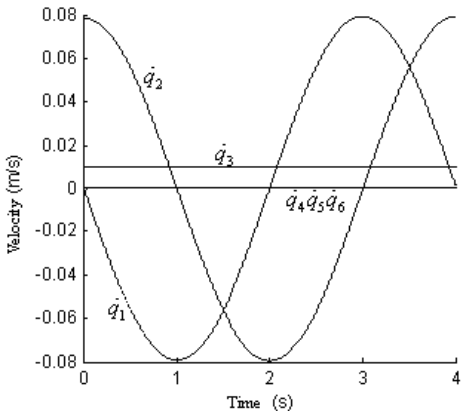

FIG. 5 THE REAL CHANGING CURVE OF THE MOVING PLATFORM CENTER VELOCITY

The conclusion that the real movement of the moving platform is in accordance with the anticipant helix movement can be gotten by comparing and analyzing Fig 2 and Fig 4.

To verify the rationality of PID controller design, error curve of the moving platform real and anticipant displacement is calculated in Fig 6.

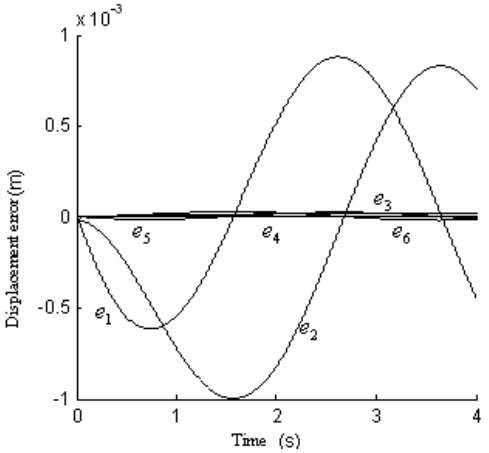

FIG. 6 ERROR CURVE OF THE REAL AND GIVEN DISPLACEMENT

Through Fig 5, the maximal error of the moving platform center displacement is about 9_m, so the rationality of the PID controller design can be confirmed. Under the control of PID controller, the changing curve of driving force which belongs to the 6UPS parallel manipulator driving leg can be shown as Fig 7:

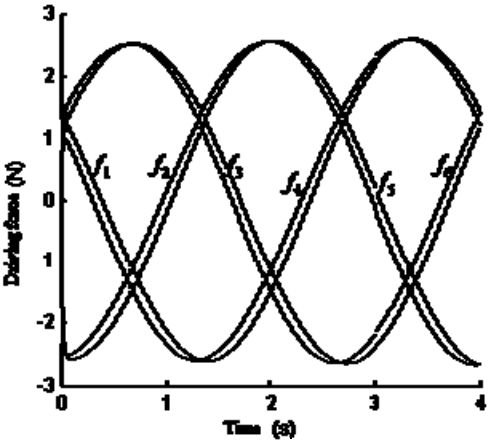

FIG. 7 THE DRING FORCE CURVES OF THE LEGS.

In Fig 7, it can be found out that the driving force of the driving legs changed periodically and increased continually in the process of the whole helix movement, which is approximately in accordance with the path programming of the moving platform. Through the movement process, the stress cyclical change of driving leg 1 and 4, 2 and 5, 3 and 6 is accordant, which is approximately in accordance with the symmetrical distribution structure. So the conclusion is that the moving platform would move cyclically while the cyclical changed driving force is added on the driving leg.

Conclusion

Lagrange-Maxwell method a simple and efficient in modeling and analysis of electromechanical coupling dynamic system is in possession of wide potential application in design and analysis of complicate electromechanical equipments. The inertia weight adaptive particle swarm optimization algorithm would not require knowledge of first or second differential coefficient, discontinuities and other assistant information, moreover, it could realize global optimization. The results of computer simulation show that it is feasible to realize the optimal control of mechanism displacement of the moving platform by this new optimization algorithm.

ACKNOWLEDGMENT

This work was financed by Inner Mongolia high school science and technology fund NJZZ120492013MS0712.

REFERENCES

Jack Hollingum, “Hexapods to take over”, Industrial Robot, IEEE Press, 1997, pp.428-431.

Khalil W, Guegan S. “Inverse and direct dynamic modeling of Gough-Stewart robots”, IEEE Transactions on Robotics, IEEE Press, 2004, pp.754-762.

Liu M J, Li C X, Li C N. “Dynamics analysis of the Gough-Stewart platform manipulator”, IEEE Transactions on Robotics and Automation, IEEE Press, 2000, pp.94-98.

Ohn M Fitzgerald, “Evaluating the Stewart platform for manufacturing”, Robotics Today, Society of Manufacturing Engineers, 1993, pp.1-3.

Stanley Modic, “Virtual axis machining–the shape of things to come”, Tooling & Production, Industrial & Manufacturing Trade Publications, 1994, pp.13-14.

Yiu Y K, Cheng H Xiong, Z H Liu, et al. “On the dynamics of parallel manipulators”, Proceedings of the 2001 IEEE International Conference on Robotics & Automation, Seoul Korea.Seoul, IEEE Press, 2001, pp.21-28.

DOI: 10.14355/ijcsa.2014.0301.11

Research and Implementation of Distributed Disaster Tolerant System

Yongjian Ren[1], Huijia Xuan[2], Jiling Zhang[3],Yuyu Yin[4], Miaofeng Shi[5]

[1,2,3,4]School of Computer Science and Technology, Hangzhou Dianzi University, Hangzhou, China

[5]Enterprise Information Management,Inc,Hangzhou,China

[1]yongjian.ren@infocore.cn; [2]cloudxhj@gmail.com; [3]jilin.zhang@hdu.edu.cn; [4]yuyu.yin@hdu.edu.cn; [5]miaofeng.shi@infocore.cn

Abstract

With the advent of the information age, the growths of data amount are explosive in various industries and the importance of data has become more and more prominent. When a disaster occurs, how to recover data completely and rapidly is one of the important issues which raise common concern in both industry and academy circles. This paper proposes a distributed disaster tolerant system based on information decentralization algorithm. The system, called NewDDR, adopts distributed architecture to ensure the high availability of data even under the condition of multi-node damage. NewDDR uses considerably fewer physical resources by employing the information decentralization algorithm which is based on erasure code. Experiments show that NewDDR can guarantee effective protection of the source data, while keeping the normal operation of the application.

Keywords

Disaster Tolerance; Distributed; Information Decentralization Algorithm; Erasure Code

Introduction

Currently, the common structure of disaster tolerant system is point-to-point or multi-to-point, namely a production center corresponds to a disaster tolerant center, or multiple production centers correspond to a disaster tolerant center (Lawler et al, 2008). In the case of the single node damage, this structure can ensure data security, but if this structure encounters continuous disasters or multi-node failure, it can't ensure data security and business continuity. Symantec's Veritas Volume Replicator system (Symantec 2002) allows multi-to-multi data disaster tolerance, but the data redundancy degree is large, and the utilization of storage resource is low. On the other hand, disaster tolerant products currently on the market mostly work on expensive disk arrays and FC (Fiber Channel) network. And they are integrated in each companies' hardware. So there are some defects in the flexibility, purchasing cost and so on. One example is EMC's SRDF (EMC, 2009) disaster tolerant system, which must be built on top of the Symmetrix storage systems. Therefore, this paper presents a distributed disaster tolerant system which has a 1+N type structure to cope with these situations.

The second chapter of this paper discusses the structure of NewDDR, and describes processes of data storage and data recovery briefly; Section 3 describes the theory of information distributed algorithm and data processing in NewDDR; In section 4, time consumption of the information distribution algorithm and the writing and reading performance degradation of application are tested; Section 5 concludes the paper.

NewDDR Architecture

System Architecture and Function of Each Module

This paper designs a distributed disaster recovery system named NewDDR based on the storage virtualization engine. Storage virtualization engine manages underlying heterogeneous storage resources by the storage virtualization technology and maps storage resources in the form of logical volumes to servers via iSCSI(iSCSI) (Internet small computer system interface) or FC network. According to user demand, NewDDR establishes a hot backup center in remote or only on local important data for disaster tolerant backup. NewDDR has no strict requirement on transmission network and does not need specialized communication link and hardware facilities, thereby reducing the cost of system deployment.

The overall system architecture is shown in fig. 1. According to the above figure, the production center maps logical volume to client for application. The logical volume in NewDDR is called source volume, which stores the source data. Coding operations take place in the disaster tolerant center and the encoded

data is stored in a logical volume of disaster tolerant center, then this logical volume is called to target volume.

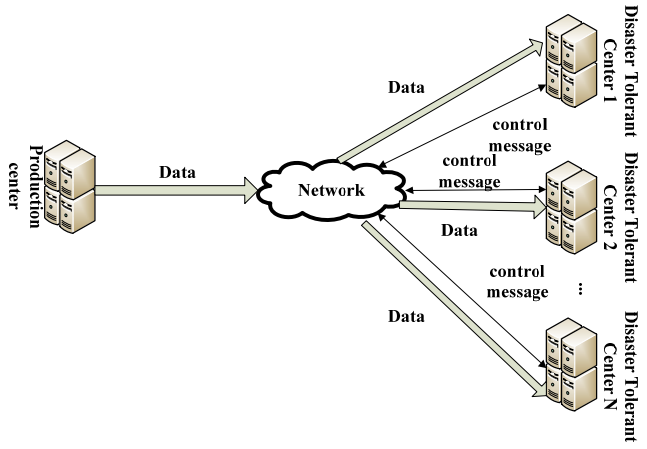

FIG.1 NEWDDR SYSTEM ARCHITECTURE

The NewDDR system is mainly composed of three modules, including I/O management module, file transfer module, coding and decoding module.

I/O management module is deployed in the production center and can access all I/O Request Packet(IRP) that is written in the source volume by NewDDR's disaster tolerant filter driver(Baker,2001, Orwick et al,2007, Zhu et al,2008) (DDR). Taking the low network bandwidth in actual into account, I/O management module adopts the asynchronous transfer mode, and IRP data will be temporarily stored in the buffer volume of production center.

File transfer model is based on Web Service (Roman et al, 2005) technology, deployed in production center and disaster tolerant center. The file transfer model is used to transmit data, including the source data and the encoded data. At the same time, the file transfer model reduces the amount of data transmission through data compression technology.

Encoding and decoding module is deployed in the disaster tolerant center. When the disaster tolerant center receives source data, encoding module parses the data and encodes every IRP by RS erasure code, and then stores the encoded data in multiple files for transfer. The decoding module is responsible for the source data recovery operation when multiple nodes are damaged.

Process of NewDDR

The process of NewDDR mainly includes disaster tolerant relationship configuration, data disaster tolerance and data recovery.

1) Disaster Tolerant Relationship Configuration

Disaster tolerant relationship configuration refers to the process of deploying multiple disaster tolerant centers into a production center. The number of disaster tolerant centers to be deployed should not exceed the one in NewDDR. Assuming that there are N disaster tolerant centers in NewDDR, now users will deploy relationship with (K, M) (M<=N) mode for a source volume. (K,M) mode means cutting the source data with length L into K parts, generating M encoded data with length L/K after encoding by RS erasure code and saving them in M target volumes.

2) Data Disaster Tolerance

After the step 1, DDR will monitor all IRPs which are written into the source volume and then stored in buffer volumes. Given the load and performance of production center, NewDDR makes disaster tolerant center encode IRP data. After the amount of data in buffer volume reaches a certain value, file transfer module will read the data and send them to the corresponding disaster tolerant center.

File transfer module in the target disaster tolerant center receives the source data and send it to encoding and decoding module through I/O control (IOCTL). After the completion of encoding, according to the recoded disaster tolerant relationship in profiles, these data will be sent to corresponding disaster tolerant volumes for storing through file transfer module.

3) Data Recovery

When no more than M-K disaster tolerant centers are damaged in the (K, M) mode, NewDDR can take advantage of the rest disaster tolerant centers and erasure decoding algorithm to construct the source data. And then according to the recovered source data, NewDDR can recover the data in the damaged disaster tolerant centers through erasure encoding algorithm.

Information Distributed Algorithm Based on RS Erasure Code

To ensure data security and high availability, NewDDR system uses data redundancy backup mechanism, and redundant data are stored in a number of target volume. Currently, data redundancy backup mechanism mainly includes complete mirror mechanism and erasure code mechanism. Complete mirror mechanism, also known as copy mechanism that multiplies copies of the source data that are stored separately. This mechanism is characterized by

simplicity, but the storage resource utilization is low, resulting in high cost. Erasure code mechanism gets the redundancy data by erasure encoding algorithm. When the part of the data is damaged, it can recover the source data according to erasure decoding algorithm. Compared with the complete mirror mechanism, erasure coding mechanism has the advantage of high disk utilization, and low redundancy.

Process of Encoding and Decoding

1) Process of Coding

Based on considerations of production center's performance, NewDDR makes encoding operation in disaster tolerant center. Once the source data are received from the file transfer module, disaster tolerant center analyzes the file and then sent to the encoding and decoding module which is followed by encoding the source data in groups of IRP and writing encoded data into distributing files. After encoding operation is completed, file transfer module transfers distributing files to target volumes.

2) Process of Decoding

The process of decoding need to be undertook by the decoding module when data is lost. If data loss occurs in disaster tolerant center while the production center takes no damage, we should reestablish the disaster tolerant centers and recode the source volume according to configuration files. If the production center is damaged, new production center should be built and the storage virtualization engine should map intact target volumes to the new production center. The remaining data will be decoded based on RS erasure decoding algorithm, and the recovery data will be written to the source volume.

Performance Evaluation

Experimental Environment Description

NewDDR system is prototyped under the laboratory environment in which the real remote disaster tolerance is simulated. Experimental environment includes a client, a production center, seven disaster tolerant centers, where the client and three disaster tolerant centers consists of virtual machines. Client, production center is in the same gigabit LAN. Production center connects with each disaster tolerant center in 10Mb network. The physical machine node configurations are shown in Table 1, and the virtual machine node configurations are shown in Table 2.

TABLE 1 PHYSICAL NODE CONFIGURATION TABLE

Role	CPU	Memory	Disk	OS
Production Center	Intel Core 2.98GHz CPU*4	4GB	500G	Windows Server 2003
Disaster tolerant Center 1	Intel Xeon 2.13GHz CPU*4	4GB	500G	Windows Server 2003
Disaster tolerant Center 2	Intel Core 2.98GHz CPU*4	4GB	500G	Windows Server 2003
Disaster tolerant Center 3	Intel Core 2.98GHz CPU*4	4GB	500G	Windows Server 2003
Disaster tolerant Center 4	Intel Core 3.10GHz CPU*2	2GB	500G	Windows Server 2003

TABLE 2 VIRTUAL MACHINE CONFIGURATION TABLE

Role	CPU	Memory	Disk	OS
Client	2	2GB	100G	Windows Server 2003
Disaster tolerant Center 5	2	2GB	200G	Windows Server 2003
Disaster tolerant Center 6	4	4GB	200G	Windows Server 2003
Disaster tolerant Center 7	4	2GB	200G	Windows Server 2003

NewDDR's Impact on Application

In this paper, four groups of experiments are made to test the impact of NewDDR on application, and experiments shows that NewDDR can guarantee the normal operation of the applications.

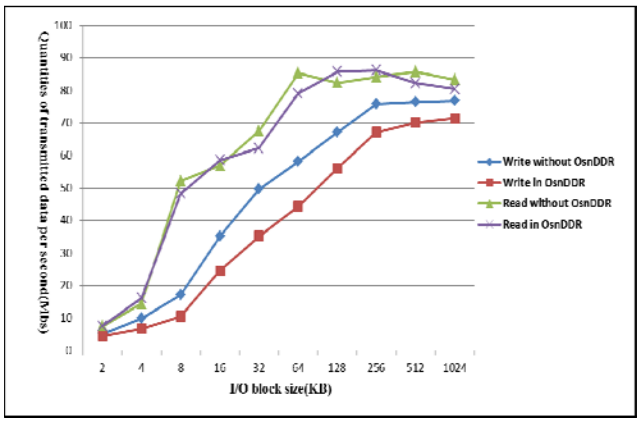

FIG. 2 PERFORMANCE OF READING AND WRITING

First of all, in Gigabit network environment, the source volume in production center is mapped to the client. The client runs software named iometer to obtain the reading and writing performance without the disaster tolerant relationship. Secondly, the source volume is configured on (2, 4) mode relationship, logging the reading and writing performance of source volume after configurition. The results are shown in fig. 2.

According to the fig. 2, the reading performance of volume is better than writing performance. The configuration of NewDDR exerts little influence on the reading performance, while the writing performance would be degraded to some extent, but the ratio is relatively low, so NewDDR can guarantee the normal operation of the application.

Performance Test of Encoding

This group of experiments presents the performance testing of encoding by RS erasure code. Firstly, disaster tolerant relationship is configured, but all operations of encoding in this relationship must be carried out in a disaster tolerant center. We use the software named dbgview to count the encoding time of different sizes of I/O block in disaster tolerant center 1. The results are shown in table 3.

TABLE 3 COMPARISON OF PERFORMANCE

I/O block size(KB)	(2,4) encoding time(s)	(3,6) encoding time(s)
2	0.000294	0.000456
4	0.000522	0.000898
8	0.001618	0.00221
16	0.004043	0.006154
32	0.016	0.022458
64	0.037234	0.052125
128	0.06726	0.10326
256	0.26809	0.369852
512	0.573648	0.71336
1024	0.926897	1.43251

As can be seen from the above results, with the increasing number of disaster tolerant center in disaster tolerant relationship, the encoding time also increases.

Conclusions

This paper designs and implements a distributed disaster tolerant system based on information decentralization algorithm. The system, called NewDDR, can ensure the safety of the source data in the case of multi-node damage. Experiments show that, NewDDR can guarantee the normal operation of the user's application and ensure source data security under the conditions of multi-node damage.

REFERENCE

Baker A H. The Windows 2000 device driver book: a guide for programmers. Prentice Hall Professional. 2001.

EMC. EMC SRDF: Zero data loss solution for extended distance replication. Technical Report. 2009.

Internet Small Computer Systems Interface (iSCSI). http://tools.ietf.org/html/rfc3720.

Lawler C M, Harper M A, Szygenda S A, et al. Components of disaster-tolerant computing:analysis of disaster recover, IT application downtime and executive visibility.International Journal of Business Information Systems. 2008,3(3):317-331.

Orwick P, Smith G. Developing Drivers with the Microsoft Windows Driver Foundatin. Microsoft Press. 2007.

Roman D, Keller U, Lausen H, et al. Web Service Modeling Ontology.Applied Ontology. 2005,1(1):77-106.

Symantec. Veritas Volume Replicator Option by Symantec-A Guide to Understanding Volume Replicator. Engineering White Paper. 2006.

Zhu G, Liangchen Z, Guonian L. The access control technology of spatial data files based on file system filter driver. 2008 11th IEEE International Conference on Communication Technology Proceedings. Hangzhou. 2008:734-737.

DOI: 10.14355/ijcsa.2014.0301.12

Interval Regression Model Using $L(p,q)$-Estimator

Mahshid Namdari[1], Seung Hoe Choi [2*]

[1] Department of Biostatistics, Faculty of Paramedical Sciences, Shahid Beheshti University of Medical Sciences, Tehran, Iran

[2] School of Liberal Arts and Sciences, Korea Aerospace University, Koyang, South Korea

[1]namdari_mahshid@yahoo.com; *Corresponding author: shchoi@kau.ac.kr

Abstract

In this paper we introduce an interval regression model, having interval coefficients and crisp input data, and propose a $L(p,q)$-estimator for the interval coefficients. The $L(p,q)$-estimator uses one L_p-norm to estimate the left end point of the interval coefficients and independently another L_q-norm for the width of the intervals. Two examples are presented showing how the results of the regression model vary as we change p and q which implies we need to find the "best" p and q. An error measure is defined and we use response surface methodology to search for the optimal values for p and q to minimize this error.

Keywords

Interval Regression Models; $L(p,q)$ -estimator; Symmetric Difference

Introduction

An interval regression model is expressed as

$$Y(\mathbf{x_i}) = A_0 + A_1 x_{i1} + \cdots + A_p x_{ip}, i = 1, 2, \cdots, n,$$

where $\mathbf{x_i} = (1, x_{i1}, \cdots, x_{ip})$ is a p-dimensional input vector and $A_i = \{x : l_i \le x \le r_i\}$ is an interval coefficient, $Y(\mathbf{x_i})$ is a predicted interval corresponding to the input vector $\mathbf{x_i}$.

Several methods were presented to estimate the interval regression model, initially developed by Tanaka[(Tanaka et al. 1982, 1987, 1989)]. Tanaka and Hong [(Tanaka and Lee, 1989), (Hong and Hwang, 2005)] proposed numerical methods that minimize the length of the estimated interval output, while Inuiguchi , Yoon and Choi [(Inuiguchi et al. 2001), (Yoon et al. 2010), (Choi and Buckley, 2006)] studied on statistical methods that minimize the difference between the estimated and observed interval outputs.

The interval least squares regression model, which was used by Inuiguchi and Yoon [(Inuiguchi et al. 2001), (Yoon et al. 2010)], is the one which applies the least squares method used in ordinary regression models to interval regression models. While, Choi [(Choi and Buckly, 2006)] applied least absolute deviation method for defining the distance and to generalize it in interval regression models. They compared its performance with least square estimators when the data contains interval outliers.

Hladik [Hladik and Cerny, 2012)] proposed a method which was motivated by tolerance analysis in linear systems. Interval regression analysis was investigated by using support vector machines by some researchers; see e.g. [(Chuang, 2008), (Hao, 2009), (Huang and Kao, (2009)].

The method of least square based on the L_2-norm has been one of the most popular techniques in the statistical inference of regression parameters. However, the least square estimators are known to be sensitive to departure from the assumption of normally distributed error. To overcome this lack of robustness, which means slightly affected either by a small number of gross errors or by a high number of small errors, a L_p-norm estimation method introduced in the regression analysis by Nyquist and Gonin [(Nyquist, 1983), (Gonin and Money, 1989)], was investigated for different values of p. The least absolute deviation estimator, the least squares estimator and the minimax estimator are particular cases of L_p-norm estimators, namely when $p = 1$, $p = 2$, $p = \infty$, respectively.

In this paper we introduce an interval regression model with interval regression coefficients and output. We propose a new interval estimator, which is based on $L(p,q)$-norms, to construct the interval regression model. Also, Two examples are given to evaluate the performance of the proposed interval regression models for different values of p and q. We also search for the optimal values for p and q.

Interval Regression Model

In this section we first consider an interval regression model, which is represented by the left endpoint and the width of the interval regression coefficient. For this, let $w_i = r_i - l_i$ denote the width of the interval A_i. Since the interval A_i can be represented as

$$A_i = [l_i, r_i] = l_i + [0, w_i],$$

we can rewrite the interval regression model as follow

$$Y(\mathbf{x_i}) = \sum_{j=0}^{p} l_j x_{ij} + \sum_{j=0}^{p} [0, (r_j - l_j)x_{ij}],$$

where $x_{i0} = 1$ and $x_{ij} \geq 0$.

In this paper we consider the following interval regression model:

$$\begin{aligned} Y_i &= Y(\mathbf{x}_i) + E_i \\ &= f(\mathbf{x}_i, L) + g(\mathbf{x}_i, W) + E_i, \end{aligned}$$

where Y_i is an observed interval with the left endpoint y_i^l and width y_i^w, f and g are real-valued functions, E_i is an interval error with the left endpoint e_i^l and width e_i^w, $L = (l_0, \cdots, l_p)$, $W = (w_0, \cdots, w_p)$. If f and g are the same the linear function, the above interval regression is the same as the interval linear regression model given by Tanaka. That is, the interval linear regression model is an important special case of our proposed model.

Now, we consider a method to estimate the interval regression model. The interval error can be expressed as

$$\begin{aligned} E_i &= e_i^l + [0, e_i^w] \\ &= y_i^l - f(\mathbf{x}_i, L) + [0, y_i^w] - [0, g(\mathbf{x}_i, W)]. \end{aligned}$$

And by separating the above equations into number term and interval term we have two equations as follows:

$$y_i^l = f(\mathbf{x}_i, L) + e_i^l. \quad (1)$$

$$[0, y_i^w] = [0, g(\mathbf{x}_i, W)] + [0, e_i^w]. \quad (2)$$

We use a distance between numbers and between intervals to construct the interval regression model. A famous mathematitian named Minkowski introduced the L_p-norm as the distance between numbers, and Heilpern [(Heilpern, 1997)] defined the distance between intervals using the Minkowski distance defined on a two-dimensional space R^2. The distance between interval $A_i = [l_i, r_i]$ and $A_j = [l_j, r_j]$ is the following real function;

$$d_p(A_i, A_j) = \begin{cases} 2^{-\frac{1}{p}} (|l_i - l_j|^p + |r_i - r_j|^p)^{\frac{1}{p}}, & \text{if } 1 \leq p < \infty, \\ max\{|l_i - l_j|, |r_i - r_j|\}, & \text{if } p = \infty. \end{cases}$$

We may adopt the method of minimizing the distance between the left endpoints of the intervals and between the widths of the intervals in order to minimize the sum of the distances between the predicted and the actual interval output. Therefore, we can introduce a new method using L_p-norms to construct the interval regression model. When crisp input data and interval output data are given as

$$\mathbf{x_i} = (x_{i1}, \cdots, x_{ip}) \quad \text{and} \quad Y_i = [y_i^l, y_i^r],$$

an interval regression estimator using a L_p-norm for estimating left endpoints and a L_q-norm for estimating widths based on $(\mathbf{x}_i : Y_i)$, denoted by $(\hat{L}^p, \hat{W}^q)$, is defined as the values minimizing the following functions

$$\begin{cases} \sum_{i=1}^{n} \left| y_i^l - f(\mathbf{x}_i, L) \right|^p, & \text{if } 1 \leq p < \infty, \\ \max\left\{ \left| y_i^l - f(\mathbf{x}_i, L) \right| : i = 1, \cdots, n \right\}, & \text{if } p = \infty, \end{cases} \quad (3)$$

and

$$\begin{cases} \sum_{i=1}^{n} \left| y_i^w - g(\mathbf{x}_i, W) \right|^q, & \text{if } 1 \leq q < \infty, \\ \max\left\{ \left| y_i^w - g(\mathbf{x}_i, W) \right| : i = 1, \cdots, n \right\}, & \text{if } q = \infty, \end{cases} \quad (4)$$

subject to

$$w_j \geq 0 \text{ for each } j,$$

where $y_i^w = y_i^r - y_i^l$.

Thus, the interval regression model using L_p-norms and L_q-norms simultaneously (IR(p,q)) is as follows:

$$\hat{Y}_i^{pq} = \left[\hat{y}_i^{l\,pq}, \hat{y}_i^{r\,pq} \right] = \left[f(\mathbf{x}_i, \hat{L}^p), f(\mathbf{x}_i, \hat{L}^p) + g(\mathbf{x}_i, \hat{W}^q) \right].$$

Specially, when $p = q = 1$, $p = q = 2$, and $p = q = \infty$, we will call the results $(\hat{L}^1, \hat{W}^1), (\hat{L}^2, \hat{W}^2)$ and $(\hat{L}^\infty, \hat{W}^\infty)$ as the interval least absolute deviation estimator, the interval least square estimator, and the interval minimax estimator, respectively.

The following example shows the IR(1,1) model, IR(2.2) model and IR(∞, ∞) model for the numerical values used by previous researchers.

Example 1. Table 1 lists the numerical values by Tanaka and Chen [(Tanaka and Watada, 1988), (Chen, 2001)] to handle an outlier problem. Like a method suggested by Yoon [(Yoon et al., 2010)], we use a response function for the left endpoint and the width as follows:

$$f(x_i, L) = l_0 + l_1 x_i$$

and

$$g(x_i, W) = w_0.$$

The right half of Table 1 explains that the intersection of the observed and estimated interval outputs using

our proposed method corresponding to each crisp input are not empty.

TABLE 1 DATA AND ESTIMATED OUTPUT IN EXAMPLE 1

Input	Output	Estimated Output		
x_i	Y_i	IR(1,1)	IR(2,2)	IR(∞,∞)
1	[6.2, 9.8]	[3,7.5]	[4.1, 9.1]	[4.1, 8.7]
2	[4.2, 8.6]	[4.9, 9.5]	[5.9, 10.9]	[5.9, 10.5]
3	[6.9, 12.1]	[6.9, 11.5]	[7.7, 12.6]	[7.7, 12.2]
4	[10.9, 16.1]	[8.9, 13.5]	[9.5, 14.4]	[9.5, 14]
5	[10.6, 15.4]	[10.8, 15.4]	[11.3, 16.2]	[11.2, 15.8]
6	[12.9, 17.5]	[12.8, 17.4]	[13.1, 18]	[13, 17.6]
7	[14.8, 19.2]	[14.8, 19.4]	[14.8, 19.8]	[14.8, 19.4]
8	[14.5, 24.1]	[16.8, 21.3]	[16.6, 21.6]	[16.6, 21.2]
9	[18.2, 22]	[18.7, 23.3]	[18.4, 23.4]	[18.4, 23]
10	[22.3, 26.3]	[20.7, 25.3]	[20.2, 25.2]	[20.2, 24.8]

In Example 1, the estimated interval outputs obtained by using the three estimators are all different. Example 1 indicates that we have to investigate a performance of the interval regression model for different values of p and q.

Optimal IR(p,q) Model

The interval regression model using a L_p-norm and a L_q-norm at the same time IR(p,q) changes according to varying values of p and q as we showed in Example 1. This section suggests a criterion to investigate the performance of the IR(p,q) model, and presents a response surface methodology to find an optimal IR(p,q) model.

Yoon [(Yoon et al., 2010)] introduced the length of the symmetric difference between intervals to compare interval regression models. The length of the symmetric difference for intervals A_i and A_j, denoted by $l(A_i \Delta A_j)$, is equal to

$$l(A_i \Delta A_j) = \begin{cases} |l_i - l_j| + |r_i - r_j|, & \text{if} A_i \cap A_j \neq \varnothing, \\ (r_i - l_i) + (r_j - l_j), & \text{if} A_i \cap A_j = \varnothing. \end{cases}$$

Now, we consider the following measure as a criterion to investigate the performance of a interval regression model

$$M_Y = \sum_{i=1}^{n} M_{\hat{Y}_i}$$

where

$$M_{\hat{Y}_i} = \begin{cases} \dfrac{m(Y_i \Delta \hat{Y}_i)}{l(Y_i)}, & \text{if} \quad l(Y_i) > 1 \\ m(Y_i \Delta \hat{Y}_i), & \text{if} \quad l(Y_i) \le 1, \end{cases}$$

where $m(Y_i \Delta \hat{Y}_i) = l(Y_i \Delta \hat{Y}_i) + \min\{|s - \hat{s}| : s \in Y_i \text{ and } \hat{s} \in \hat{Y}_i\}$ and $l(Y_i)$ denotes a length of the interval Y_i. Then, the performance of interval regression models can be compared using the measure M_Y.

Now we consider a method to find suitable exponents p and q when the value of p and q are unknown. Since the proposed criterion M_Y, based on length of the symmetric difference between the estimated and the observed interval outputs, depends on values p and q, we regard the measure M_Y equal to a function relationship $F(p,q)$ between the value p and q. In order to suggest an optimal IR(p,q) model which has less error than another interval regression model we have to develop a good approximation for the function $F(p,q)$ because the form of the function $F(p,q)$ is unknown. For this we consider a response surface methodology(RSM) which searches for the input combination optimizing the output of real system or its simulation. The RSM is a collection of statistical and mathematical techniques useful for developing, improving, and optimizing a process [(Myers and Montgomery, 2002)]. In this paper we use a Minitab program to obtain response surface result. The regression procedure in the Minitab program uses the method of least squares to fit quadratic response surface regression model which focuses on characteristics of the fit response function and in particular, where optimum estimated response values occur. The steps in this paper for finding the optimal exponents p and q are as follows:

1. The value of p and q are chosen randomly from the uniform distribution.

2. Estimate the interval regression coefficient $\hat{L}^p$ and $\hat{W}^q$ using equations (3) and (4).

3. Predict the shape of the response surface function $F(p,q)$ using the regression procedure in the Minitab program.

4. Find the optimal values $\hat{p}$ and $\hat{q}$ satisfying as

$F(\hat{p},\hat{q}) \le \max\{F(p,q), F(\infty,\infty)\}$ for $(p,q) \in [1,\infty) \times [1,\infty)$.

The following example shows the optimal interval regression model for the numerical values used in Example 1.

TABLE 2 EXPONENT AND ERROR IN EXAMPLE 2.

p	q	M_Y	p	q	M_Y	p	q	M_Y
8	3	5.34	20	16	6.44	12	18	6.5
20	6	6.16	18	19	7.12	19	2	5.02
1	9	5.83	14	17	6.93	17	4	6.21
19	10	6.73	6	2	4.93	7	15	6.58
2	4	5.54	8	16	6.56	5	1	4.75
2	5	5.78	6	8	6.35	2	8	6.15
12	8	6.27	10	11	7.25	8	8	6.34
2	5	5.78	18	10	6.96	1	1	4.72
9	7	6.27	8	20	6.59	2	2	4.85

Example 2. The data in Table 2 shows results of

choosing randomly from the descrete uniform distribution $U[1, 20]$ and the error M_Y corresponding to each p and q.

By response surface analysis using the regression procedure in the Minitab program for the data in Table 2 we obtain a response surface as

$$F(p,q) = 4.251 + 0.072p + 0.298q - 0.003p^2 + 0.001pq - 0.011q^2,$$

where a P-value is less then 0.001 and $R^2 = 0.9$. The surface of $F(p,q)$ is presented in Fig. 1. The Second Derivative test (Stewart, 2007) show that $F(p,q)$ has a maximum at $(14.37,14.22)$. The graph of the function $F(p,q)$ using Matlab and the test of Second derivative imply that $F(p,q)$ has a minimum point at (∞,∞).

$F(p,q)$ has a minimum point 4.63 at (∞,∞) from equation (3) and (4). So, we believe that the IR(∞,∞) model is an optimal model for the data in Table 2. This surface is really just the first step in the response surface technique.

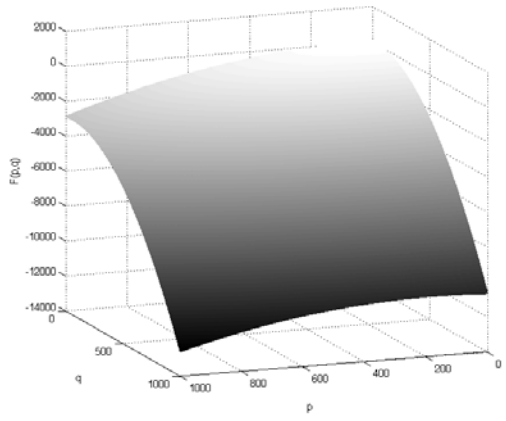

FIG. 1 THE SURFACES OF $F(p,q)$ IN EXAMPLE 2.

Example 3. In this example we use data of speed and surface roughness in [10] (See Table 3).

TABLE 3 DATA IN EXAMPLE 3.

Input	Output
x_i	Y_i
1	[0.19, 0.29]
1.5	[0.24, 0.32]
2	[0.20, 0.27]
2.5	[0.20, 0.46]
3	[0.22, 0.38]
3.5	[0.22, 0.33]
4	[0.35, 0.56]
4.5	[0.37, 0.60]
5	[0.41, 0.89]

The values of M_Y for a random selection of p and q from the response function for the left endpoint $f(\mathbf{x}_i, L) = l_0 + l_1 x_{i1} + l_2 x_i^2$ and the width $g(x_i, W) = w_0 + w_1 x_i$, are given in Table 4.

TABLE 4 EXPONENT AND ERROR IN EXAMPLE 3.

p	q	M_Y	p	q	M_Y	p	q	M_Y
1	1	0.786	19	1	1.81	17	7	1.92
2	2	0.714	15	11	2.11	3	1	0.74
2	1	0.755	18	12	2.22	19	15	2.26
5	2	0.706	5	14	0.78	17	14	2.22
12	9	1.8	18	3	1.91	11	8	1.73
13	6	1.84	12	14	2.09	2	14	0.78
2	18	0.81	2	13	0.78	11	13	1.72
8	16	1.19	15	18	2.17	1	11	0.81

The regression procedure in the Minitab program with the data in Table 4 gives a response function as following

$$F(p,q) = 0.504 + 0.086p + 0.031q - 0.001p^2 + 0.002pq - 0.002q^2,$$

where a P-value is less then 0.0001 and $R^2 = 0.95$. The surface of $F(p,q)$ for example 3 is presented in Fig. 2. The Second Derivative test shows that $F(p,q)$ has a maximum at $(101.5,58.5)$. Since it is difficult to find a minimum foint of the $F(p,q)$, we can use a finite set of integers for p and q such as

$$A = \{\{(p,q) \mid 1 \le p \le 20, 1 \le q \le 20, p,q \in Z\} \cup \{(-\infty,+\infty)\}\}.$$

So, by this set $F(p,q)$ has a minimum at $(1,20)$.

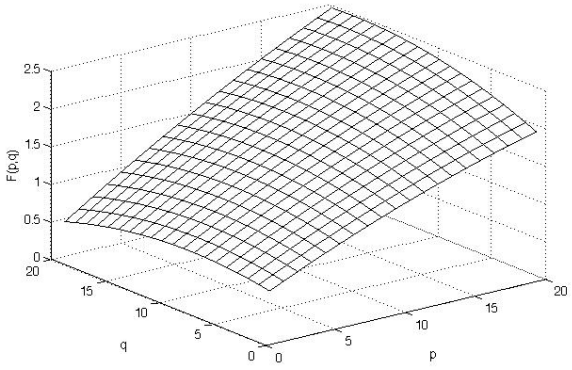

FIG. 2 THE SURFACES OF $F(p,q)$ IN EXAMPLE 3.

Summary and Conclusions

We studied an interval regression model having crisp input, interval coefficients and interval output. To estimate the interval regression model we separately estimate the left end points of the interval coefficients using one L_p -norm and another L_q -norm for the widths of the interval coefficients. We called this a $L(p,q)$-estimator.

It is obvious that the predicted interval output and the error in the model will vary considerably as we vary p and q form one to ∞ and we showed this result in our first example. This leads us to the question: "what

are the best values for p and q?" The optimal values will minimize the error in the model. We defined an error measure E and E will be a function of p and q, or $E = F(p,q)$ for unknown function F.

We found the optimal interval regression model IR(p,q) by using the $L(p,q)$ -estimator and the response surface methodology. Response surface methodology is now the technique which can be employed to search for the values of p and q to minimize the response function F. The same example is continued and we tentatively choose $p = q = \infty$, the minimax estimator, as optimal. We showed that the IR(1, 20) is an optimal model for data of speed and surface roughness.

For furthure studies we will consider how to find the optimum values of p and q in IR(p,q).

REFERENCES

Chen, Y.S. "Outliers detection and confidence interval modification in fuzzy regression". Fuzzy Sets and Systems, 119,259-272, 2001.

Choi, S.H. and Buckley, J. "Fuzzy regression using least absolute deviation estimators". Joint Conference on Information Sciences, JCIS, Kaohsiung, Taiwan, 2006.

Chuang, C. "Extended support vector interval regression networks for interval input output data". Information Science, 178(3),871-891,2008.

Diamond, P. and Tanaka, H. "Fuzzy regression analysis", in Fuzzy sets in Decision analysis, Operation Research and Statistics, Kluwer, MA,349-387, 1998.

Gonin, R. and Money, A.H. "Non-linear L_p -norm estimation". Dekker, New York (1989).

Hao, Y. "Interval regression analysis using support vector networks". Fuzzy Sets and System 160(17), 2466-2485,2009.

Heilpern, S. "Representation and application of fuzzy numbers". Fuzzy Sets and Systems, 91,259-268,1997.

Hladak, M. and Cerny, M. "Interval regression by tolerance analysis approach". Fuzzy Sets and systems, 193,85-107,2012.

Hong, D.H. and Hwang, C. "Internal regression analysis using quadratic loss support vector machine". IEEE Transactions on Fuzzy Systems, 13,229-237, 2005.

Huang, C.H. and Kao, H.Y. "Interval regression analysis with soft-margin reduced support vector machine". Lecture Notes in Computer Science, vol. LNAI 5579, 826-835, 2009.

Inuiguchi, M., Fujita, H. and Tanino, T. "Interval linear regression analysis base on Minkowski difference". Proc. International Conference on Information Systems. Analysis and Synthesis, 7, 112-117, 2001.

Myers, R. H. and Montgomery, D. C. "Response surface methodology". John Wiley and Sons, New York, NY 2002.

Nyquist, H. "The optimal L_p -norm estimators in linear regression models". Communication of Statistics-Theory and Method, 12,2511-2524,1983.

Stewart, James., Essential calculas. Thomson Press, 2007.

Tanaka H. and Watada J., "Possibilistic linear systems and their applications to the linear regression model". Fuzzy Sets and Systems, 27,275-289, 1988.

Tanaka, H. and Lee, H. "Interval regression analysis by quadratic programming approach". IEEE Transactions on Fuzzy Systems, 6,473-481,1998.

Tanaka, H., Hayashi T., and Watada J. "Possibilistic linear regression analysis for fuzzy data". European Journal of Operational Research, 40,389-396, 1989.

Tanaka, H., Hayashi, T., and Watada J.,"Interval regression analysis". 3rd Fuzzy System Symposium, 9-12,1987.

Tanaka, H., Uejima, S., and Asai, K. "Linear regression analysis with fuzzy model". IEEE Trans. Systems. Man Cybernet, 12,903-907,1982.

Yoon, J. H., Jung, H. Y., and Choi, S.H. "Interval regression using symmetric difference". Fuzzy Systems and Knowledge Discover, Shandong, 478–482, 2010.

Mahshid Nmadari obtained his M.S. in Biostatistics from Shiraz University of Medical sciences, Iran in 2007. Currently, she is a PhD candidate in Biostatistics at Shahid Behesti University of Medical Sciences, Iran.

Seung Hoe Choi obtained his PhD in Mathematics from Yonsei University, South Korea in 1994. Currently, he is a Professor at the School of Liberal Arts and Sciences, Korea Aerospace University, South Korea.

International Journal of Computer Science and Application (IJCSA) Volume 3 Issue 1, February 2014 www.ij-csa.org
DOI: 10.14355/ijcsa.2014.0301.13

Modern CAD Technique to Design Gyrocompass for UAVs and Robot, Ships, Aircrafts Navigation Systems

M. S. Zaghloul

Arab Academy for Science, Technology, and Maritime Transport, Electronic, Communication Department[2], P.O.1029, Alex, Egypt

dr_mszaghloul@yahoo.com

Abstract

This paper concerns the practical design and implementation of gyrocompass required for operation of all installed navigation equipments on robot, aircrafts, ships, also for UAVs. Most navigation systems today use some type of compass to determine heading direction. Using the Earth Õs magnetic field, electronic compasses based on magneto-resistive (MR) sensors can electrically resolve better than 0.1 degree rotation and accuracy from 1 to 2 degree. Most of installed equipment on aircrafts, ships, and spaceship are form of computer-based navigation information system that complies with International regulations. These equipments can be Global position System (GPS), Radar, speed, direction, electronic chart display, height finder for aircrafts and spaceship, echo sounder for ships etc. In our design, Compass Module was utilized with Honeywell's HMC5883L 3-Axis Magnetometer, I²C, 2.7-6.5V, TTL-USB and microcontroller 16F877. For programming of the microcontroller, software PIC Basic pro was used, a window based Software. We are trying to use a cheap and good resolution within a small size Using Anisotropic Magneto resistive (AMR) technology that provides advantages over other magnetic sensor technologies. These anisotropic, directional sensors feature precision in-axis sensitivity and linearity. These sensors' solid-state construction with very low cross-axis sensitivity is designed to measure both the direction and the magnitude of Earth's magnetic fields, from milli-gauss to 8 gauss. The complete designed system has three outputs, the first one is USB port friendly user interface, the other two outputs are control logic state outputs. We used the designed gyro output to interface with Radar display so the targets direction can be measured in true mode instead of relative mode; as well, our designed module was employed in car protection in driver safety.

Keywords

Microprocessor; CAD; Ship Control, Radar; Signal Processing; Sensors

Introduction

From very long time, the magnetic compass has been used in navigation. It appears that Mediterranean seamen of the 12th century were the first to use a magnetic compass at sea

Today, the balanced needle compass is only a slight variation of this early discovery. In our design, we make use of advances in technology that have led to the solid state electronic compass based on MR magnetic sensors and acceleration based tilt sensors. In our design, he Honeywell HMC5883L is implemented which is a surface-mount, multi-chip module designed for low-field magnetic sensing with a digital interface for applications that enables 1° to 2° compass heading accuracy. Plus a friendly user interface USB which can be used with any equipment fitted with USB port; moreover, we use the micro controller 16 F877. The I²C serial buses for the gyro allows for easy interface. The gyro sensor converts any magnetic field into a differential voltage output on three axes. This voltage shift is the raw digital output value, which then can be used to calculate headings or sense magnetic fields coming from different directions. Output of the gyro compass is fed to the microcontroller that is programmed using Basic pro which allows accepting the data from the gyro module, then we have three outputs from the microcontroller, one output to the TTL-USB, and the other two outputs are fed to two transistors which will give control using two relays. Compasses are commonly used with accelerometers, where the data from both the compass and accelerometer can provide extended information to compensate for any tilt of the compass because the reading is affected if the compass is not level. The Memsic 2125 Dual-axis Accelerometer and MMA7455 3-Axis Accelerometer Module are available companion accelerometers for the 3-Axis Compass module. Newer solid state accelerometer tilts sensors that measure the earth Õs gravitational field by means of an electromechanical circuit.

The Compass Module with 3 –Axis HMC5883L

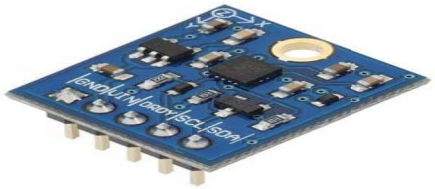

FIG.1 COMPASS MODULE WITH 3 –AXIS HMC5883L

This is a breakout board for Honeywell's HMC5883L, a 3-axis digital compass. Communication with the HMC5883L is simple and all done through an I²C interface. This model can measures the earth's magnetic field in three axes, with 1–2 degree accuracy, providing individual readings for each axis, which may be used separately or together for 3D calculations, and measures raw strength (gauss) of a nearby magnetic source. The 3-Axis Compass module measures magnetic fields in three directions–or axes, labelled X, Y, and Z. In its most simple form, the module can be used as a basic compass to find earth's magnetic north. The compass module can also sense the relative strength of a nearby magnetic source, such as those caused by magnets or electric fields. As the sensor detects magnetism in three dimensions, relative distance and direction to these sources can be determined. One application of adding an accelerometer is to compensate for any tilt of the compass. As with most compasses, the reading is affected if the compass is not level. The Mimic 2125 Dual-axis Accelerometer and MMA7455 3-Axis Accelerometer Module are good companion accelerometers for the 3-Axis Compass module. The International Geomagnetic Reference Field (IGRF) is a series of mathematical models describing the earth's field and its time variation

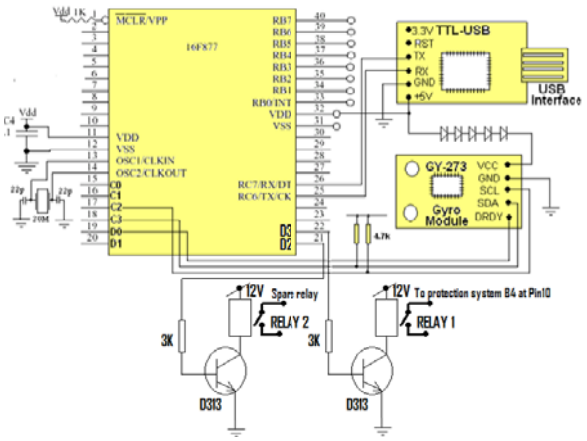

FIG. 2 GYRO COMPLETE CIRCUIT DIAGRAM

The System Design

The designed system is 3-axis digital compass. We are trying to use a cheap and good resolution with a small size. The Used Anisotropic Magneto-resistive (AMR) technology provides advantages over other magnetic sensor technologies. These anisotropic, directional sensors feature precision in-axis sensitivity and linearity. These sensors' solid-state construction with very low cross-axis sensitivity is designed to measure both the direction and the magnitude of Earth's magnetic fields, from milli-gauss to 8 gauss.

To get the data from the module, we need I²C interface so a micro controller chip 16F877 is applied to read this data. The design includes a small PCB with Micro Chip "Pic16F877" micro controller and the supporting hardware. We get the I²C data to C_2, C_3 and an interrupt pin to D_0 to indicate data ready. Still it is required to read the data on a PC. The microcontroller is connected to TTL-USB converter to read Data from Microcontroller. Then a small 5 v power is made. To supply the Module with 3.3 volts, we applied the 5 v to 4 diodes forward to have the required voltage drop. We made an external pull up resistor (4.7K) to the SCL & SDA. The I²C software is listed as S/W 2_6, From this gyro complete circuit, we get two outputs, the first of which is from the USB and this can be fed into computer or display system to give the three reading x, y, and z where x indicates the direction, y for roll, and z for beach; while the second output is taken from D_3 and used to be fed to another circuit to control and change status, in addition, we have spare output D_2 which can be used for any other application.

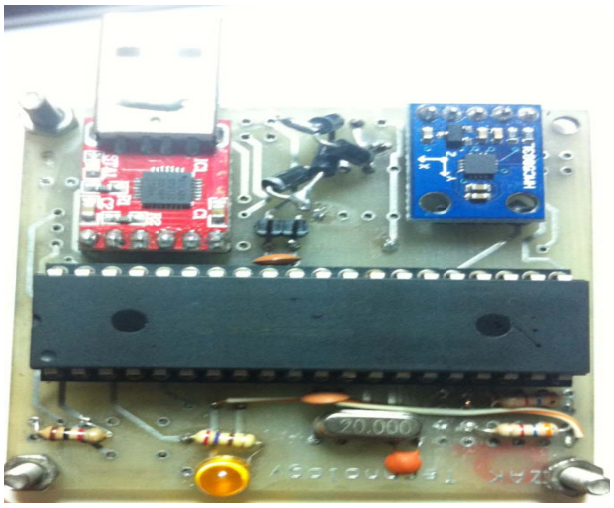

FIG. 3 FINISHED DESIGNED MODULE

The HOST Computer Software

We used a V Basic program as shown in appendix (A) or under request from the author which is mainly to read the data from module, 6 data bytes (2 for each word) which are x, y, z angles. The program has a

given name COMVB and the given three outing angles in three boxes. The rate of reading the angles by computer is every 2 seconds with width of 1-2 degree accuracy, and the real reading of the computer is shown in figure 5. Moreover, figure 6 represents Radar display with the use of our gyrocompass input via USB.

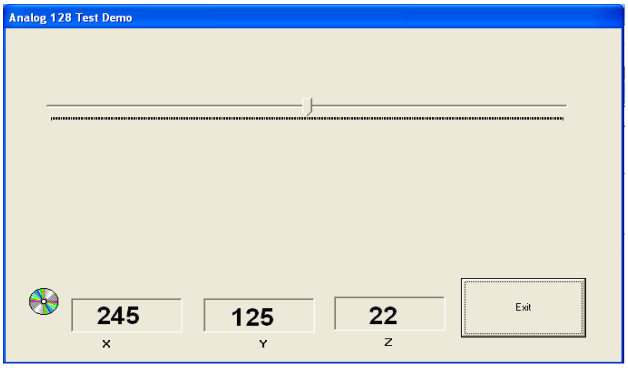

FIG. 4 READING OF 3 ANGLES X, Y AND Z ON COMPUTER DISPLAY

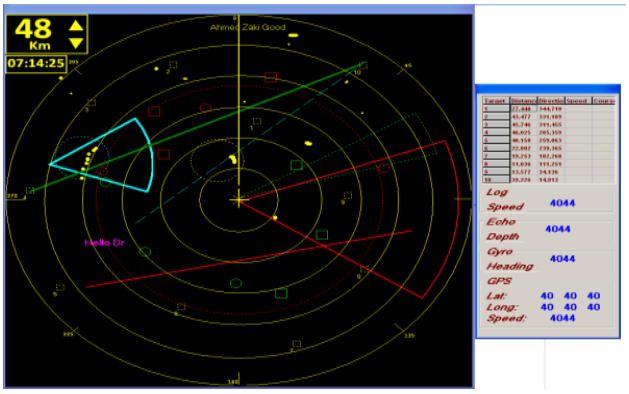

FIG. 5 RADAR DISPLAY USE GYROCOMPASS INPUT FROM USB

Our design was implemented in two application, the first of which is in design of open architecture system to reduce the likelihood of a vehicle getting stolen or carjacking and driver safety in which e the gyro is employed to detect the sleep of the driver, the second application is in Radar display which will be shown and explained in next part of the paper. By applying the gyro output from the USB port, all the target direction can be read with respect to the true north (north up), and when the this input is stopped, all our reading for the tracks direction will be in relative to ships heading (ships head up), and the target directions will be from 00 to 1800 right (green) or left (red).

Practical Implementation of the Gyrocompass Output to a Ship Navigation Radar.

We used to have a view of a relative motion display i.e. the ships heading is the zero angle for display as shown in Fig. 6.

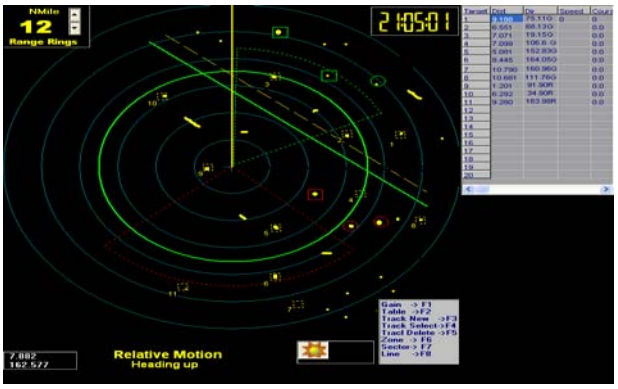

FIG. 6 RADAR DISPLAYNOT USE GYROCOMPASS INPUT

When gyro is implemented after 40 mints of operation as a hard ware and soft ware in the display program, a true motion display can be obtained in which North is taken as the zero angles for the display, which is more realistic and easier to identify true target angle and locations regardless of our ship heading. This is indicated in Fig. 7, and it is noticed that all targets and graphics are rotated by the gyro heading angle being 90 degrees, which is the gyro reading at that time.

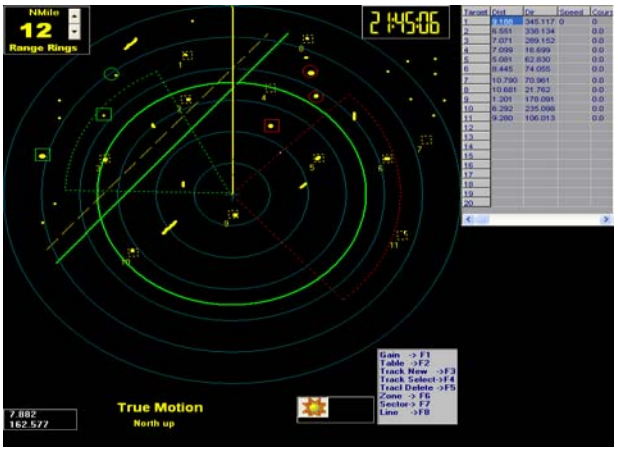

FIG. 7 RADAR DISPLAY WHEN GYROCOMPASS INPUT IMPLEMENTED

Conclusions

The designed system is friendly user with TTL USB interface, most sensitive, reliable low-field sensors in the industry, and low cost gyro having a one degree accuracy requirement due to the choice for the HMC5883L utilizing Honeywell's Anisotropic Magneto-resistive (AMR) technology that provides advantages over other magnetic sensor technologies. It is available to have directional sensors feature precision in-axis sensitivity and linearity. These sensors' solid-state construction with very low cross-axis sensitivity is designed to measure both the direction and the magnitude of Earth's magnetic fields, from milli-gauss to 8 gauss. We can electrically resolve better than 0.1 degree rotation and accuracy from 1 to

2 degree. Adding to that for tilt compensation, an accelerometer needs to be used along with this module. A low cost compass has been discussed here having a one degree accuracy requirement. At the heart of the compass is a three-axis MR magnetic sensor. If a compass system has a requirement higher than one degree of accuracy, then it is important to break down the error caused by the tilt sensor and the magnetic sensor and it is determined that the level of signal processing is required. [3] The designed compass can be used in car protection for driver safety and with Radar display where relative motion picture of the displayed tracks is obtained.

REFERENCES

A Dual Axis Tilt Sensor Based on Micro machined Accelerometers, Mike Horton, Charles Kitchin, Sensors Magazine, April, 1996.

Applications of Magneto resistive Sensors in Navigation Systems Michael J. Caruso, Honeywell Inc.

Applications of Magnetic Sensors for Low Cost Compass Systems Michael J. Caruso Honeywell, SSEC.

National Geomagnetic Information Centre, website URL http://geomag.usgs.gov/.

National Geophysical Data Centre, website URL http://www.ngdc.noaa.gov/.

Sensor Products Data Sheet, "1 and 2 Axis Magneto-resistive Microcircuits", Honeywell SSEC, 5/99, <www.magneticsensors.com>.

The Ship's Compass Grant, George A, and Klinkert, John. , 2d ed. (1970).

1st international conference on computer science and application (ICOCSA 2014). January 10 to 11, Indianapolis, Indiana, USA, 2014, M. S. Zaghloul .

International Journal of Computer Science and Application (IJCSA) Volume 3 Issue 1, February 2014 www.ij-csa.org
DOI: 10.14355/ijcsa.2014.0301.14

Technology Adoption and Trademarks

Ayesha Saleem, Kiyohide Higuchi

Graduate School of Global Information and Telecommunication Studies

Waseda University , Tokyo Japan
dua@fuji.waseda.jp

Abstract

Technology adoption in industries and firms is the current quest. Business sector growth the questionable in the global market. Intellectual Property (IP) rights data is the indicator for the research and development in the business sector. Patents have gained attraction as indicator by researchers to analyses technology adoption, Research and Development (R&D) and the economic growth. However, trademark is relatively new concept to use it for economic analysis. Trademarks are the most prominent type of Intellectual Property used in most of the developed and developing countries. The analysis used secondary data from different sources. We downloaded trademarks data from the WIPO (World Intellectual Property Organization), Goods and Services data from the United Nations Statistics Division, and OECD database.

This study is important in spite of its measurement difficulties. This study is in depth analysis of the trademarks that distinguishes the role of trademarks as technology adoption indicator. This study is twofold. Firstly, describes the details about trademark classification. Secondly, it indicates the technology adoption trend by using trademark data.

Keywords

Technology Adoption; Industries/Firms; Trademarks; Economic Development;

Introduction

Many economic studies have found that technology adoption is faster in some industries than others. The reason behind is the industry characteristics. Industry characteristics include business, technology, behaviour, product quality, demand and research & development. Some researcher used patents to evaluate the industry characteristics. The patent is the major indicator of the innovation. However, trademark can be used to measure the business growth in the specific industry.

"A trademark is a distinctive sign which identifies certain goods or services as those produced or provided by a specific person or enterprise. Trademarks may be one or a combination of words,letters, and numerals. They may consist of drawings, symbols, three dimensional signs such as the shape and packaging of goods, audible signs such as music or vocal sounds, fragrances, or colours used as distinguishing features".Trademark can be any sign that is suitable for distinguishing goods or services of a particular enterprise from that of other enterprises. Any owner of a registered trademark should use the mark. If a trade mark is not used within a period of five years after registration, it can be cancelled, upon request or legal action, on grounds of revocation. Trademarks are of different types. Trademark are registered under these main types such as word mark, figurative mark, word and figurative mark, three-dimensional mark, sound mark, tracer mark and others.

NICE Classification (NCL) is the international classification of goods and services for the registration of marks. Nice classification is published online by the WIPO (World Intellectual Property Organization). Nice classification is important to evaluate the trademark. Trademark applications consist of a list of goods and services to specify the type in which trademark is registering. The countries did agreement to use alphabetical list of the Nice classification for specify goods and services and classifies trademark applications received according to the Nice agreement rules. Therefore, Nice classification is a very useful tool for carrying out trademark analysis in detail.

The Central Product Classification (CPC) is an international standard for organizing and analysing data for production of industry, trade, national accounts, prices etc. CPC is the major internationally accepted classification for good and services. United Nation is managing the data for CPC Classification. "The CPC covers products that are an output of economic activities, including transportable goods, non transportable goods and services."(OECD Glossary of Statistical Terms, 2007).

Therefore, we can measure the technology adoption trend in the specific industry by using the data of

trademarks and its concordance with Nice and CPC classification.

Literature Review

There is few literature about the trademark regarding technology adoption indicator. However, many studies have utilized the patent information as the indicator of the technology adoption. Therefore, we use the patent as technology adoption literature as base of our research.

The patent is considered the important indicator for estimating the technology strength in the companies. The 0.88 correlation was found between the expert opinion of the the number of patents granted to the pharmaceutical company and the expert opinion of the technology strength (Narin & Noma, 1987).

The relationship between patent and innovation process has investigate to prove patent data as technology indicator. The studies have three differnt directions to evaluate the patent statistic as technology adoption indicator. The most important direction is to analyse the relationship of patent statistics with the technological changes and economic development. The second direction is to compare the technology adoption capacities within countries (Schiffel and Kitti, 1978; Paci & Sassu, 1997. The third direction is to evalute the outcome of the research and development activites and innovation process (Basberg, 1987; Liu and Shyu, 1997; Archibugi and Pianta, 1996; Mogee, 1991).

Patent statistics provide information on both sides the technology strength in a specific sector and the market intentions of potential competitors. The other side they have ability to perform as a useful input into strategic planning of business. "Flows of technology are reflected in part by the international pattern of patenting behaviour" (Bosworth, 1983).

Patent data has analysed the firm`s R & D capability (Liuand Shyu, 1997) and trend of foreign markets (Shipman, 1967). One study use the patent statistics to find the relationship within technology sectors and industrial sectors and in Austria. The patent data served as the indicator for measuring the inventive and innovative activity (Gassler et al., 1996).

Patent claimed data is more effective indicator for technology adoption rather to just count the number of patents (Tong and Frame, 1994). An analysis evaluate the Indian patent data to measure its suitability for assessing technology adoption trend. It is concluded that public policy measure could make the data more reliable for technology adoption in firms. (Abraham & Moitra, 2001).

The statistics is divided in two sectors, economical and product statistics. Product statistics is further divided in industry statistics and goods & services statistics. The both types of data are used for different purpose, such as the industry statistics are used for employment, investment and value added etc. While the goods statistics are used for evaluating the market condition and trend in trade (John W Houghton, Michael Pucar, Catherine Knox, 1996).

"The concordance provides a powerful tool for analysing the relationship between sectors and technologies and between technological and economic performance" Schmoch et al. (2003). However,the concordance is really difficult to understand. Therefore, very few researcher correspondence to this type of research. There are few research that show some changes in the scheme of classes (Heiko Wongel, Antonios Farassopoulos). One study analysed the linking between patent and economic activity.(Lybbert, T. and N. Zolas , 2012). An analysis focused on the structure of the Nice, ISIC and SITC. They concluded that Nice system is structured very differently it is designed to facilitate the registration of trademarks protection of their legal scope. (Lybbert, T., P. Bhattacharyya and N. Zolas, 2012).

One researcher analysed the one classification system of controlling wind motors, as the author was the searcher in this field. He compared this classification in different systems of WIPO, EPO, DPMA, JPE, USPTO, and Derwents' World Patent Index (Bernd Wolter, 2012) . Another study proposed two dimensional IT map to represent goods and industry based classification systems (John W Houghton, Michael Pucar, Catherine Knox, 1996).

Trademark as Technology adoption Indicators

Trademarks is the prominent type of Intellectual Property (IP) in developing and developed countries. In most of the countries the ratio of residents are higher than the non-resident of trade mark application. Therefore, this is very relevant to evaluation the

International Journal of Computer Science and Application (IJCSA) Volume 3 Issue 1, February 2014 www.ij-csa.org

technology adoption with respective to research and development activities. "Firms show different propensity to rely on TM and to penetrate foreign markets…..This may be due to factors such as the size of the target market, the presence and location of foreign affiliates, economies` industrial specialisation , trade agreements, and participation in global value chain."(OECD, 2013)

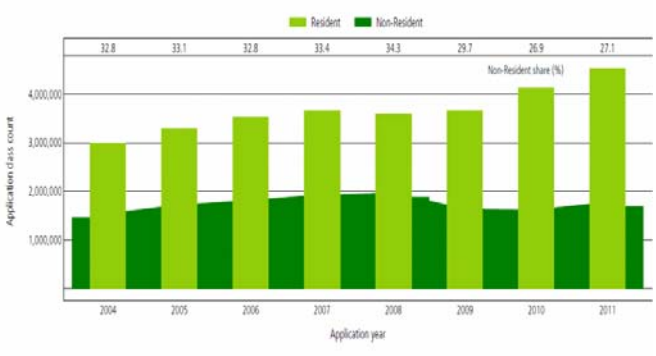

FIGURE 1: TREND IN TRADEMARK APPLICATION CLASS COUNTS FOR SELECTED OFFICES

(Source: WIPO Statistics Database, October 2013)

The trademark application has doubled from 1995 to 2011 that has become around 2 to over 4 million. The trademark application are increasing in the emerging countries such as India and Brazil the application class count is drastically increasing while in the developed and high income countries is decreasing. . (WIPO, 2013).

TABLE 1: TOP 10 CLASSES BY THE REGISTRATIONS FOR DIRECT APPLICATIONS (SOURCE: WIPO STATISTICS DATABASE)

	Class	Class Description	Number of Application
1	Class 35	Advertising; business management; business a	831118
2	Class 09	Scientific, nautical, surveying, photographic, c	742138
3	Class 41	Education; providing of training; entertainmen	527047
4	Class 42	Scientific and technological services and rese	500359
5	Class 25	Clothing, footwear, headgear.	466709
6	Class 16	Paper, cardboard and goods made from thes	384534
7	Class 05	Pharmaceutical and veterinary preparations; s	323655
8	Class 30	Coffee, tea, cocoa and artificial coffee; rice; t	278941
9	Class 03	Bleaching preparations and other substances	270597
10	Class 38	Telecommunications.	244789

Analysis

We organized the database, sort some data and use Imlinker Software(Imalinker system developed for the OECD by IDENER, Seville, 2013) to find the linking between these classes.

We used the SQL query to extract the data from the software and matched that data with the OECD database. The results of the automatic matching of software were further checked manually, in order to optimise the precision of the match and minimise false positive matches. In this step, for each Nice keyword we rank all matches according to their score and we assign a maximum score.

Further, we analysed the occurrence of different keywords in trademark applications, based on the OHIM trademark database. Then we counted the occurrence of the different key words in the Goods and Services description of OHIM trademarks.

The top 50 keywords are found in the Class 35,16,9,41, 3,18, 39, 42, 30, 29, 32 and 20.

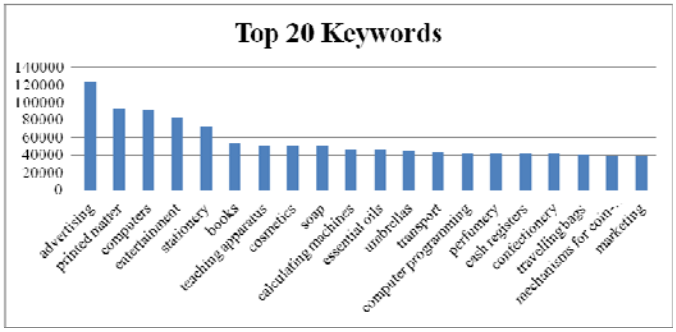

FIGURE 2: TOP 20 KEYWORDS

The keyword "advertising" belongs to class 35 and Nice ID 3632and CPC ID 3632. The trademark applications for class 35 is 204130 in OHIM database, 618417 in USPTO and 894605 in JPO database.

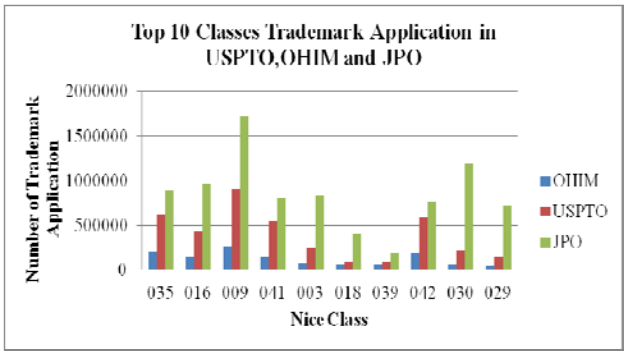

FIGURE 3: TOP 10 CLASSES

Note: In this table we count the relevant match and ignore the lower matches of the same class.

Conclusions

The purpose of this study is to use the trademark as the technology adoption indicator. The result of the trademarks by industrial sectors could be compared in order to evaluate the technology adoption trend. However, this paper is preliminary and short part of the work conducted.

ACKNOWLEDGMENT

I would like to thank the Organization for Economic Co-operation and Development (OECD) Paris, for giving me the opportunity to work with them. I used their software and database. I am profoundly indebted to my Ms. Mariagrazia, Senior Economist, Head of OECD Unit (Industry, innovation and IP, WPIA Secretariat) for the guidance and advice. This work could not complete without her support.

References

Abraham, B. P., & Moitra, S. D. (2001). Innovation assessment through patent analysis. *Technovation*, 21(4), 245-252.

APO (2013), *APO Productivity Databook 2013,* Asian Productivity Organization, Tokyo.

Archibugi, D., & Planta, M. (1996). Measuring technological change through patents and innovation surveys. *Technovation*, 16(9), 451-519.

Basberg, B. L. (1987). Patents and the measurement of technological change: a survey of the literature. *Research policy*, 16(2), 131-141.

Bernd Wolter, It takes all kinds to make a world – Some thoughts on the use of classification in patent searching, *World Patent Information, Volume 34, Issue 1, March 2012,* Pages 8-18, ISSN 0172-2190.

Bosworth, D. L. (1984). Foreign patent flows to and from the United Kingdom. *Research Policy*, 13(2), 115-124.

Gassler, H., Frohlich, J., & Kopcsa, A. (1996). Selective information on the national system of innovation as an important input for the technology management of firms. *International Journal of Technology Management*, 11(3-4), 3-4.

Heiko Wongel, Antonios Farassopoulos, Changes to the IPC effective from January 2011, *World Patent Information*, Volume 34, Issue 1, March 2012, Pages 4-7, ISSN 0172-2190.

Houghton, Pucar, Knox (1996), Mapping information technology, *Futures*, Volume 28, Issue 10, December 1996, Pages 903-917, ISSN 0016-3287.

http://ipstatsdb.wipo.org/ipstatv2/ipstats/searchresultsTable United Nations Statistics Division (2013).

http://unstats.un.org/unsd/cr/registry/regdnld.asp.

Johnson, D. K. (2002), The OECD Technology Concordance (OTC): Patents by Industry of Manufacture and Sector of Use, *OECD Science, Technology and Industry Working Papers*, 2002/05, OECD Publishing.

Liu, S. J., & Shyu, J. (1997). Strategic planning for technology development with patent analysis. International Journal of Technology Management, 13(5), 661-680.

Lybbert, T. and N. Zolas (2012), Getting Patents and Economic Data to Speak to Each Other: An 'Algorithmic Links with Probabilities' Approach for Joint Analyses

Lybbert, T., P. Bhattacharyya and N. Zolas (2012), Matching Trademarks to Trade and Industry Data: An 'Algorithmic Links with Probabilities' Approach Getting Patents and Economic Data to Speak to Each Other: An Algorithmic Links with Probabilities' Approach, *World Intellectual Property Organization*, March 2012.

Mogee, M. E. (1991). Using patent data for technology analysis and planning. *Research-Technology Management*, 34(4), 43-49.

Narin, F., Noma, E., & Perry, R. (1987). Patents as indicators of corporate technological strength. *Research policy*, 16(2), 143-155.

OECD (2007), Glossary of Statistical Terms, retrived on 3rd October, 2013.

OECD (2013). *OECD science, technology and industry scoreboard 2013*. Paris: OECD.

of Patenting and Economic Activity, *WIPO Economics & Statistics Series*, Working Paper No.5, October 2012.

Paci, R., Sassu, A., & Usai, S. (1997). International patenting and national technological specialization. *Technovation*, 17(1), 25-38.

Schiffel, D., & Kitti, C. (1978). Rates of invention: international patent comparisons. *Research Policy*, 7(4), 324-340.

Schmoch U, Laville F, Patel P, Frietsch R (2003) Linking Technology Areas to Industrial Sectors , *Final report to the European Commission, DG Research*.

Schmoch, U. (2008). Concept of a technology classification for country comparisons. *Final report to the World Intellectual Property Organization (WIPO)*, Fraunhofer Institute for Systems and Innovation Research, Karlsruhe.

Tong, X., & Frame, J. D. (1994). Measuring national technological performance with patent claims data. *Research Policy*, 23(2), 133-141.

Treaty, P. C. (2008). International Search Report, International Application No. PCT/US, 97, 21458.

WIPO (2013). http://www.wipo.int/ipstats/en/wipi/.